



Calhoun: The NPS Institutional Archive DSpace Repository

Theses and Dissertations

1. Thesis and Dissertation Collection, all items

1969-06

A theoretical and experimental study of the impingement of two subsonic jets

Gungor, Nihat

Monterey, California. U.S. Naval Postgraduate School

<http://hdl.handle.net/10945/13262>

Copyright is reserved by the copyright owner

Downloaded from NPS Archive: Calhoun



<http://www.nps.edu/library>

Calhoun is the Naval Postgraduate School's public access digital repository for research materials and institutional publications created by the NPS community.

Calhoun is named for Professor of Mathematics Guy K. Calhoun, NPS's first appointed -- and published -- scholarly author.

Dudley Knox Library / Naval Postgraduate School
411 Dyer Road / 1 University Circle
Monterey, California USA 93943

NPS ARCHIVE

1969

GUNGOR, N.

A THEORETICAL AND EXPERIMENTAL STUDY
OF THE IMPINGEMENT OF TWO
SUBSONIC JETS

by

Nihat Gungor

United States
Naval Postgraduate School



THEESIS

A THEORETICAL AND EXPERIMENTAL STUDY
OF THE IMPINGEMENT OF TWO SUBSONIC JETS

by

Nihat Gungor

June 1969

This document has been approved for public release and sale; its distribution is unlimited.

1133243

Graduate School
Lodi, California 93940

A Theoretical and Experimental Study
of the Impingement of Two Subsonic Jets

by

Nihat Gungor
Lieutenant, Turkish Navy
Turkish Naval Academy, 1959

Submitted in partial fulfillment of the
requirements for the degree of

MASTER OF SCIENCE IN MECHANICAL ENGINEERING

from the

NAVAL POSTGRADUATE SCHOOL
June 1969

NPS ARCHIVE
1969
GUNGURU, N.

Thes C 8645 c 1

ABSTRACT

A theoretical and experimental investigation has been performed on the determination of the characteristics of two impinging plane turbulent jets for the purpose of understanding the performance of proportional fluid amplifiers and momentum-exchange devices. The jet deflection angle was determined through the application of the free-streamline theory for two normally impinging jets with arbitrary throat widths and wall set-backs. The deflection angle and the velocity and turbulence distributions across and at various distances along the jet were determined through the use of a hot-wire anemometer system. The results are presented in terms of normalized parameters suitable for comparison with the theoretical predictions. The deflection angles predicted theoretically were found to be in good agreement with those obtained experimentally.

DUDLEY KNOX LIBRARY
NAVAL POSTGRADUATE SCHOOL
MONTEREY, CA 93943-5101

TABLE OF CONTENTS

I.	INTRODUCTION	11
II.	THEORETICAL ANALYSIS OF THE JET DEFLECTION	16
III.	EXPERIMENTAL EQUIPMENT	23
IV.	EXPERIMENTAL PROCEDURE	29
V.	DISCUSSION OF RESULTS AND CONCLUSIONS	39
VI.	RECOMMENDATIONS FOR FURTHER WORK	98
	BIBLIOGRAPHY	99
	APPENDIX A	100
	APPENDIX B	102
	APPENDIX C	103
	COMPUTER OUTPUT	105
	INITIAL DISTRIBUTION LIST	114
	FORM DD 1473	117

LIST OF ILLUSTRATIONS

Figure	Title	Page
1.	Proportional Amplifier	13
2.	Schematic Drawing of the Jet Assembly	14
3.	Definition of Various Flow Planes	19
4.	Schematic Drawing of Experimental Apparatus	26
5.	General Experimental System	27
6.	Jet Assembly and Calibrator	28
7.	Calibration Curve	31
8.	Visual Jet Configuration	36
9.	Schematic of Velocity Traversing Line	37
10.	Jet Deflection Angle ($\frac{t}{a} = -0.5$)	40
11.	Jet Deflection Angle ($\frac{t}{a} = -1.0$)	41
12-29.	Normalized Velocity Profiles (\bar{U}/U_m vs. x/a)	44 - 61
30-35.	Normalized Velocity Profiles (Combined for each angle)	62 - 67
36-41.	Normalized Velocity Profiles (\bar{U}/U_c vs. x/d ; combined for each angle)	68 - 73
42-59.	Turbulence Intensity Profiles ($\sqrt{\bar{u}^2}/\bar{U}$ vs. x/a)	79 - 91
60-65.	Turbulence Intensity Profiles (combined for each angle)	92 - 97

LIST OF SYMBOLS

a	width of the auxiliary jet channel
a_n, b_n	coefficients of the polynomials
B	a constant
C	a constant
c	width of the resultant jet in the analysis
CF(P)	Pressure Correction Factor
\bar{E}	Anemometer output with flow, volts
\bar{E}_o	Anemometer output with no flow, volts
$\Delta \bar{E}$	$E - E_o$
d	The distance to any station of the jet axis from the intersection of two channel inner walls.
e	Width of the Main Jet Channel
$\sqrt{\bar{e}^2}$	Root Mean Square (RMS) value of the voltage output of anemometer corresponding to $\sqrt{\bar{e}^2}$
f	a parameter
h	a parameter
k	a parameter
M	a constant
n	a constant
ΔP	Manometer Reading of pressure head
q	Magnitude of the velocity vector, $\sqrt{u^2 + v^2}$
s	Relative set-back on the Main Jet Channel
t	Relative set-back on the Auxiliary Jet Channel
\bar{U}	Temporal Mean velocity at a given point on the jet
u	Velocity component in x-direction

$\sqrt{\bar{u}^2}$	Root Mean Square (RMS) value of the fluctuating component of velocity
U_a	Velocity in the Auxiliary Jet Channel
\bar{U}_c	Velocity on the Jet Center
U_m	Velocity in the Main Jet Channel
U_j	Free Stream line Velocity
U_{OR}	Velocity through the Calibration Orifice
v	Velocity Component in Y Direction
w	Complex Potential
Z	Complex Variable
α	Jet Deflection Angle Measured from Main Jet Direction
β	Jet Deflection Angle Measured from Auxiliary Jet Direction
δ	A Parameter U_a/U_j
ζ	Variable, $-u + iv$
η	A Parameter U_m/U_j

ACKNOWLEDGEMENT

The study and experiment was made possible through the sponsorship of the Harry Diamond Laboratories of the United States Material Command, Washington, D. C.

The author wishes to express his sincere appreciation to Professor T. Sarpkaya for his patience, guidance and encouragement during the course of the investigation. A special thanks is also due Messrs. K. Mothersell, J. Beck, and J. McKay of the Mechanical Engineering Machine Shop.

I. INTRODUCTION

In recent years considerable interest has been shown in the research, development, and design of fluid amplifiers with no moving parts. These devices are finding many applications in various fields of engineering, especially in control systems. The main feature of most of these devices is the use of a controlled fluid jet. The power jet or the primary jet may or may not attach to one or the other sidewall depending on whether the amplifier is a wall-attachment type bistable amplifier or a proportional amplifier. In the former type, the deflection of the jet from one stable to another stable position is accomplished by a combination of momentum exchange and pressure build-up in the separation bubble. In the proportional or momentum-exchange devices, however, the deflection of the jet is accomplished by and proportional to the exchange of momentum between the primary and control jets.

Despite the simplicity of their design, the complex combinations of fluid dynamic phenomena which take place inside these devices make it very difficult to produce a mathematical model able to predict their operation. The need for gaining a better understanding of the basic phenomena involved in the fluid amplifiers has brought a new interest in the area of small flows in closed passages and chambers, and many new works on these subjects have appeared in the last few years.

Some work on the research and development of fluid amplifiers and rate sensors has been undertaken by the Department of Mechanical Engineering of the Naval Postgraduate School through a research grant from the Harry Diamond Laboratories of the U. S. Army Materiel Command. The present work is part of this general research program and deals with only the proportional amplifiers.

A schematic diagram of a typical proportional amplifier is shown in Fig. 1. The interaction region of the amplifier is shaped to prevent the attachment of the supply (power) flow to an output via the Coanda effect. With no input (control) flow present, the supply flow strikes the splitter and divides equally through the two outputs. If pressure is applied to one of the inputs, the resultant control flow strikes the supply flow which deflects more of the supply flow to the opposite output. The deflection of the supply flow varies proportionally with the input flow. The greater the input pressure, the greater is the deflection of the supply flow to the opposite output. If the input pressure differential is reduced, the deflection of the supply flow is reduced proportionately. Since a variation in the control flow conditions causes a larger variation at the receivers, the device can be considered as an amplifier.

One can introduce parameters such as differential flow gain, a differential pressure gain, and differential power gain to describe the static characteristics of the amplifier. Until recently, these characteristics were determined purely experimentally without a serious effort to theoretically predict the jet deflection, momentum interaction, velocity and turbulence distributions, and the division of flow between the two outputs and vents.

In an attempt to lay a theoretical foundation for the prediction of the characteristics of proportional amplifiers with one or two control flows, the present study was undertaken. Furthermore, in order to partly simplify the problem, two two-dimensional, normally-impinging jets were considered with different jet widths and side-wall set-backs. Obviously, such a configuration (Fig. 2) corresponds to a simple momentum exchange proportional amplifier as encountered in several logic devices such as a

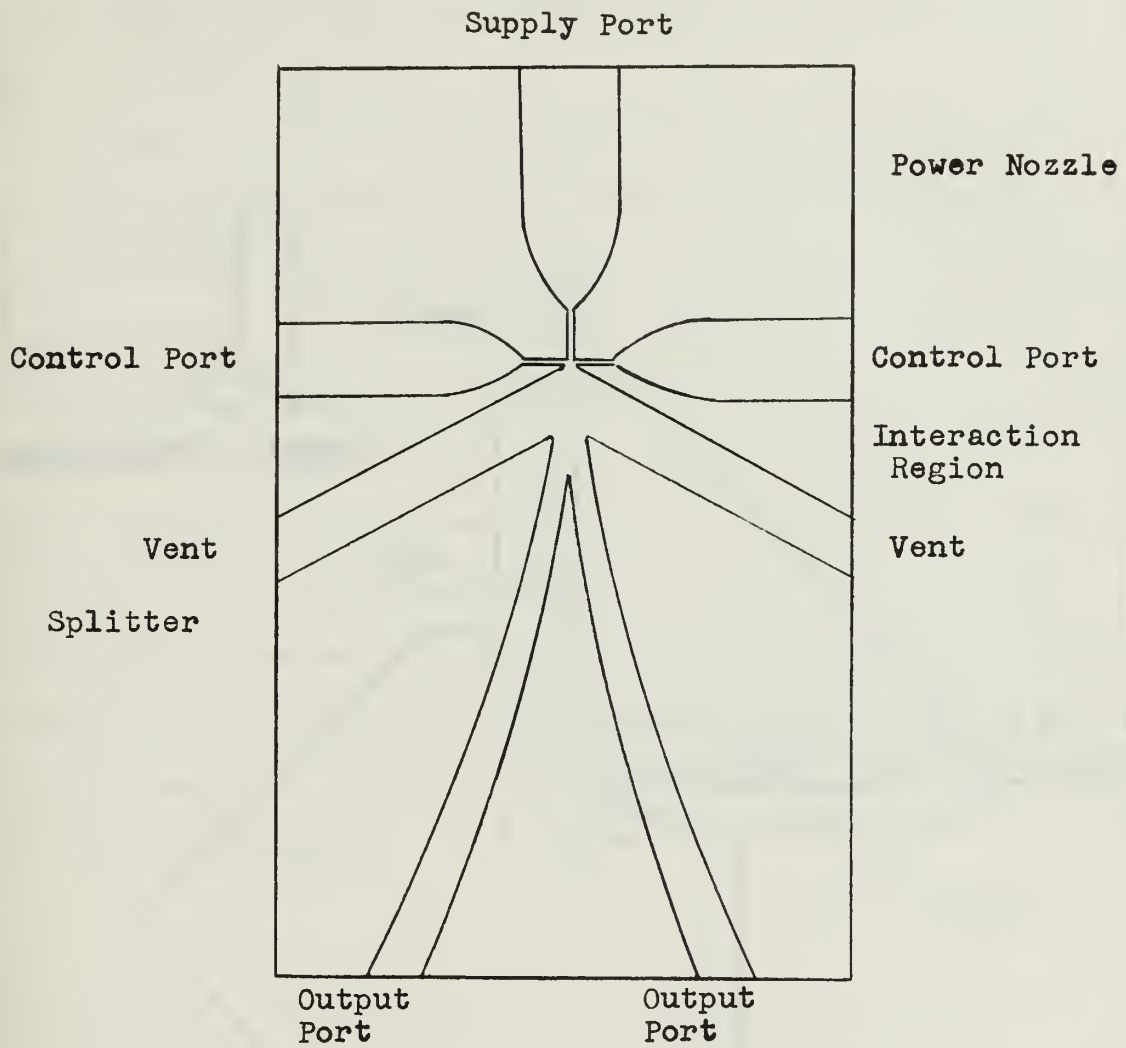


FIGURE 1. PROPORTIONAL AMPLIFIER

1. Auxiliary jet
2. Main jet

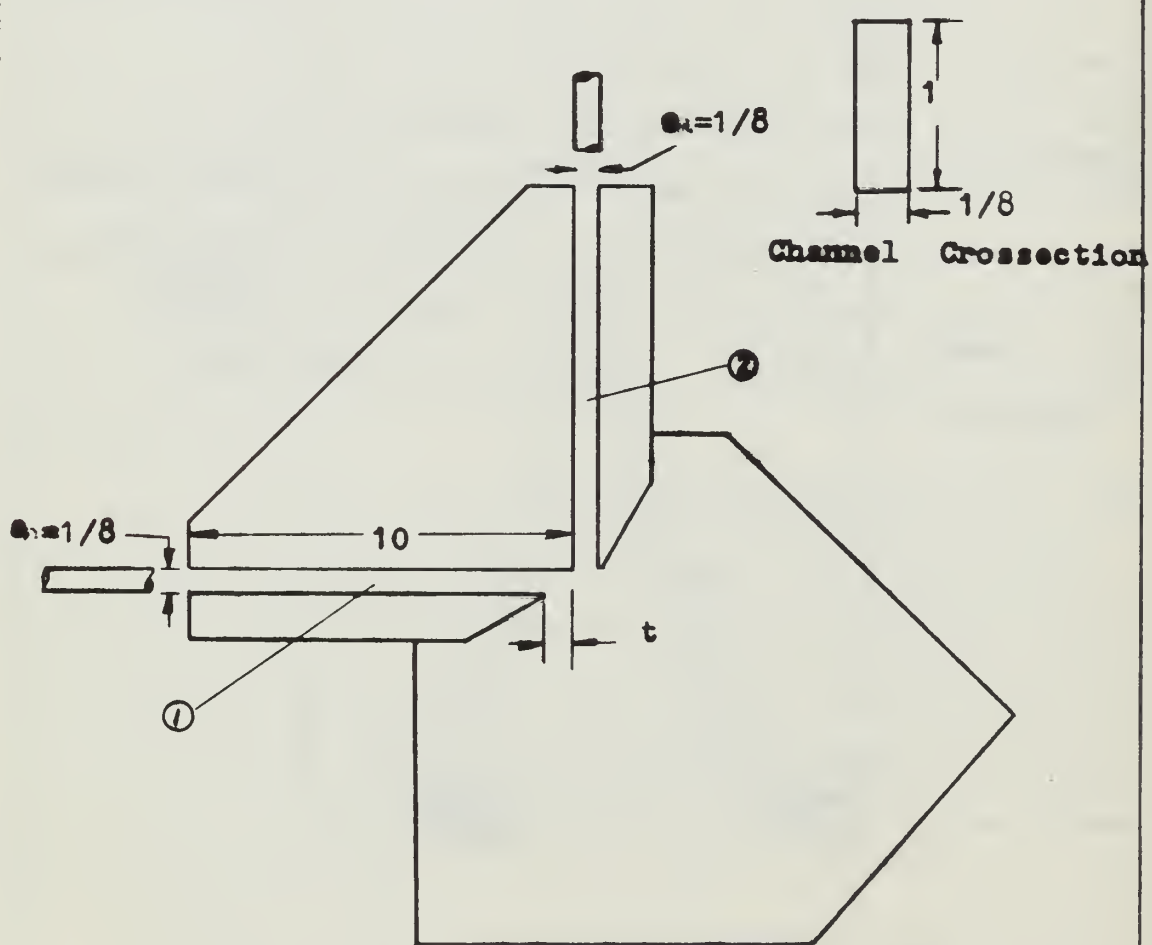


FIGURE 2. SCHEMATIC DRAWING OF THE JET ASSEMBLY

"half adder" and "transverse impact Modulators" [1]. The understanding of the fluid mechanics of such a jet configuration could then be extended through the use of similar but perhaps more complicated theoretical and experimental means to the study of the complete proportional amplifier shown in Fig. 1.

In connection with this and other current and anticipated investigations in the laboratory, it was decided to study the impingement of two semi-confined jets between two parallel plates, with special regard to the influences of the velocity ratios of the two jets and the wall set-back. A large scale model was used having dimensions that are large compared with the power of resolution of the flow measurement instruments. Velocity and turbulence measurements were carried out through the use of a hot-wire anemometer system for various velocity combinations and at various sections along the jet. The theoretical analysis, based on the free-streamline theory, was used to calculate the jet deflection angle as a function of the velocity ratio of the jets assuming the fluid to be inviscid.

II. THEORETICAL ANALYSIS OF THE JET DEFLECTION

Many plane irrotational flow patterns which include the formation or deflection of free or partly bounded jets can be analyzed satisfactorily by the theory of free-streamlines by Helmholtz [2] and Kirchhoff [3]. The results obtained may be significant not only for the corresponding two-dimensional flows of real compressible and incompressible fluids but, in many instances, for their three-dimensional counterparts as well. The analysis consists of the definition of successive conformal transformations involving a hodograph, or velocity plane, and the application of the Schwartz-Christoffel transformation [4]. The fact should be emphasized that from a mathematical point of view, the direct calculation of free-streamline flows is restricted to two-dimensional irrotational flows of compressible and incompressible fluids which are free from gravitational effects. Hence, the formation of a jet by two two-dimensional streams impinging obliquely is well suited to free-streamline analysis because of the dominance of inertia and pressure in the establishment of the resulting flow pattern and because of the negligible effect of gravity on gas jets. As will be discussed later, however, difference in the free-streamline velocities of the two jets enhances the shear in the mixing region of the two jets. The larger is the velocity difference, the larger the energy dissipation becomes. The free-stremaline analysis may be applied, however, only when the velocities along both sides of the jet are assumed to be identical and equal to an unknown free-streamline velocity. Thus the region in which the momentum-exchange and the turbulent mixing take place does not, strictly speaking, follow the

assumptions made in the free streamline theory. Hence the validity of the analysis depends on the experimental demonstration of the uniformity of the velocity profiles at the formation region of the resulting jet.

For the development of the following analysis, the free-streamline velocities are assumed to be identical and the validity of the assumption is discussed later in connection with the comparison of the theoretical results with those obtained experimentally. Mindful of the restrictions and limitations of the applicability of this method, the solution of the problem under consideration proceeds as follows:

If z and w are used for the complex variable and the complex potential, then the variable ζ defined as dw/dz is given by

$$\zeta = -u + iv - qe^{-i\theta} \quad (1)$$

in which u and v are the velocity components in the x and y directions, q is the magnitude of the velocity vector, and θ is the angle of its inclination.

If the variable Ω is introduced,

$$\Omega = \ln \left(-\frac{U_j}{\zeta} \right) = -\ln \frac{q}{U_j} + i\theta \quad (2)$$

the flow region in the physical plane (Fig. 3a) can be mapped onto a corresponding region in the Ω -plane, as indicated in Fig. 3b. Either ζ or Ω must be related to w by means of known methods through still another complex variable designated as t . This relationship completes the rather complicated functional analysis because, as has already been seen, either ζ or Ω can be expressed in terms of dw/dz .

Any polygonal boundary in one complex plane can be transformed into the entire real axis of another through application of Schwartz-Christoffel theorem, the interior of the polygon being transformed into either the

upper or the lower half of the second plane [4]. Thus the outline in the Ω -plane is directly transformable into the real axis of the t -plane. Therefore, the Ω -plane shown in Fig. 3b may be transformed to the t -plane shown in Fig. 3c. The transforming function can be written as follows:

$$\Omega = \int \frac{M dt}{\sqrt{(t+1)(t-h)}} \quad (3)$$

Upon integration, one has

$$\Omega = 2M \ln C (\sqrt{t+1} + \sqrt{t-h}) \quad (4)$$

in which M and C are found to be $1/2$ and $\sqrt{1+h}$ by substituting into the equation the coordinates of the points B and D . The final form of Ω thus reduces to

$$\Omega = \ln \frac{\sqrt{t+1} + \sqrt{t-h}}{\sqrt{h+1}} \quad (5)$$

In particular, it will be noticed that at $t = 0$, $\Omega = i\beta$ (at point C) and one has

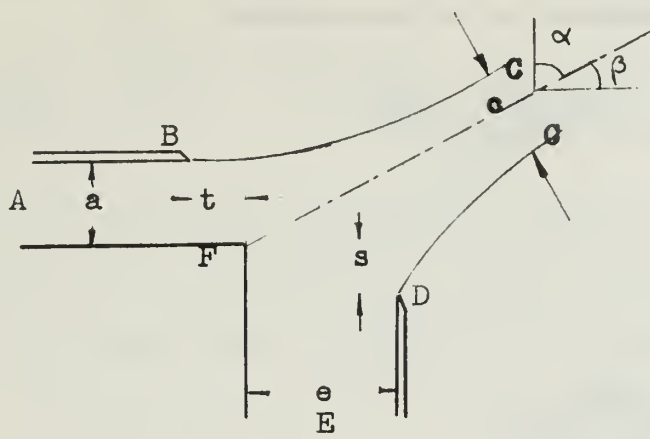
$$i\beta = \ln \frac{1 + i\sqrt{h}}{\sqrt{1+h}} = i \tan^{-1} \sqrt{h}$$

or

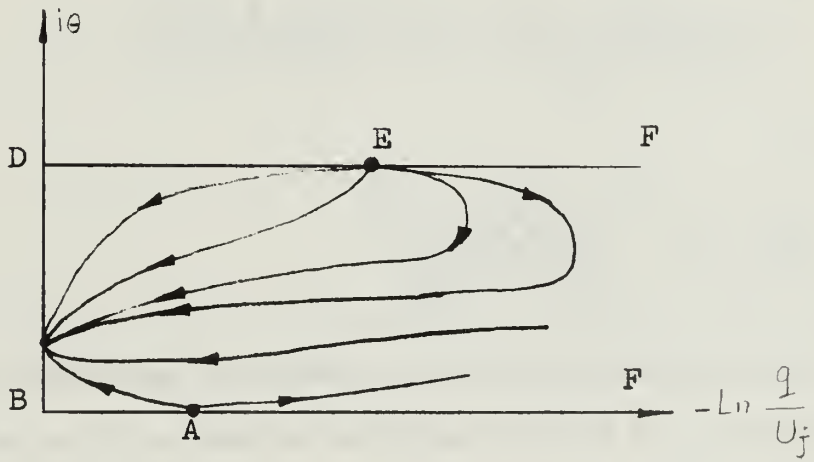
$$\tan \beta = \sqrt{h} \quad (6)$$

Obviously, the angle of the deflection of the main jet, α , is related to β by the simple relationship

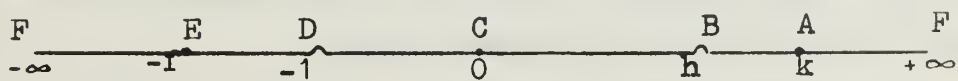
$$\alpha + \beta = \pi/2 \quad (7)$$



(a) Physical Plane



(b) Ω - Plane



(c) t - Plane

FIGURE 3. DEFINITION OF VARIOUS FLOW PLANES

The velocities are related to various parameters in the t -plane via the Ω transformation. At A, for example,

$$\Omega = \ln \frac{U_j}{U_a} = \ln \frac{\sqrt{k+1} + \sqrt{k-h}}{\sqrt{h+1}}$$

or

$$\frac{U_a}{U_j} = \delta = \frac{\sqrt{h+1}}{\sqrt{k+1} + \sqrt{k-h}} \quad (8)$$

Likewise, at E

$$\Omega = \ln \frac{U_j}{U_m} + i \frac{\pi}{2} = \ln \frac{\sqrt{1-f} + i \sqrt{f+h}}{\sqrt{h+1}}$$

or

$$\frac{U_m}{U_j} = \eta = \frac{\sqrt{h+1}}{\sqrt{f-1} + \sqrt{f+h}} \quad (9)$$

Before proceeding further, it should be pointed out that the parameters (f , h , k) could have been selected at other points or special use could have been made of the symmetry of the points B and D. A careful analysis of the various possibilities has shown that the t -plane selected herein will yield the least amount of difficulty in the evaluation of the integrals to be performed later.

The complex potential w can be expressed in terms of t by the method of sources and sinks as

$$w = \frac{U_j c}{\pi} \ln t - \frac{U_a a}{\pi} \ln(t-k) - \frac{U_m \cdot \bullet}{\pi} \ln(t+f) \quad (10)$$

From this relationship and from the definition of ζ , one obtains

$$z = -\frac{1}{\pi\sqrt{h+1}} \int [\sqrt{t+1} + \sqrt{t-h}] \left[\frac{c}{t} - \frac{a\delta}{t-k} - \frac{e\eta}{t+f} \right] dt \quad (11)$$

The integrals appearing in the above equation may be evaluated for various intervals in the t -plane or for various distances between various points in the physical plane. The position of the point B relative to the point F is given by:

$$-t + ia = |z| \Big|_{t=h}^{t=\infty}$$

which, upon evaluation in a straightforward manner, yields

$$\begin{aligned} \frac{t}{a} = & -\frac{1}{\pi\sqrt{h+1}} \left[-\frac{c}{a} \ln \frac{\sqrt{h+1} + 1}{\sqrt{h+1} - 1} + \delta\sqrt{k+1} \ln \frac{\sqrt{k+1} + \sqrt{h+1}}{\sqrt{k+1} - \sqrt{h+1}} \right. \\ & \left. + \frac{c}{a} \pi\sqrt{h} - 2\eta \frac{e}{a} \sqrt{f-1} \tan^{-1} \sqrt{\frac{f-1}{h-1}} - \pi\eta \frac{e}{a} \sqrt{f+h} \right] \end{aligned} \quad (12)$$

It should be noted that c/a , δ , e/a , and η are related by the equation of continuity as

$$\frac{c}{a} = \delta + \frac{e}{a} \eta \quad (13)$$

The evaluation of the integrals indicated in Eq. (11) from $t = -\infty$ to $t = -1$ and the separation of the real and imaginary parts similarly yields

$$\begin{aligned} \frac{s}{a} = & -\frac{1}{\pi\sqrt{h+1}} \left[\frac{c}{a} \pi - \pi\delta\sqrt{k+1} + \frac{e}{a} \eta\sqrt{f+h} \ln \frac{\sqrt{f+h} + \sqrt{1+h}}{\sqrt{f+h} - \sqrt{1+h}} \right. \\ & \left. - \frac{c}{a} \sqrt{h} \ln \frac{\sqrt{1+h} + \sqrt{h}}{\sqrt{1+h} - \sqrt{h}} - 2\delta \sqrt{k-h} \tan^{-1} \sqrt{\frac{k-h}{1+h}} \right] \end{aligned} \quad (14)$$

It is thus apparent that the velocity ratios and the relative setbacks t/a and s/a and the angle β may be evaluated by assigning various values to the parameters f , h , and k in the t -plane. It is further obvious that the width of the jet at C may be evaluated without difficulty by carrying out similar integrations from D to C and from B to C. Since the jet width or the contraction coefficient is not needed in the present analysis, the results concerning the contraction coefficient will not be presented here.

The expressions for t/a and s/a are of such nature that one cannot assign special values to them and expect to find the corresponding values of f , g , and k and the angle β . The nonlinearity of the equations makes it mandatory that one assign arbitrary values to the parameters in the t -plane in a fairly systematic manner and obtain the corresponding values of t/a , s/a , and β . In this manner, one obtains an infinite variety of possible solutions and then selects those which conform to the selected geometry. This procedure which is common to all free-streamline problems, has been applied to the present problem through the use of the IBM 360 computer and the results obtained for both $t/a = -1$, $s/a = 0$, $e/a = 1$ and for $t/a = 0.5$ $e/a = 1$, and $s/a = 0$ are plotted in terms of the jet deflection angle α versus the ratio of the velocities. These will be discussed later in connection with the discussion of the results. The information for other combinations of t/a , s/a , and e/a is available in the form of computer print-out and they will not be reproduced here for it is practically impossible to cover the entire range in the form of a simple plot. Thus only those cases which are of practical significance are presented herein and compared with those obtained experimentally. The computer program which will generate solutions for all ranges of the parameters encountered in the analysis is presented in the Computer Output Section.

III. EXPERIMENTAL EQUIPMENT

The experimental apparatus consisted of the jet assembly, supply system, hot wire anemometer system, and the velocity calibrator.

Jet Assembly

The jet assembly was made of plexiglass for ease of machining and flow visualization. As shown in Fig. 2, two ten inch long, one inch deep and one-eighth inch wide channels were cut out and sandwiched between two one half inch plexiglass plates. The axes of the two jets (referred to hereafter as the main jet and auxiliary jet) were normal to each other since in the majority of the momentum-exchange amplifiers these two jets are made to intersect each other at an angle of 90 degrees. In order to prevent premature wall-attachment via Coanda effect, the outer edges of the two jets were sharply curved back. The three-eighths inch diameter supply lines were connected to the inlets of the two channels and a smooth transition was provided between the circular and the rectangular sections. In addition, several wire screens were placed near the transition region for the purpose of eliminating secondary swirling flows which might have developed in the long circular supply line. The outer wall of the auxiliary-jet channel was made movable for the purpose of adjusting the relative set-back (see Fig. 2). All channel surfaces were polished carefully and the dimensions were set with gage blocks to an accuracy in the order of 0.001".

Supply System

The working fluid (air) was supplied from a 50 Hp compressor. Air was then passed through a microfilter for the purpose of removing oil, dust, and other impurities and was directed to pressure regulators

and Fischer-Porter rotometers. Both the main jet and the auxiliary jet were supplied air independently from the main flow line coming out of the primary pressure regulator. Each jet had, in addition, a series of pressure regulators ranging from ten to 130 psig and an independent flowrator whose capacity was identical with that of the other flowrator. The maximum capacity of each flowrator was 14.6 SCFM at 14.7 psia and 70 degrees with a 3/4-27G-10/83 tube and 3/4-GNSVGT-54 float. Finally, in order to determine the actual flow rate passing through the flowrators at pressures other than 14.7 psia, each flowrator was equipped with a pressure gage and the flow rates were obtained by:

$$Q = \text{flowrator meter reading} \times 100\% \text{ full flow} \times CF(P)$$

where

$CF(P)$ is the pressure correction factor and is provided by Fischer-Porter Company in the form of a chart for each flowrator.

Hot-Wire Anemometer and Calibrator

The Model 1050 constant temperature hot-wire anemometer of the Thermo-Systems, Inc., was used in the measurement of velocities and turbulence intensities. The hot-wire probe holder was mounted on a micrometer block capable of providing a translation (along a slot along the edges of the top and bottom cover plates) and a rotation (in the mid-plane of the jets) to the sensor holder. The micrometer enabled the measurement of distances along any section in the mid-plane between the top and bottom cover plates to an accuracy of 1/160".

The probe used in the tests had a cold resistance of 6.45 ohms and an operating resistance of 9.70 ohms. The probe was calibrated with the Model 1125 calibrator of Thermo-Systems, Inc. All calibrations were carried out with the high-range calibration orifice of the calibrator which had a 0.150" diameter.

In order to calculate the velocity of the flow through the orifice, the pressure of the calibration chamber was connected to water manometers of three different ranges to augment the accuracy of the calibration.

A schematic of the experimental layout is shown in Fig. 4. Figures 5 and 6 are the photographs of the experimental system, the calibrator, micrometer assembly, and the plexiglass test model.

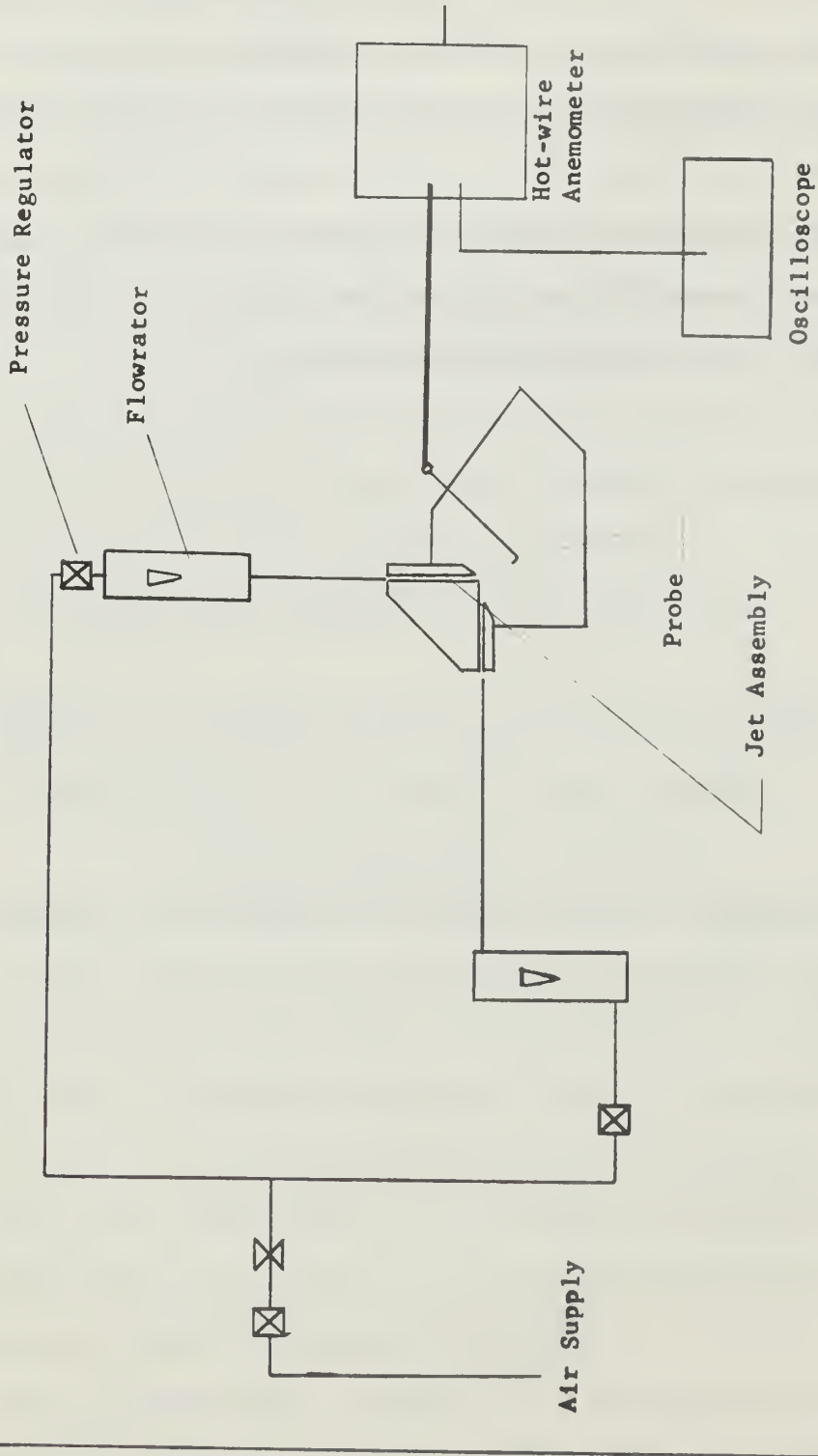
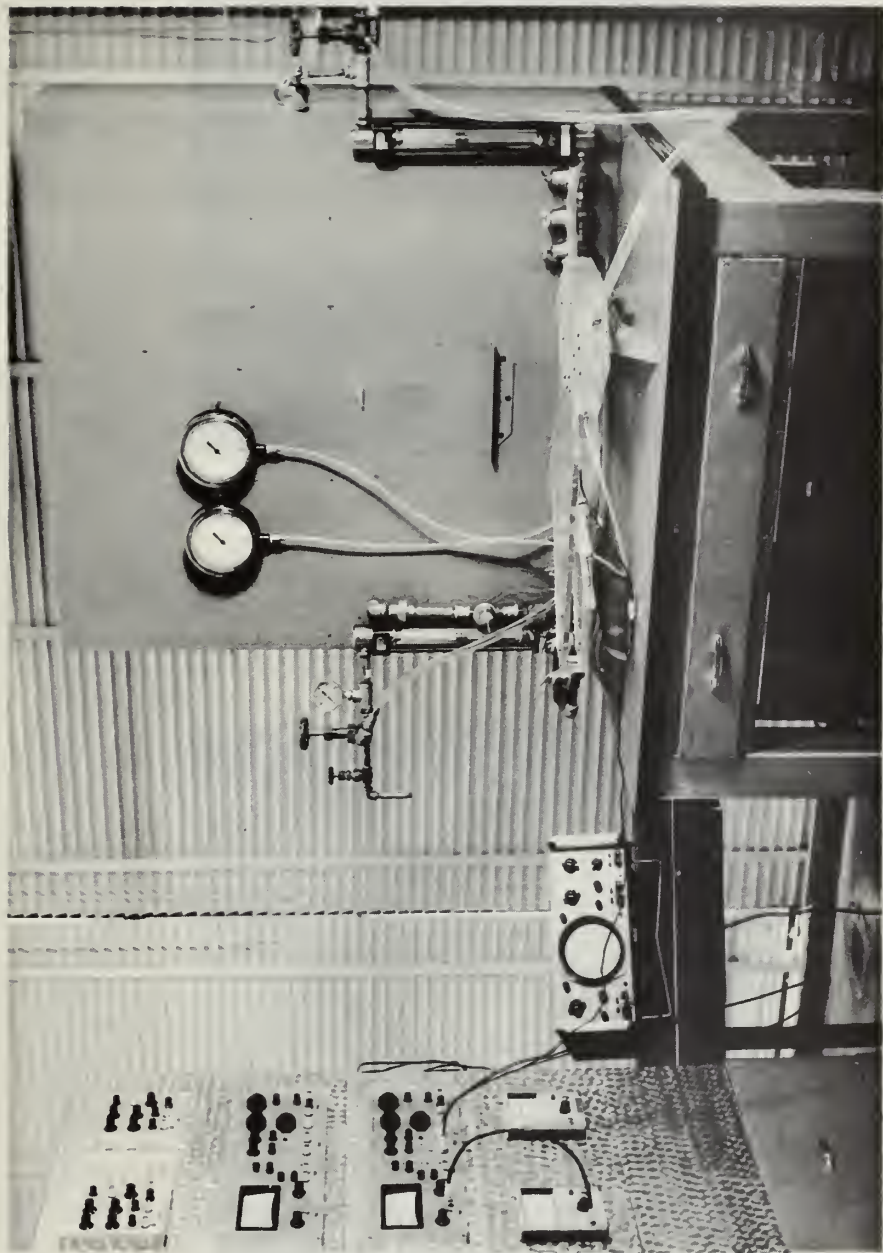


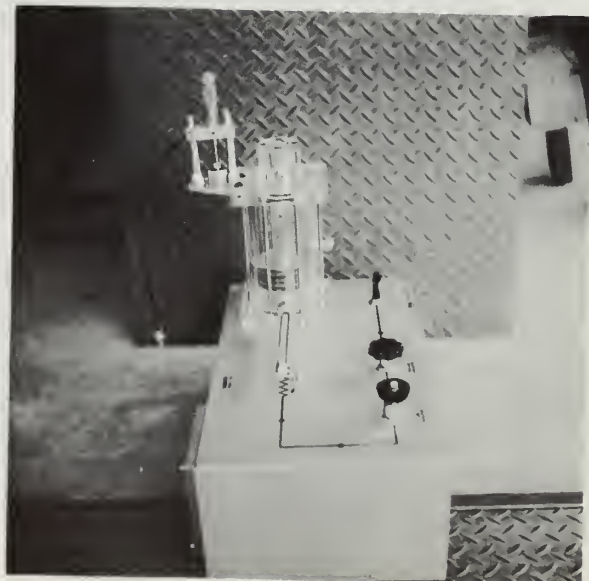
FIGURE 4. SCHEMATIC DRAWING OF THE EXPERIMENTAL APPARATUS

FIGURE 5. GENERAL EXPERIMENTAL SYSTEM.





Plexiglass jet assembly.



Model 1125 calibrator.

FIGURE 6. JET ASSEMBLY AND CALIBRATOR.

IV. EXPERIMENTAL PROCEDURE

The experiments consisted of the setting of proper dimensions to the jet channels, the calibration of the hot-wire probe, setting of the anemometer, setting of the selected flow rates for each jet, the determination of the jet deflection angle α through the use of a flow visualization method, and the measurement of velocities and turbulence intensities along lines normal to the jet axis in the mid-plane of the jet at various distances from the nozzle exit.

Setting of the Channel Dimensions

It is apparent that an infinite variety of geometrical configurations may be tested even if the jet impingement angle is maintained at 90 degrees. For this reason, attention was given only to those geometries which have considerable practical significance as far as the momentum-exchange amplifiers are concerned. In the majority of such devices, the channel widths are kept identical and the side-wall of the auxiliary jet is set back a distance equal to either the nozzle width or one-half of the nozzle width. Thus, in the present study, the channel widths were kept identical ($1/8"$) and two different set-backs were used for the auxiliary jet, i.e., t/a was chosen in the first series of tests equal to -0.5 and in the second series of tests equal to unity. All dimensions were, as cited before, set with gage blocks to an accuracy of 0.001".

Calibration of the Hot-Wire Probe

The hot-wire probe was placed $1/16"$ above the axis of the calibration orifice as recommended by the manufacturer [5] and the pressure tap of the calibrator was connected to a water manometer. In order to increase the accuracy of the pressure measurement, three different

manometers were used. These consisted of manometers 0 to 0.2" range with 0.01" increments, 0 to 2" range with 0.1" increments, and a manometer with 0-36" range with 0.1" increments. The first two manometers were of inclined type for further increase of the accuracy in the reading of the water elevations. The velocities through the orifice were then calculated through the use of the following equation:

$$U_{OR} = \sqrt{\frac{2 \Delta P}{\rho}} \quad (15)$$

where

ΔP is the manometer readings and ρ the density of air. The corresponding voltage output on the hot-wire anemometer was recorded for each manometer setting and then a velocity vs. volts "calibration curve" was plotted as shown in Fig. 7.

The calibration curve as obtained above is of limited use because of the difficulty it introduces in the evaluation of velocity for each anemometer reading corresponding to velocity and turbulence measurements along various lines, at various distances from the nozzle, and for various combinations of the flow rates. It is, therefore, obvious that one has to fit one or more polynomials to the calibration data and calculate, through the use of the computer, the velocities and turbulence intensities corresponding to each anemometer and Root Mean Square meter reading. For this purpose, various degrees of polynomials were tried for the representation of the entire calibration data and it was found that two 4th degree polynomials with a common ordinate and tangent at the point of intersection would be most satisfactory. The polynomials chosen were of the following type:

$$\bar{U}(\bar{E}) = a_1 + a_2 \Delta \bar{E} + a_3 (\Delta \bar{E})^2 + a_4 (\Delta \bar{E})^3 + a_5 (\Delta \bar{E})^4 \quad (16)$$

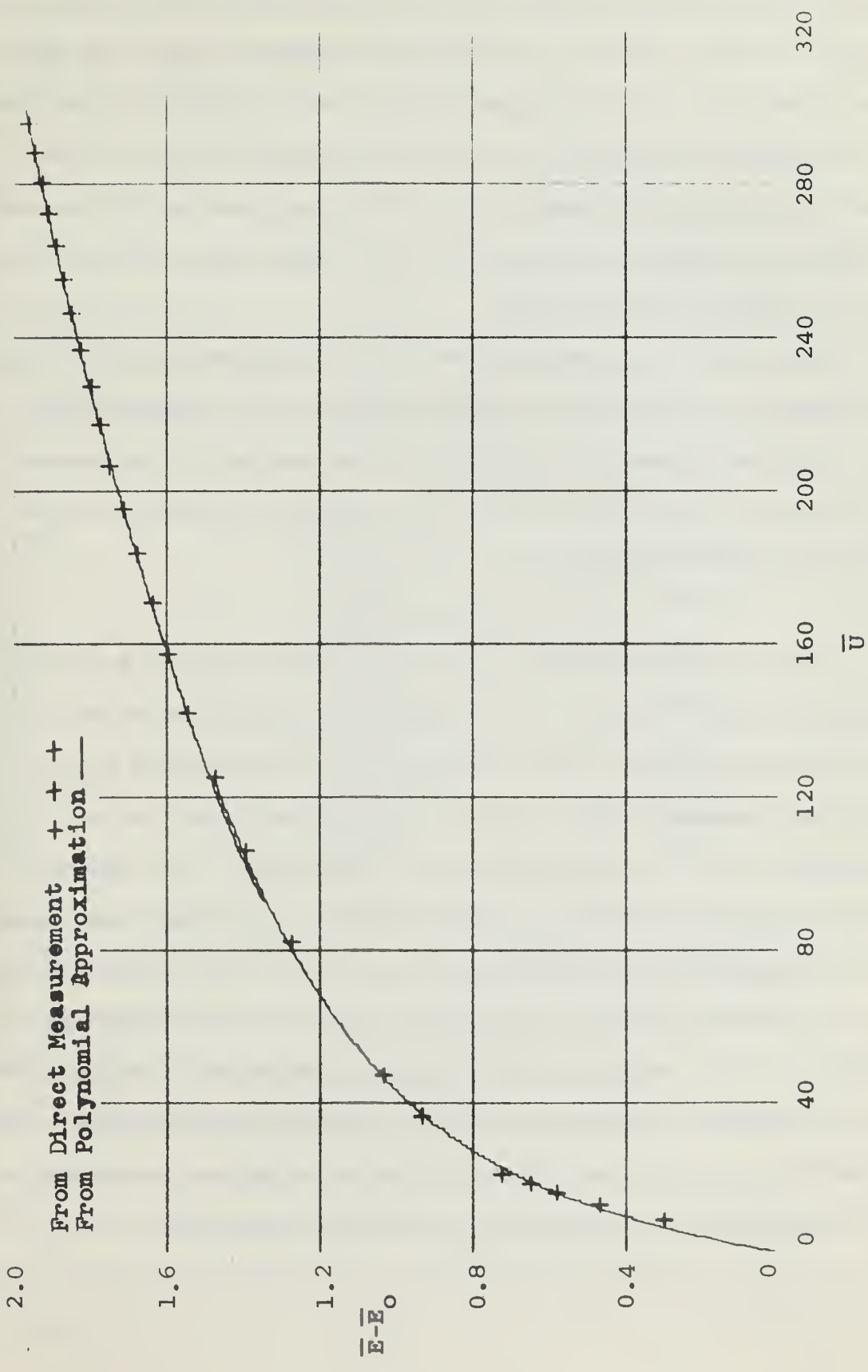


FIGURE 7. CALIBRATION CURVE

where $\Delta \bar{E} = \bar{E} - \bar{E}_0$ and \bar{E}_0 is the anemometer output at zero flow velocity and \bar{U} is the temporal mean velocity at a given point. The coefficients a_n of the above polynomial were determined through the use of an IBM 360 (see Appendix B). One 4th degree equation with coefficients a_n was used for differential anemometer output equal or below $\bar{E} - \bar{E}_0 = 1.460$ and another 4th degree polynomial with coefficients b_n was used for anemometer differential outputs greater than $\bar{E} - \bar{E}_0 = 1.460$. The coefficients a_n and b_n are tabulated in Appendix B.

The calibration curve described above was checked frequently during experiments (at least once after the completion of the velocity and turbulence measurements for a given flow combination) for the purpose of ensuring that neither the probe nor the anemometer system had drifted from their original conditions.

Setting of the Anemometer

Prior to each experiment, the anemometer was turned on and set to warm up for about one-half hour. Then the cold resistance of the hot-wire probe was checked to make sure that it had not deviated from its previously measured value. Then the operating resistance was set in accordance with the regular operational instructions of the anemometer [5] and the system was set to 'RUN' position. One of the output channels of the anemometer was connected to an oscilloscope and the flow was turned on and increased gradually until an oscillation, due to feedback instability in the amplifier circuitries, was encountered. Then the 'TRIM' on the anemometer was adjusted and the oscillation was eliminated. This procedure was, of course, carried out for all velocities encountered in the experiments by increasing and decreasing the flow rate.

The oscilloscope was, of course, observed at all times during the actual measurement to make sure that no system-generated noise interfered with the actual turbulence of the flow.

Setting of the Selected Flow Rates

The flow rates through each channel were selected on the basis of the Reynolds numbers encountered in the application of large momentum-exchange devices. The velocity of the main jet was maintained at 173.200 ft/sec which corresponded to a flowrator reading of 60% of the full capacity and to a Reynolds number of 11300. The flow rates of the auxiliary jet ranged from 60% to 10% at increments of 10%. These flow rates and the corresponding velocities and Reynolds numbers are tabulated below.

<u>Flow Rate</u>	<u>Velocity ft/sec</u>	<u>Reynold Number</u>
60%	173.200	11300
50%	146.500	9550
40%	113.200	7380
30%	84.096	5485
20%	56.064	3660
10%	28.032	1832

During the experiments, a flow rate was selected for the auxiliary jet from the above table and the flow through each jet was maintained constant (within the limits of the experimental uncertainty) with the use of separate pressure regulators described previously.

The Determination of the Jet Deflection Angle

The jet deflection angle α was determined through the use of several different procedures. The first two of these procedures consisted of the use of lamp-black and oil mixture and the use of powdered color paint.

These gave the jet deflection angle to an accuracy within $\pm 2^\circ$.

The third method which yielded the jet deflection angle to a finer degree of accuracy was the use of the measured velocity profiles.

The lamp-black and oil were mixed at more or less arbitrary quantities and the inner face of the base plate was carefully painted with a brush. Prior to painting, the valves and the pressure regulators were adjusted in such a manner that when the main flow was turned on, the flow combination would correspond to the desired flow rates in each channel. Obviously this latter procedure was easily carried out by adjusting the flows prior to the painting and then shutting off the main valve rather than the secondary valves. Then when the main valve was turned on, the resultant jet partly washed the surface of the paint and left a clear print of the jet configuration. It is, of course, fully realized that the boundary layer may yield a flow configuration on the paint somewhat different from that which would be encountered in the mid-plane. Nevertheless, the method yielded the jet deflection angles which were fairly satisfactory as far as the preliminary determination of the velocity and turbulence traversing planes was concerned. The jet deflection angle was measured relative to the main jet by placing two graph papers above and below the test section and by lining up the paint trace with the lines on the graph papers.

The second method used in the determination of the jet deflection angle consisted of the preparation of a white oil-painted paper and the introduction, into the supply lines, of small amounts of powdered, colored, dry paint (different color for each channel). The painted paper was glued to the inner face of the bottom plate with rubber cement. The powdered paint released from the supply line followed the jet configuration and stuck on the freshly painted paper. Thus, this method quickly

yielded the jet configuration and the deflection angle and also gave a pretty good idea about the mix-up of the jets in the interaction region. In all the experiments cited herein, the mixing region and of course the remainder of the jet came out at a color which one would have obtained by mixing them thoroughly in a separate container. A sample jet configuration as obtained in this manner is shown in Fig. 8.

The Measurement of Velocity and Turbulence Intensities

The velocities were measured along the lines normal to the jet centerline determined through one of the flow visualization techniques cited above. The hot-wire probe was moved at suitable increments along lines normal to the jet centerline and both the velocity and Root Mean Square (RMS) meters were read and recorded. The velocities and, of course, turbulence intensities were measured at six different stations for six different flow combinations. These stations were located at 0.15", 0.3", 0.8", 1.5", 2.5", and 4" from the point where the inner walls of the two jets intersected. As will be mentioned later, only 34 velocity and 34 turbulence intensity traces are presented instead of 36 of each. (Because the flow rates of 1/6 and 2/6 made it impossible to maneuver the hot-wire probe at the first station (0.15" from the nozzle) due to the fact that the traversing line fell within the auxiliary jet channel.) Figure 9 is a schematic drawing of the velocity traversing line relative to the jet channels.

The turbulence intensity $\sqrt{\bar{u}^2}/\bar{U}$ was calculated by

$$\sqrt{\bar{u}^2}/\bar{U} = \frac{\sqrt{\bar{e}^2}}{\bar{U}} \cdot \frac{d\bar{U}}{dE} \quad (17)$$

where $\sqrt{\bar{e}^2}$ is the output of the RMS meter and $d\bar{U}/dE$ is the derivative of Eq. 16 or, in other words, the complement of the slope of the

$$\begin{aligned} U_a/U_m \quad (173.2/173.2) &= 1.000 \\ Re \quad (\text{auxi. jet}) &= 11300 \\ Re \quad (\text{main jet}) &= 11300 \end{aligned}$$



FIGURE 8. VISUAL JET CONFIGURATION.

1. Main jet channel
2. Auxi. jet channel
3. Deflection angle
- 4-5 Sweeping path
6. Jet centerline
7. Station distance (d)

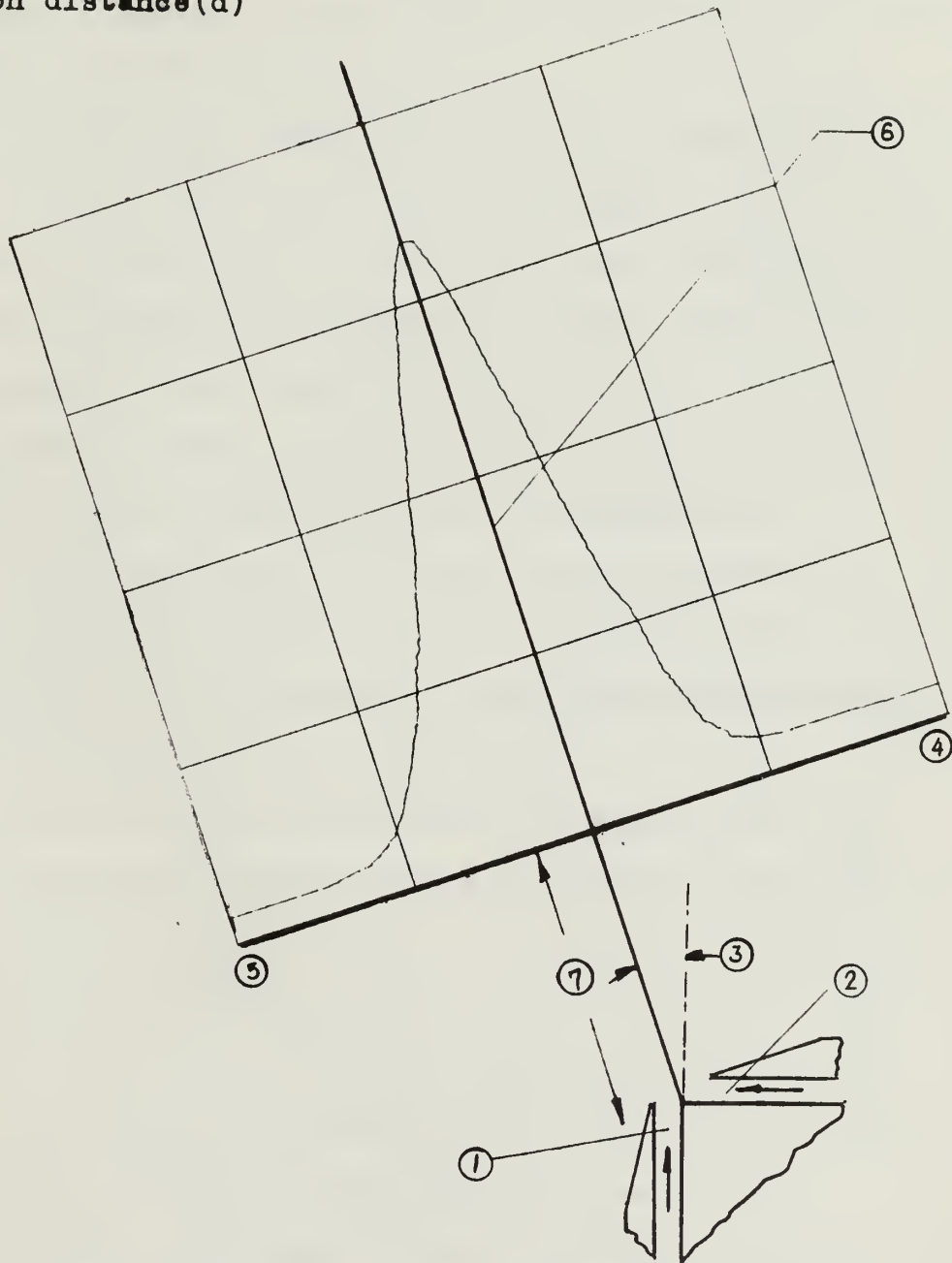


FIGURE 9. SCHEMATIC OF VELOCITY TRAVERSING LINE

calibration curve. The derivation of the above equation is shown in Appendix C. The turbulence intensity profiles were plotted like the velocity profiles by means of an IBM 360 computer and will be discussed subsequently.

V. DISCUSSION OF RESULTS AND CONCLUSIONS

The purpose of the present investigation was the understanding of the characteristics of the impingement of two plane jets. These characteristics essentially were the deflection angle of the resulting jet, and the velocity and turbulence distributions.

The deflection angles obtained experimentally are shown in Fig. 10 for a 1/16" set-back ($t/a = -0.5$). The similar data for a 1/8" set-back ($t/a = -1.0$) are shown in Fig. 11. Also shown on both figures are the results obtained theoretically through the use of Eqs. (12) and (14).

It is apparent from the examination of Figs. 10 and 11 that the agreement between the theoretical and experimental results is quite satisfactory, at least for the flow rates and set-backs used.

The velocity distributions for various angles of deflection at various distances along the nozzle exit are shown in Figs. 12-29 in a normalized form, i.e., \bar{U}/U_m versus x/a . The following facts become apparent upon a brief examination of these figures:

(a) The velocity profiles become flatter and perfectly symmetrical as the distance increases from the nozzle exit to the section where the velocity is measured. This, of course, is an observation which is true for all jet flows.

(b) The mixing of the two jets takes place more quickly for the smallest jet velocity ratios such as $U_a/U_m = 1/6$. As the velocity ratio increases, the velocity profile exhibits two maximums with a trough in the middle. This points out that the mixing of high velocity jets requires larger distances along the jet but certainly a distance less than approximately $d/a = 6$. The significance of this observation

50

$t/a = -0.5$
Analytic Solution
Experimental values ■ ■ ■

40

30

20

10

00

 α

40

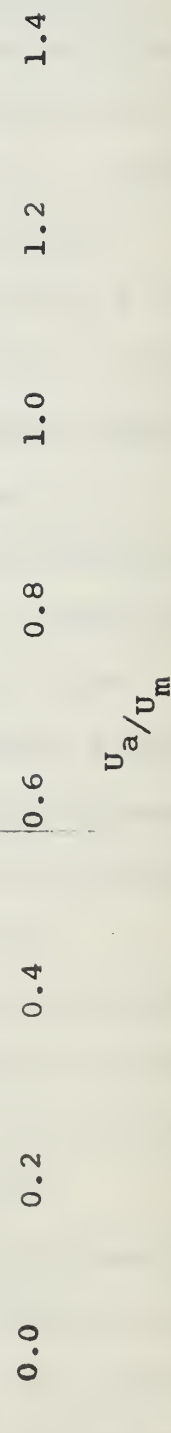


FIGURE 10. JET DEFLECTION ANGLE, F

50

$t/a = -1.0$
Analytic Solution
Experimental Values ■ ■ ■

40

30

20

10

0

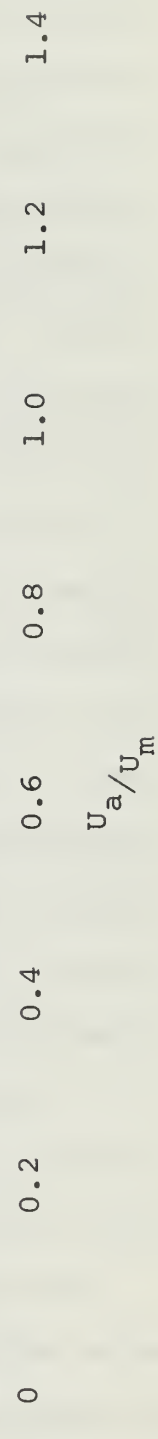
 α 

FIGURE 11. JET DEFLECTION ANGLE

is in relation with the theoretical analysis. As has been cited in the development of the theoretical analysis, the free-streamline velocities on the two sides of the inviscid jet had to be assumed to be identical. (The velocity profiles for all velocity ratios, near the nozzle where the free-streamline analysis is supposed to hold true, show an almost uniform distribution with the exception of two peaks and a trough whose amplitude is about 1/8 of the maximum of the normalized velocity. The velocity profiles for each angle are combined in Figs. 30-35 for the purpose of giving a quick idea about the evolution of the jet from the nozzle downstream.

Figures 30-41 are plotted using the parameters \bar{U}/\bar{U}_c vs. x/d . The purpose of these plots was to explore the similarity in the velocity profiles in the initial region of jet development. Previous studies [6] on the evaluation of single two-dimensional and axi-symmetric jets have shown that plots prepared in the manner cited above resulted in a single normalized curve. This was, to be sure, no mixing occurs with the exception of that with the surroundings. The plots presented herein show that such a similarity exists only for distance of $d/a > 2.4$. This is evidenced by the fact that the two velocity profiles at distances of $d/a = 1.2$ and $d/a = 2.4$ do not fall on the rest of the velocity profiles exhibiting similarity. This may be interpreted as a consequence of the mixing of two jets of unequal velocity.

The turbulence intensities were plotted as a function of x/a for various angles of deflection and for various stations along the jet and are shown in Figs. 42-59. The main characteristic of all the turbulence distributions is that there are two high regions of turbulence and a region of relatively low turbulence in the central core of the jet. The result is not unexpected in view of the fact that each jet has the

highest shear and mixing with the surrounding ambient flow at its two sides. It is also apparent from these figures that the intensity of turbulence increases with increasing distances along the jet. This is not so much because of the absolute increase of the RMS value of the local values of velocity fluctuations, but rather because of the relative decrease of the magnitude of velocity along the jet. The turbulence intensity profiles for each angle are combined in Figs. 60-65.

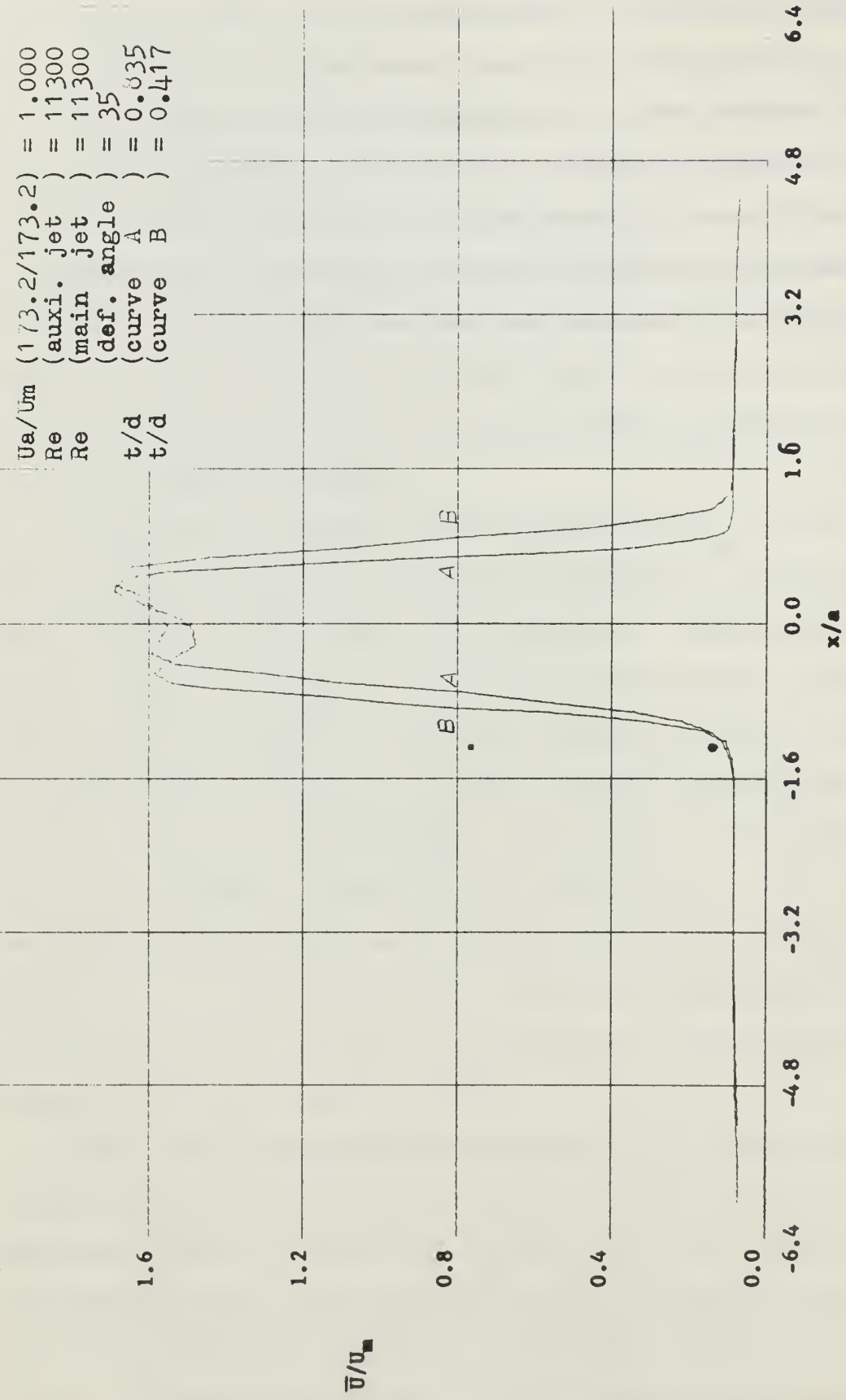


FIGURE 12 NORMALIZED VELOCITY PROFILES

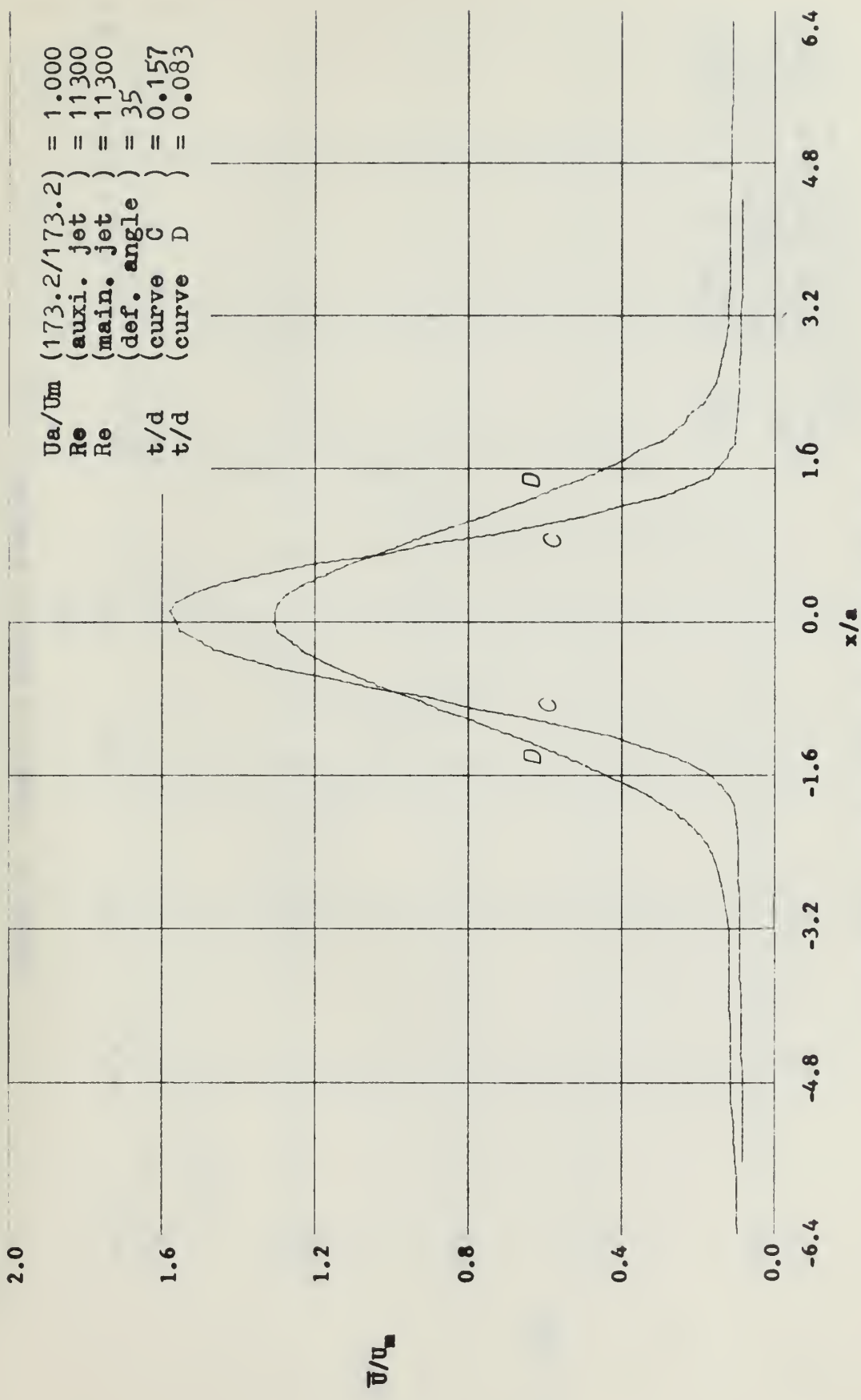


FIGURE 13 NORMALIZED VELOCITY PROFILES

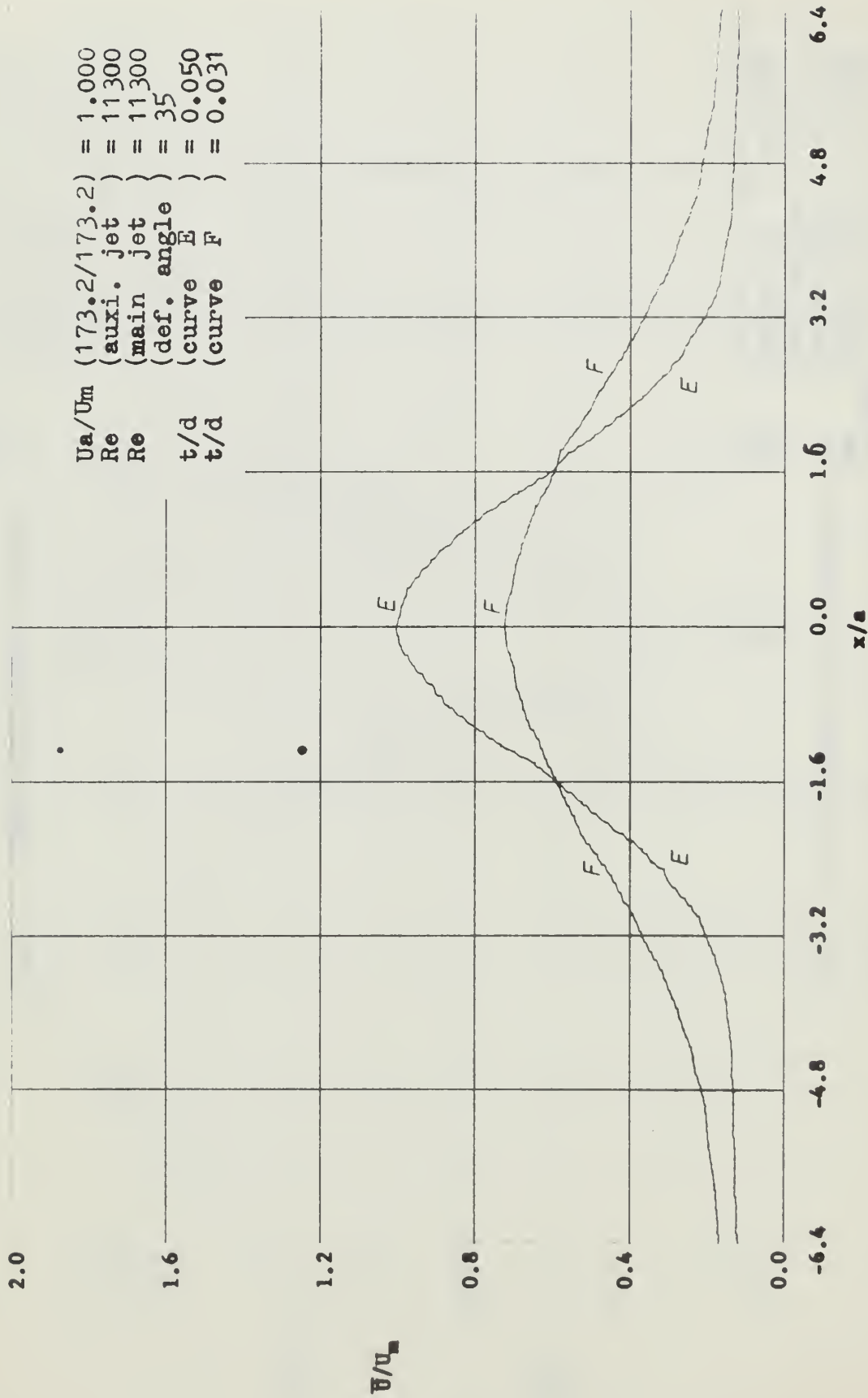


FIGURE 14. NORMALIZED VELOCITY PROFILES

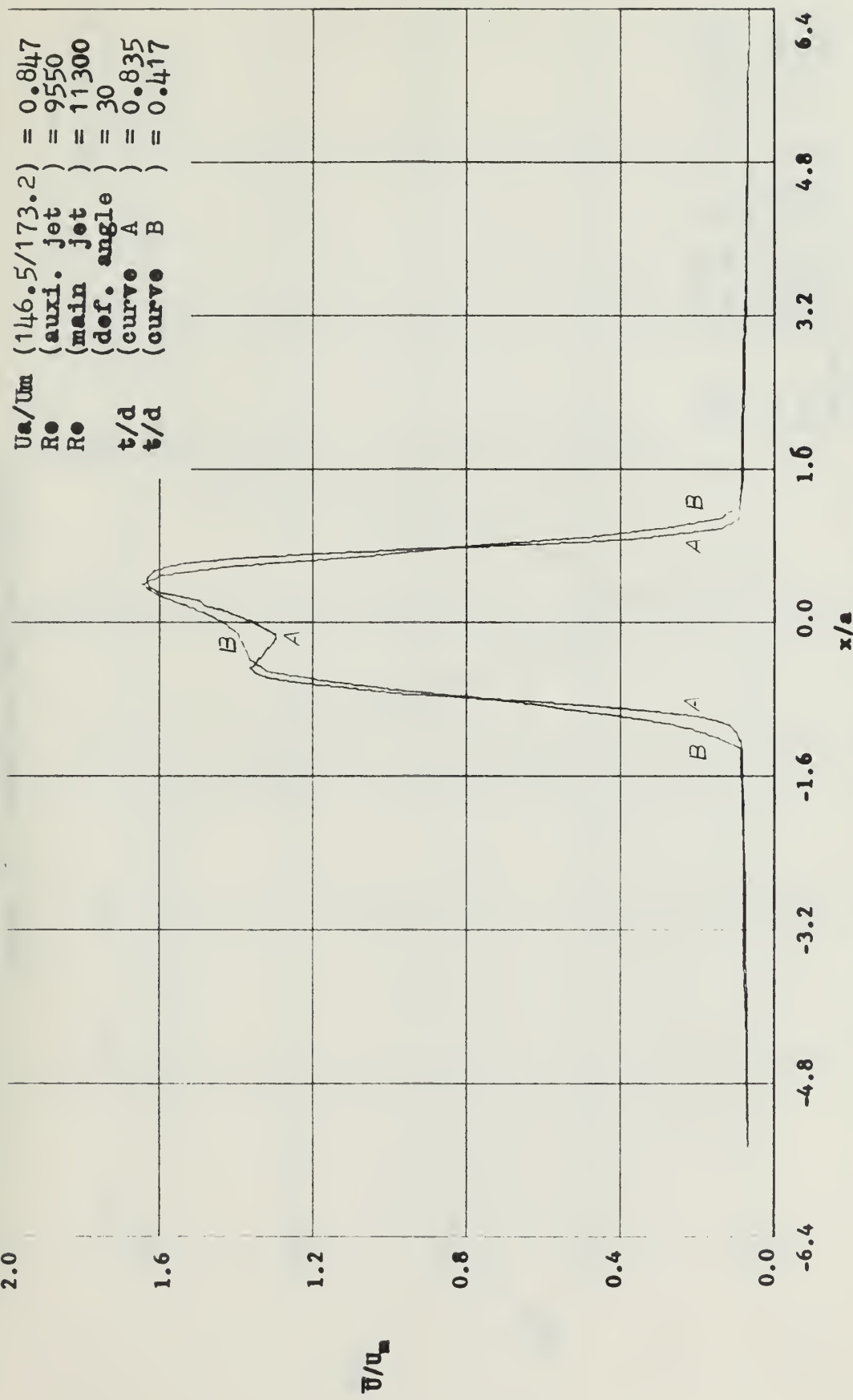


FIGURE 15 NORMALIZED VELOCITY PROFILES

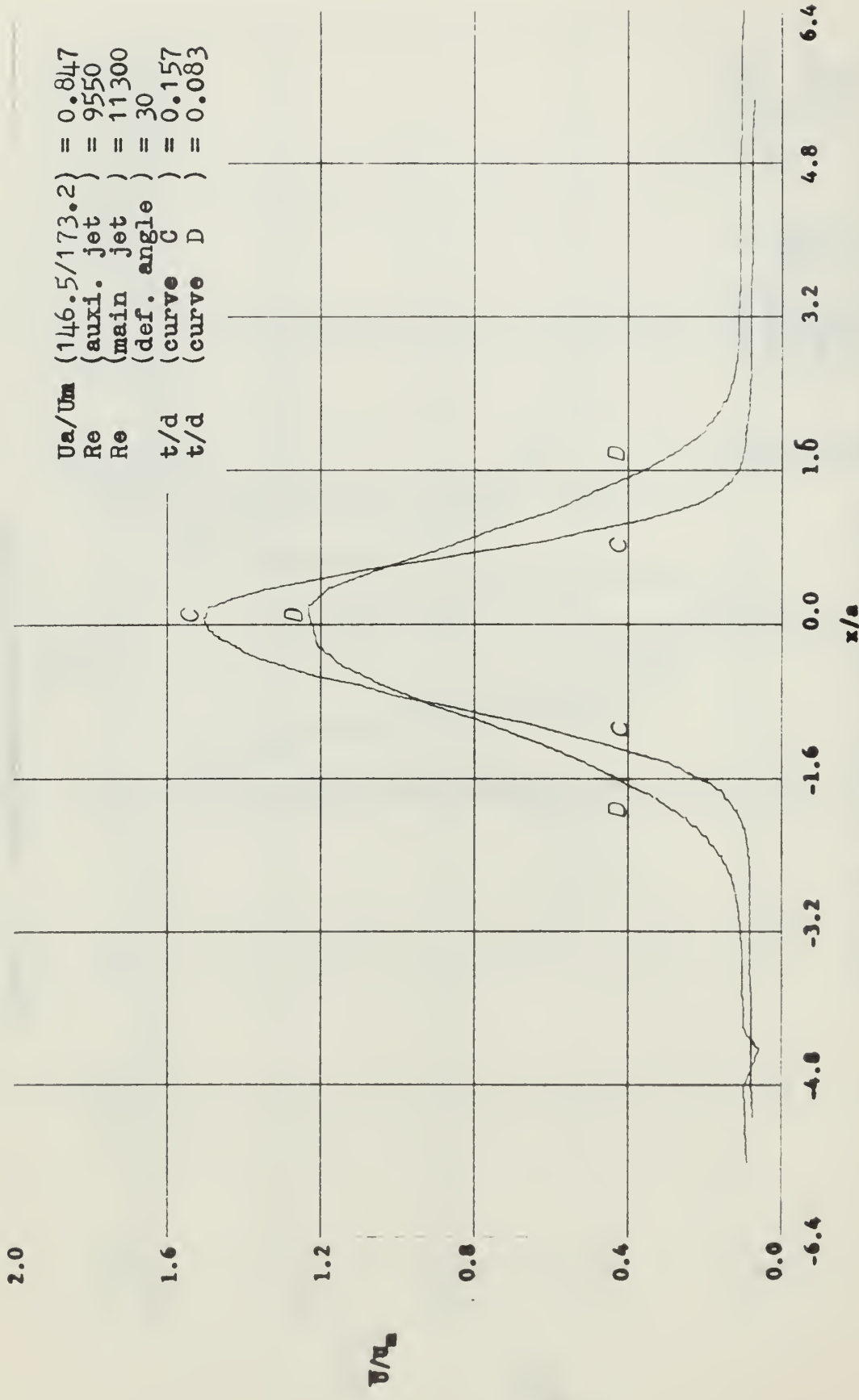


FIGURE 16 NORMALIZED VELOCITY PROFILES

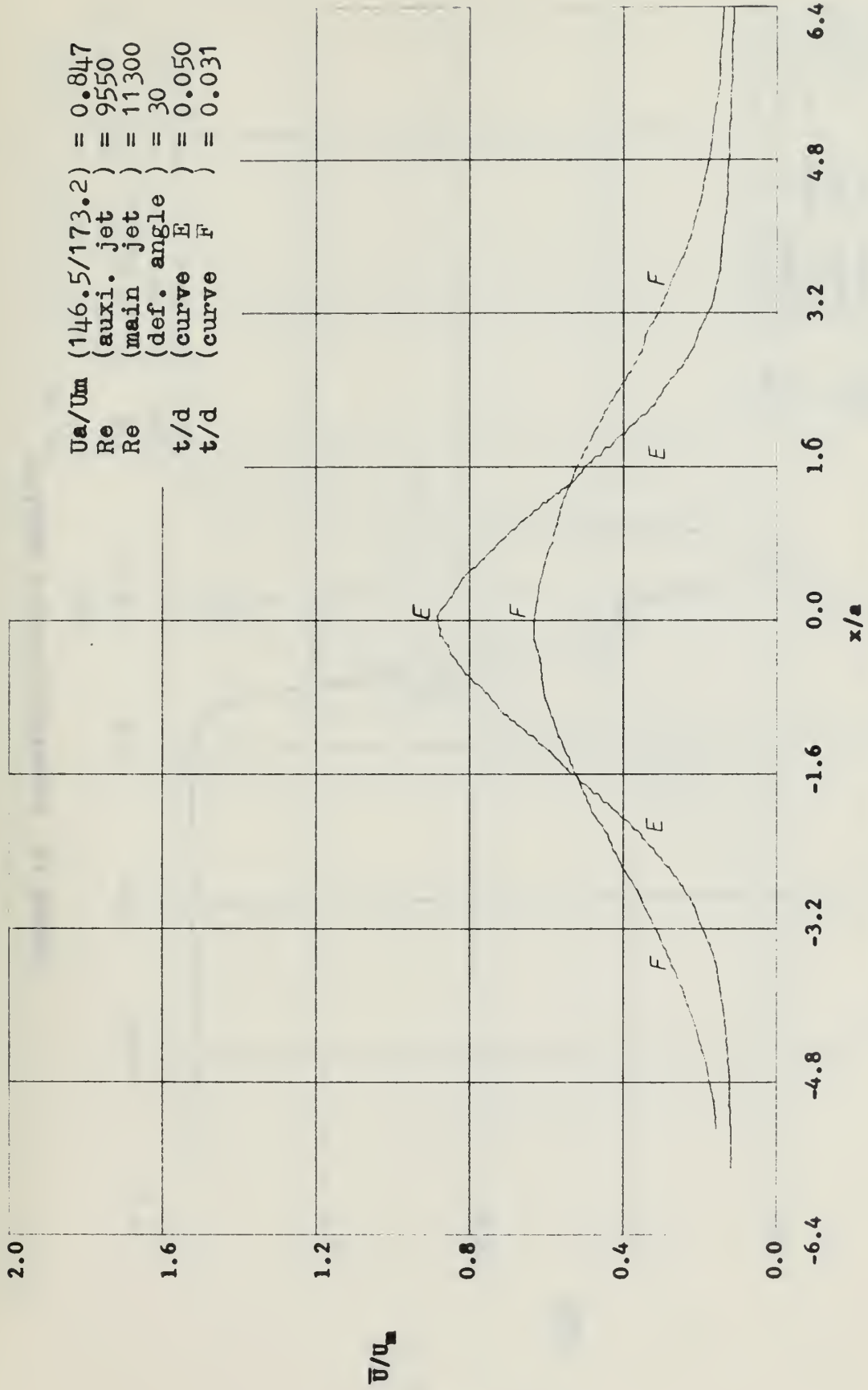


FIGURE 17 NORMALIZED VELOCITY PROFILES

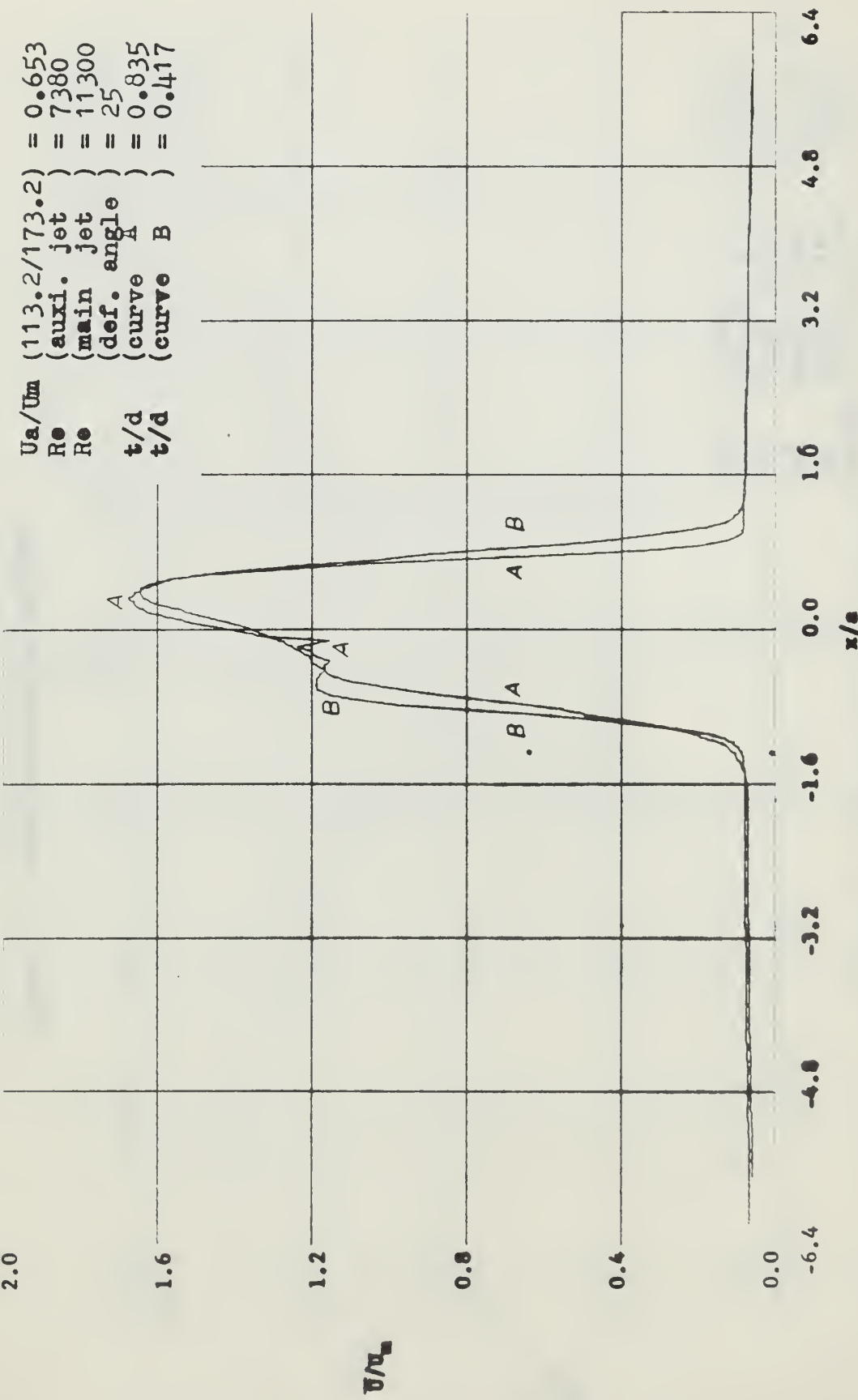


Figure 18 Normalized velocity profiles

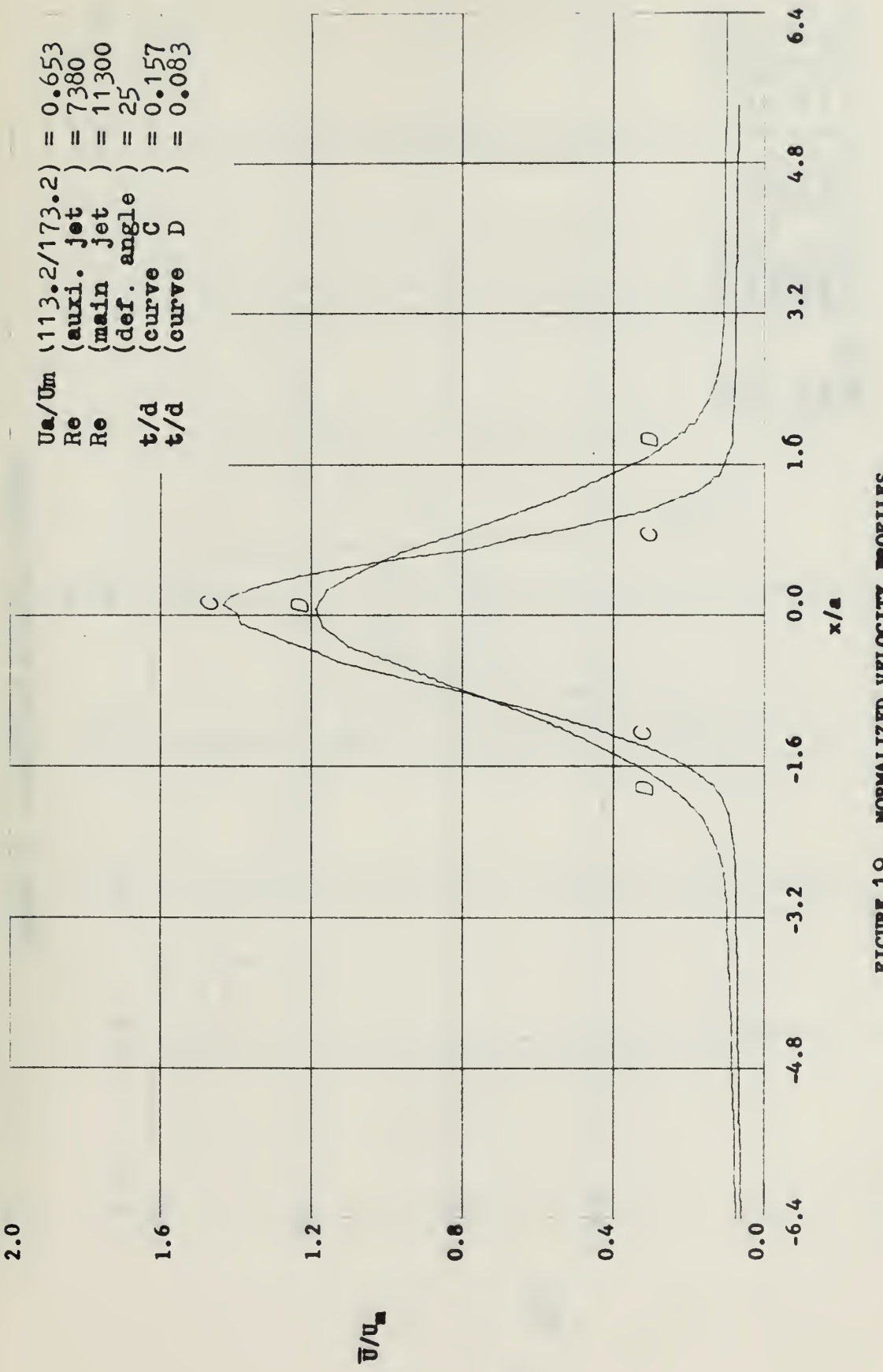


FIGURE 19 NORMALIZED VELOCITY PROFILES

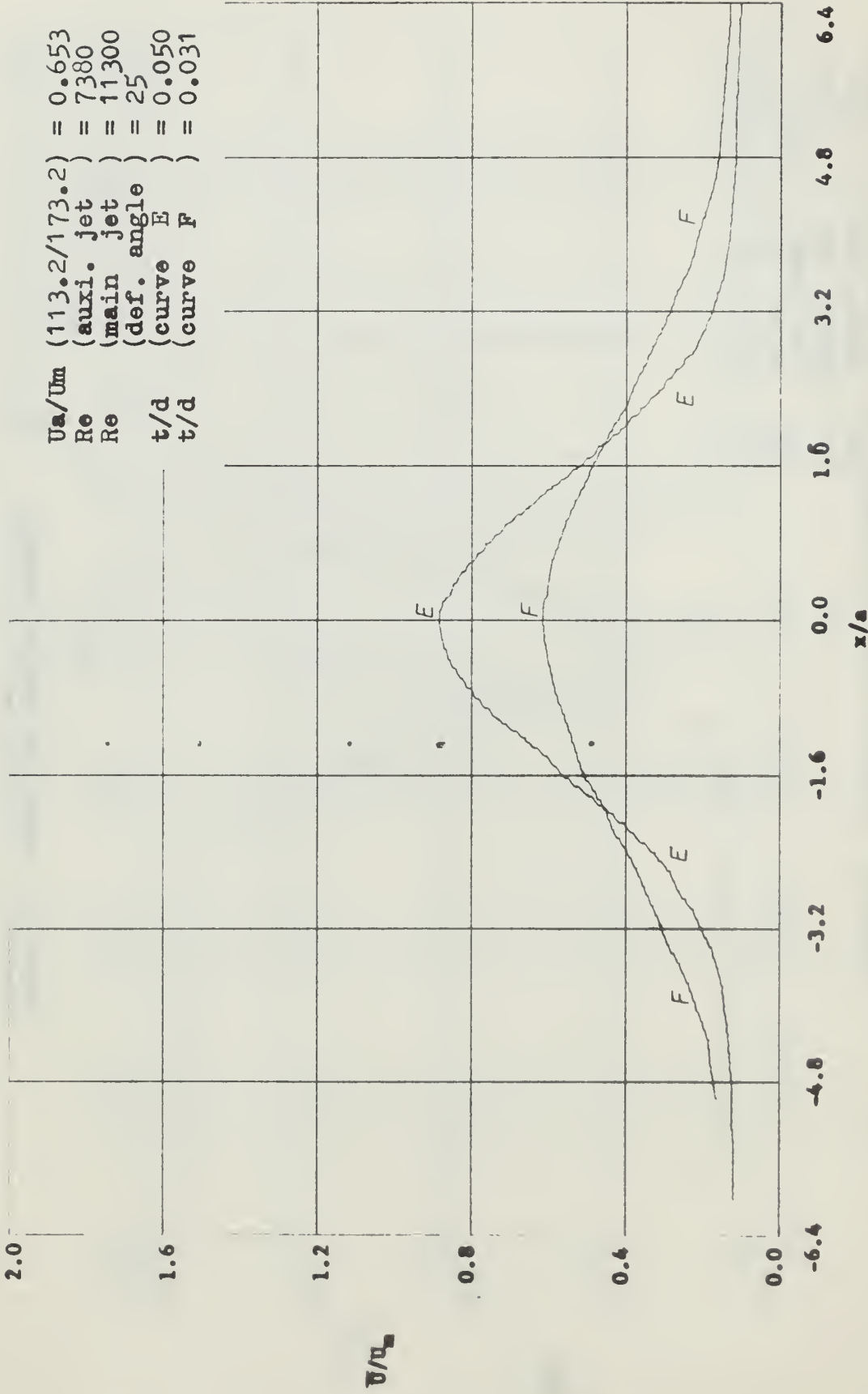


FIGURE 20 NORMALIZED VELOCITY PROFILES

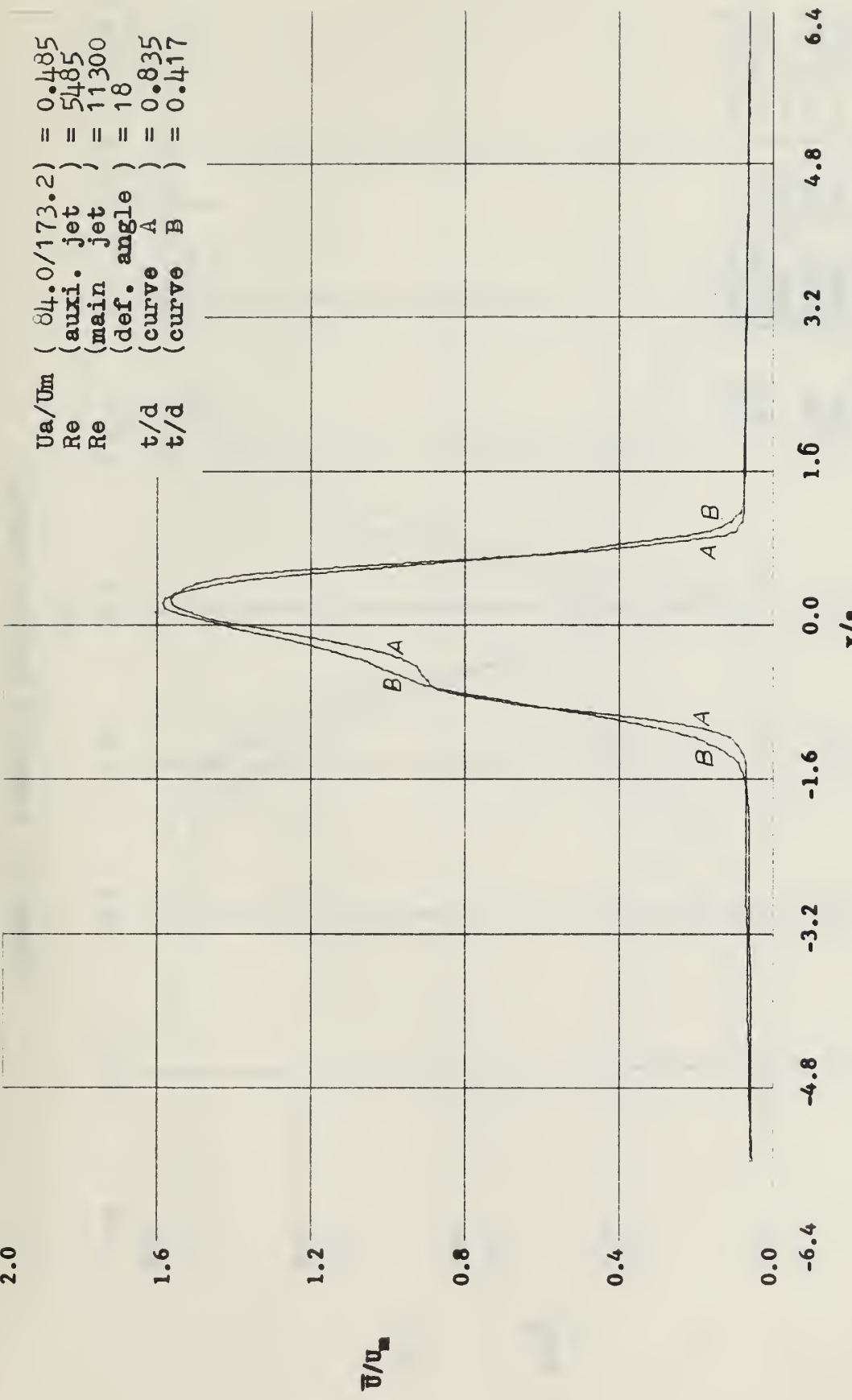


FIGURE 21 NORMALIZED VELOCITY PROFILES

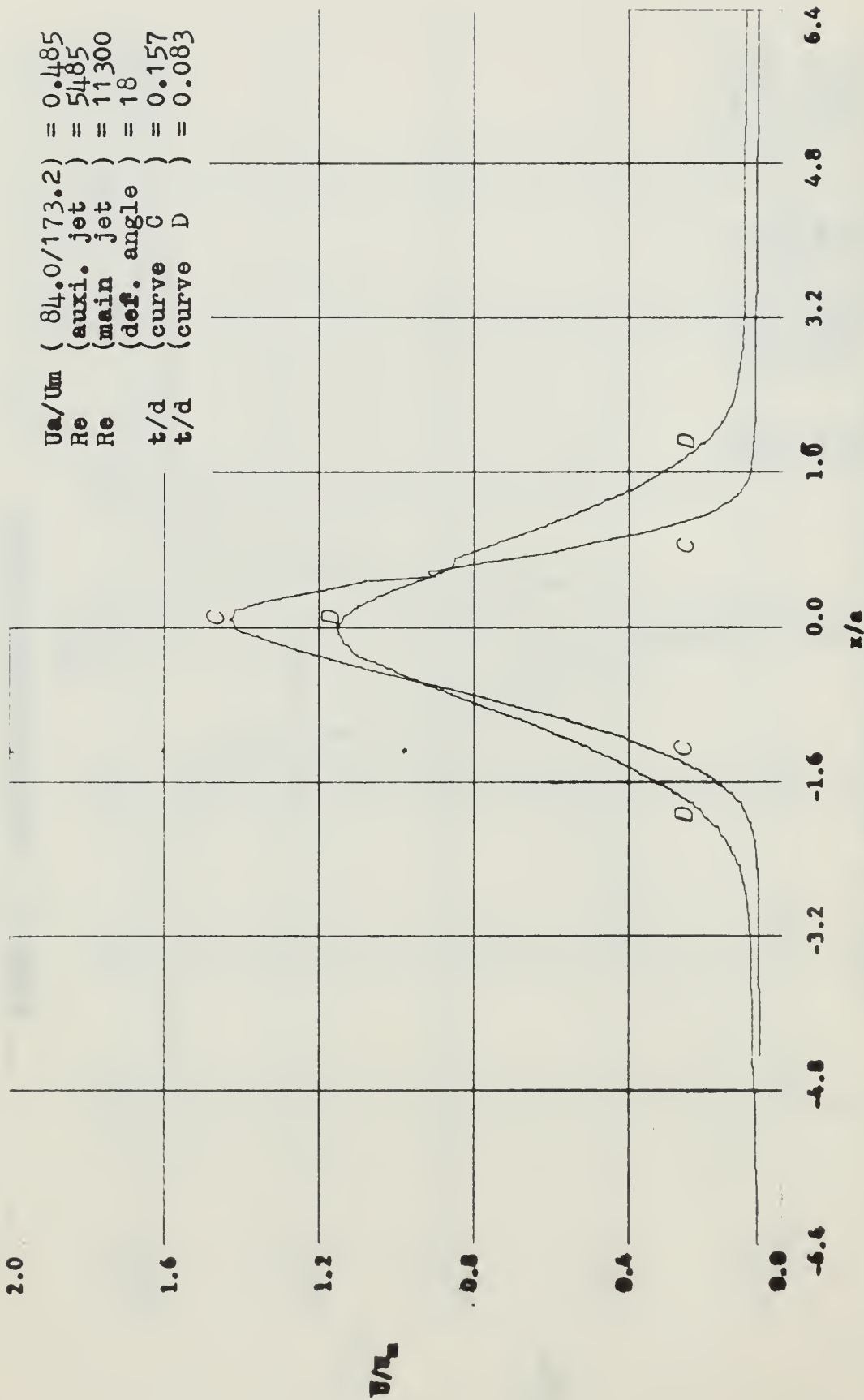


FIGURE 22 NORMALIZED VELOCITY PROFILES

2.0

$$\begin{aligned}
 \frac{U_a}{U_m} &= 0.485 \\
 Re_{aux. jet} &= 5485 \\
 Re_{main jet} &= 11300 \\
 (\text{def. angle}) &= 18^\circ \\
 (\text{curve } E) &= 0.050 \\
 (\text{curve } F) &= 0.031
 \end{aligned}$$

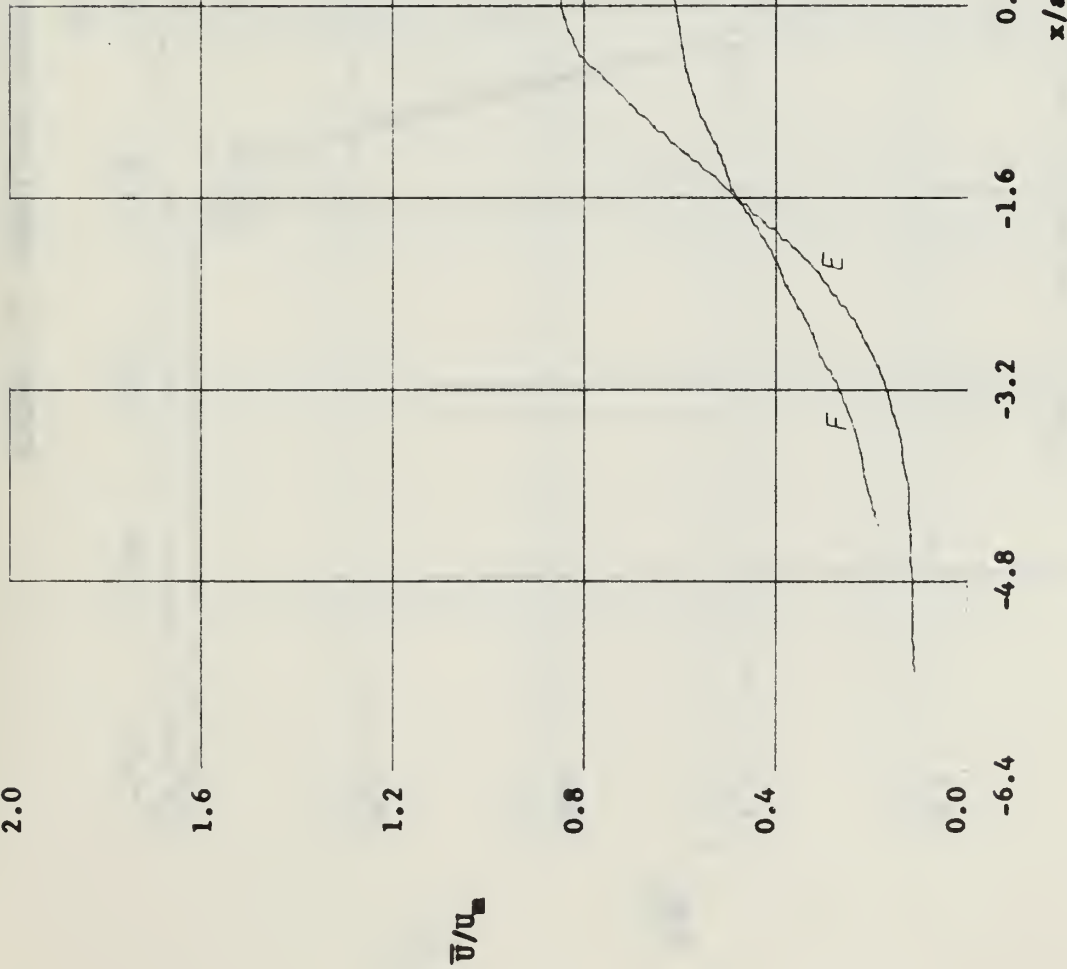


FIGURE 23 NORMALIZED VELOCITY PROFILES

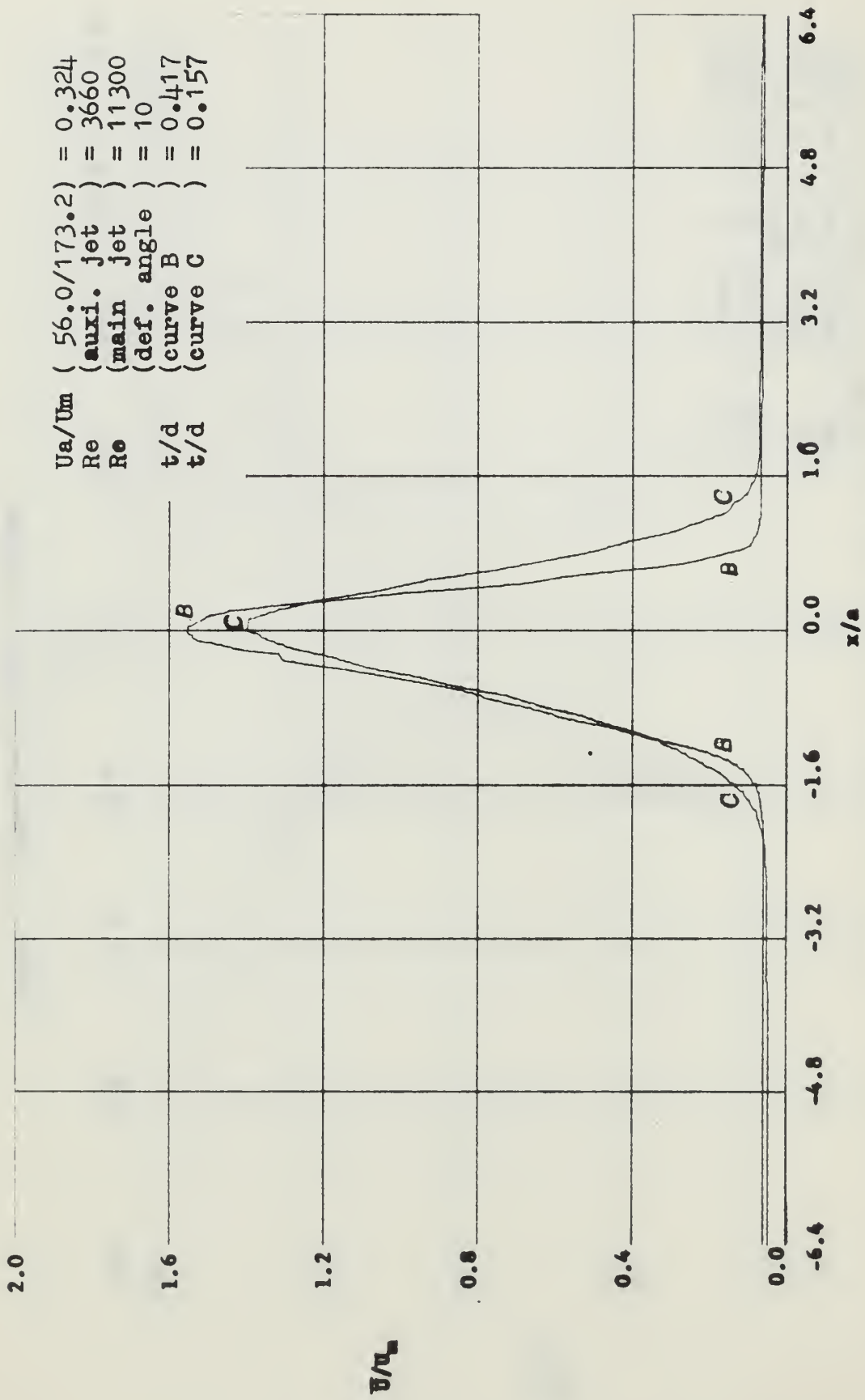


FIGURE 24 NORMALIZED VELOCITY PROFILES

U_a/U_m	($56.0/173.2$)	=	0.324
R_e	(auxi. jet)	=	3660
R_e	(main jet)	=	11300
(def. angle)	=	10	
t/d	(curve B)	=	0.083
t/d	(curve E)	=	0.050

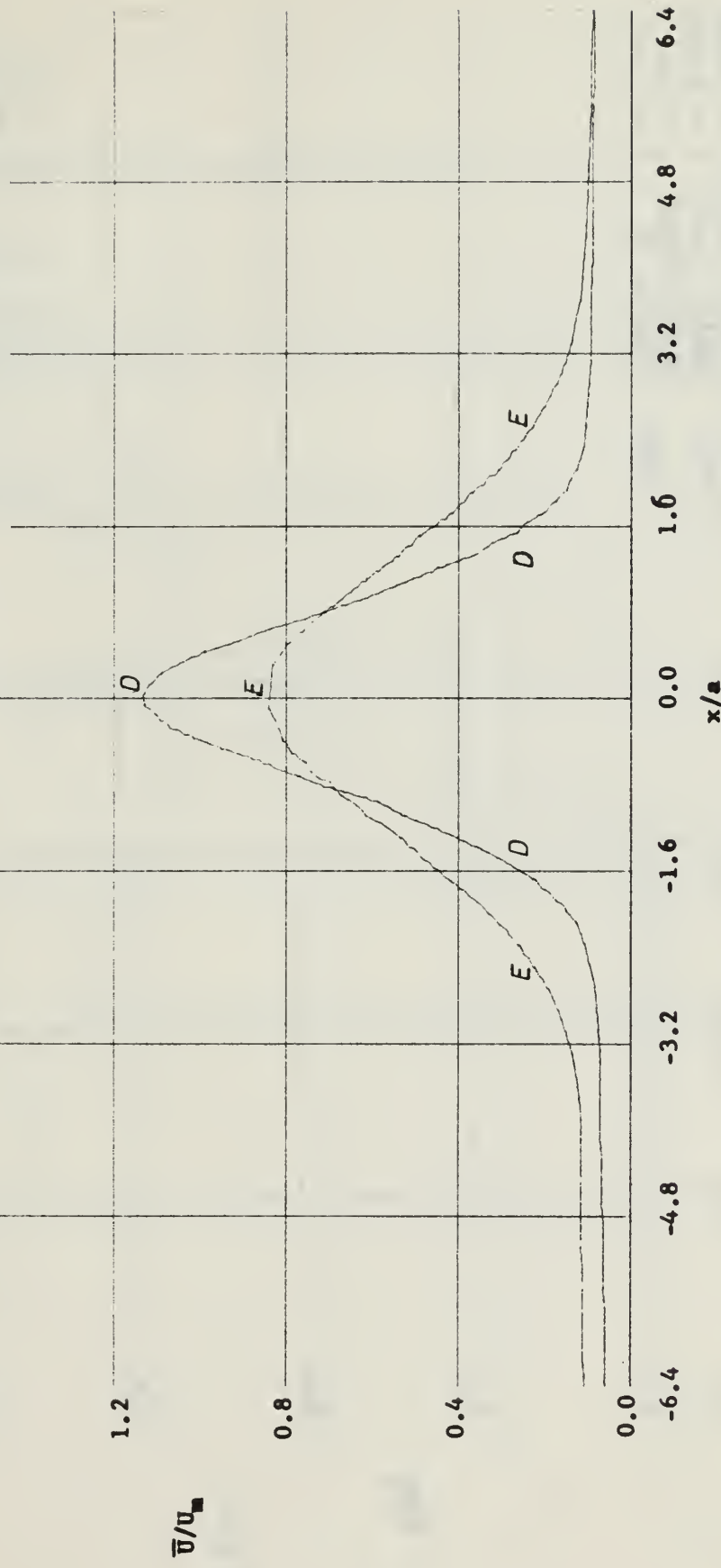
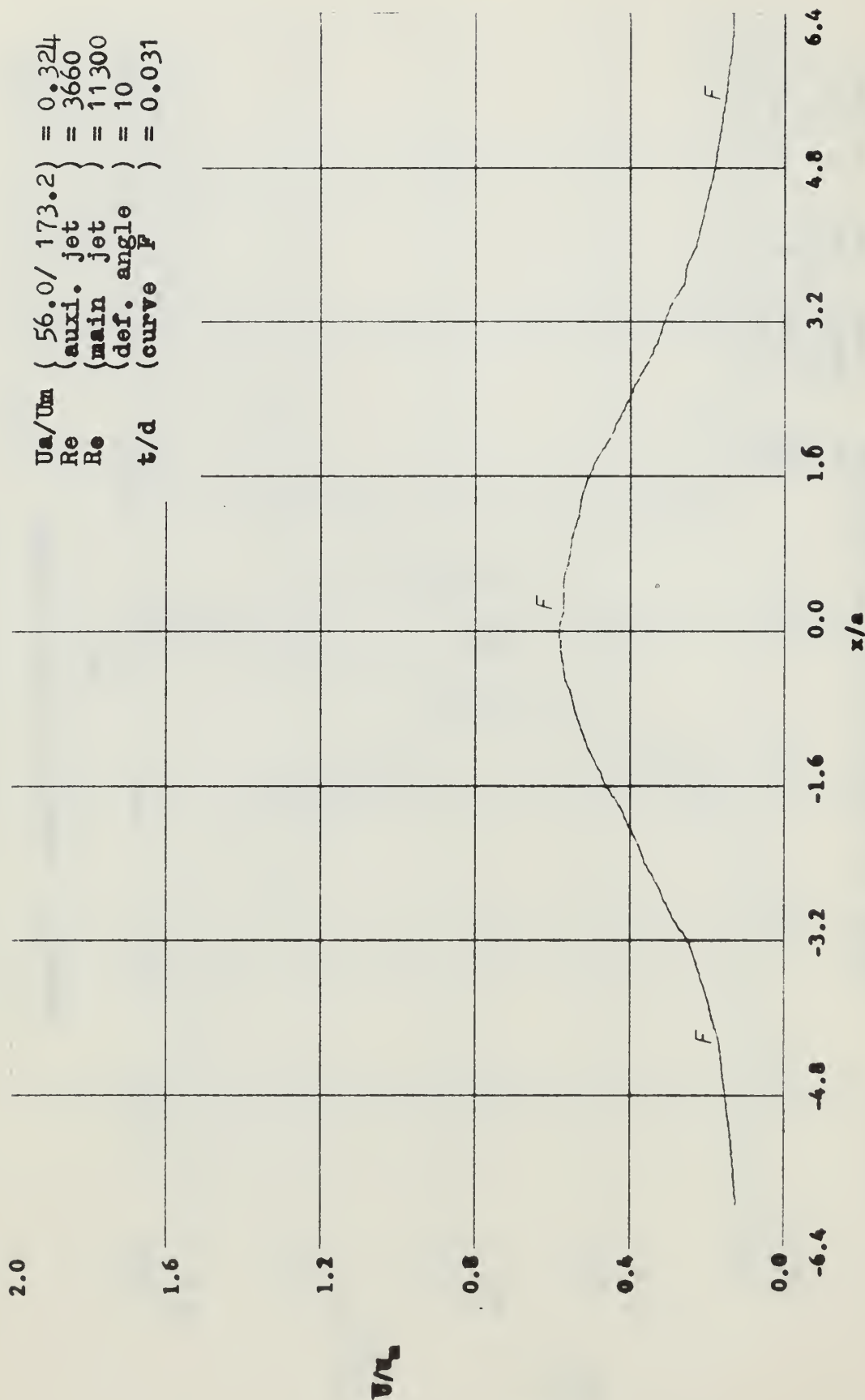


FIGURE 25 NORMALIZED VELOCITY PROFILES



PREGNANCY 26 MONILIZED VIOCETIN MOWILE

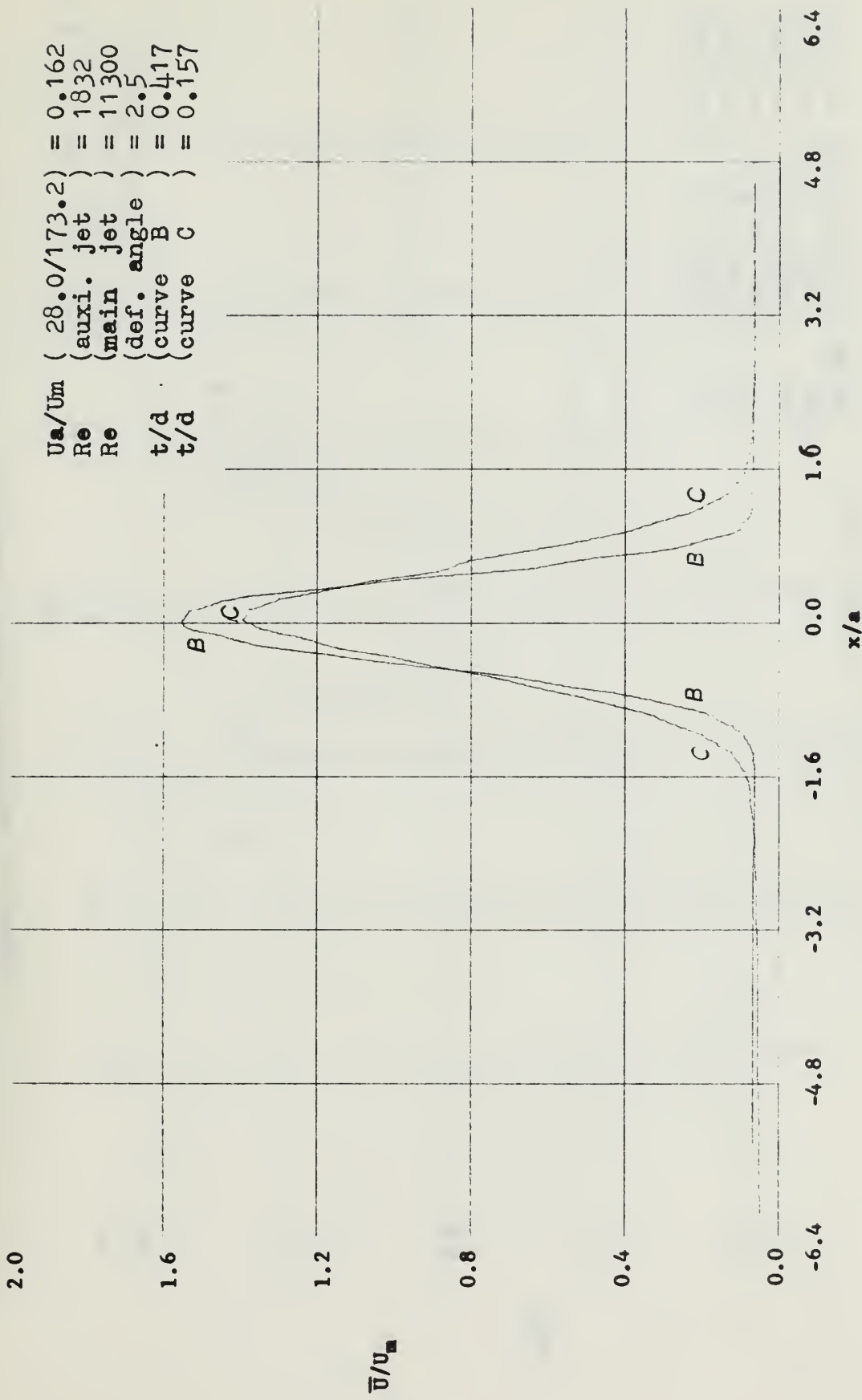


FIGURE 27 NORMALIZED VELOCITY PROFILES

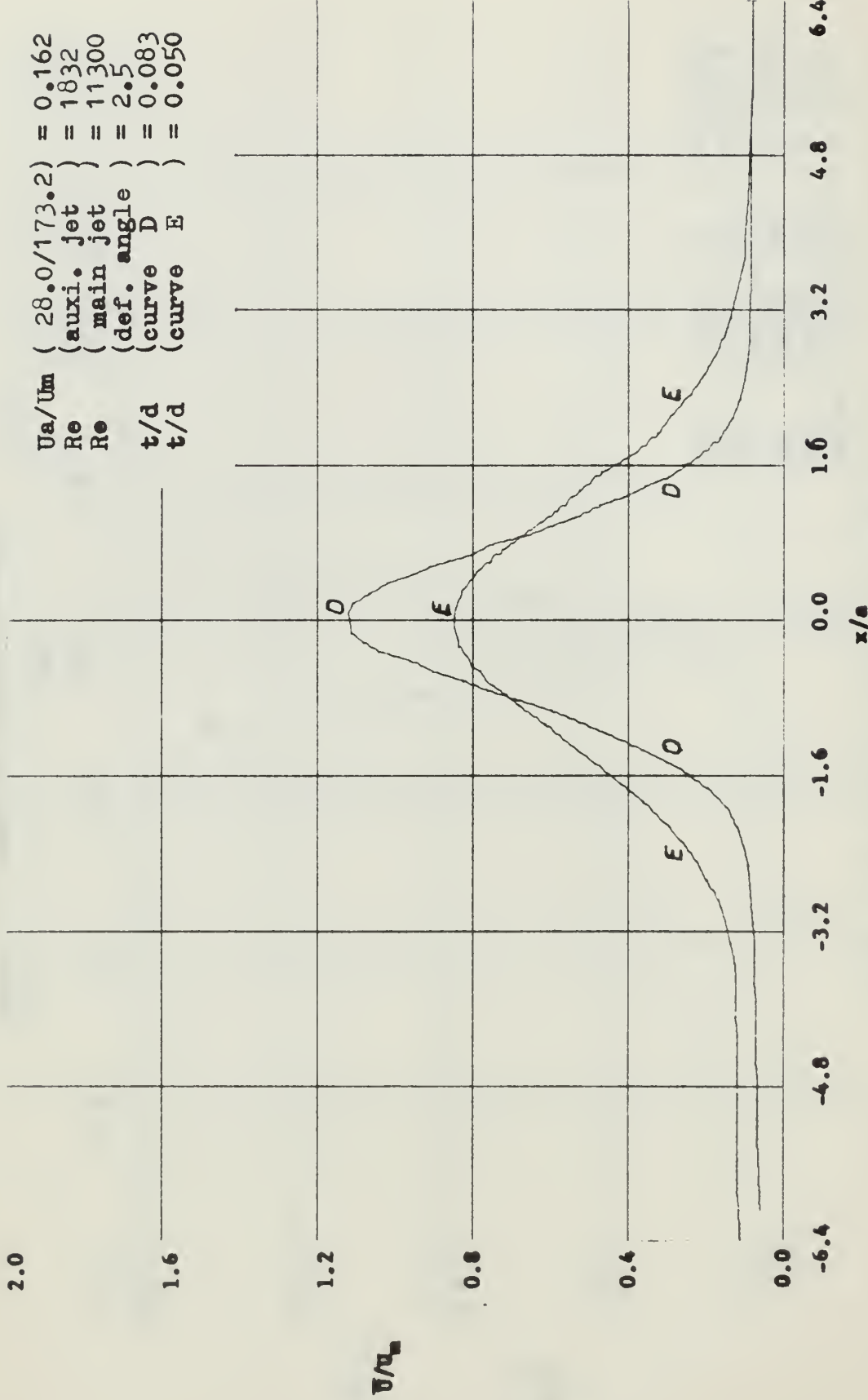


FIGURE 28 NORMALIZED VELOCITY PROFILES

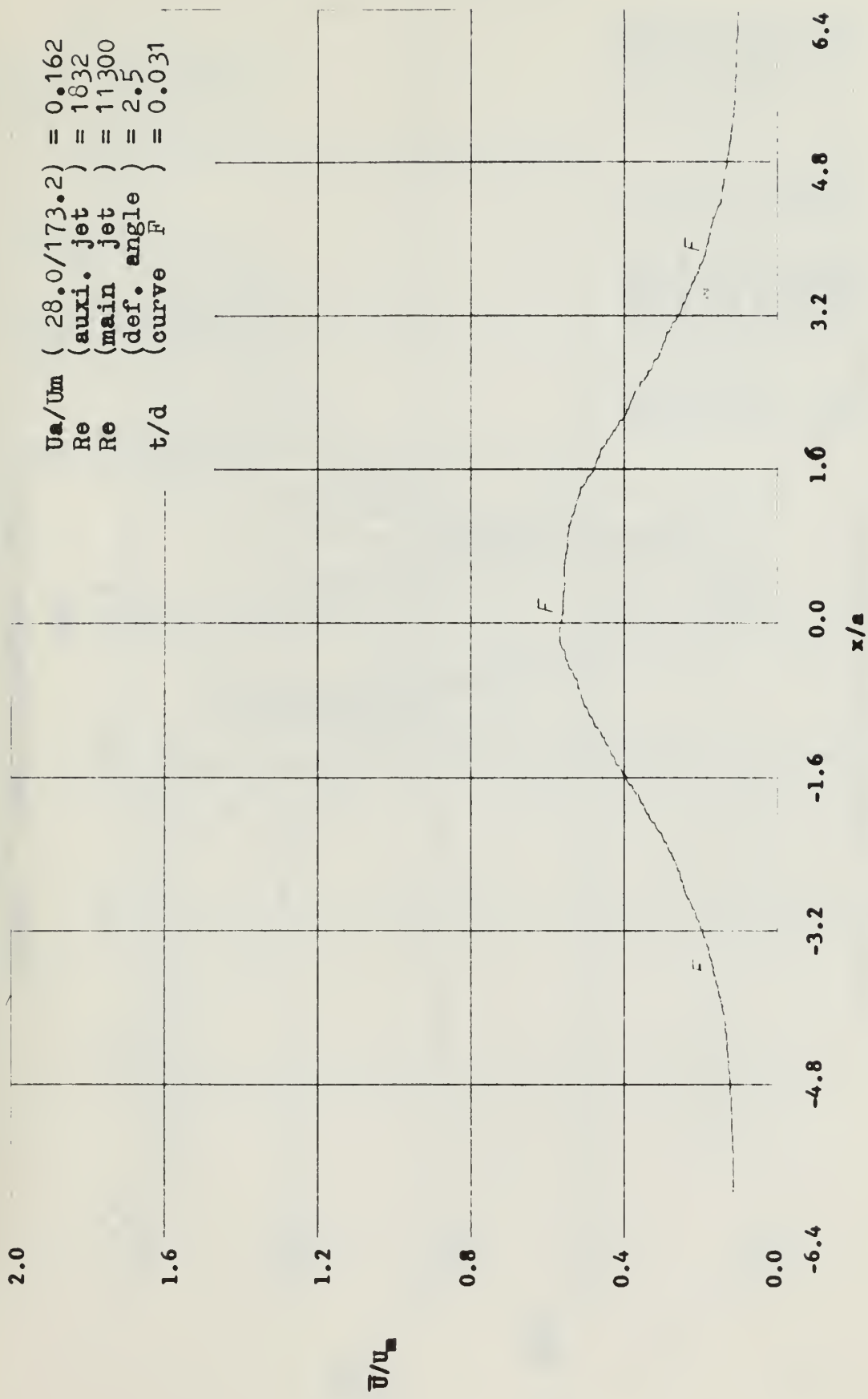


FIGURE 29 NORMALIZED VELOCITY PROFILES

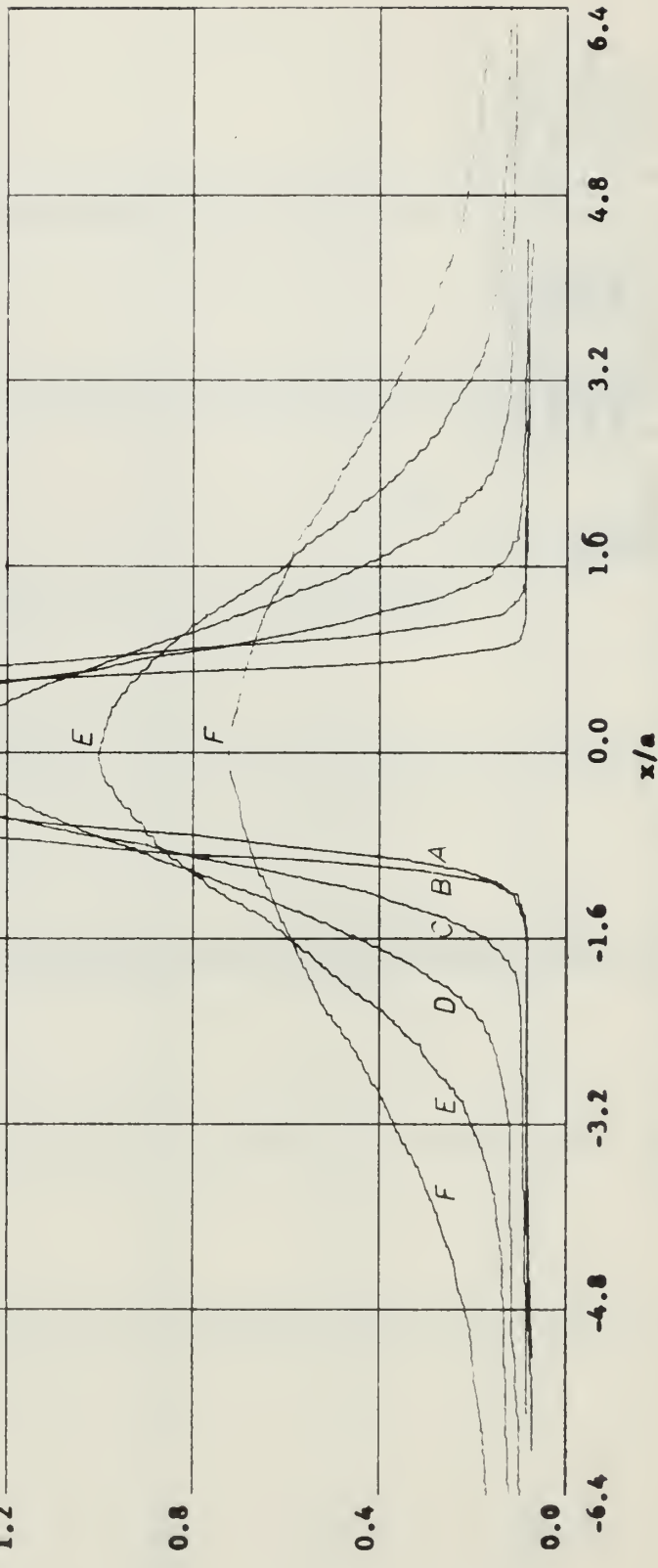
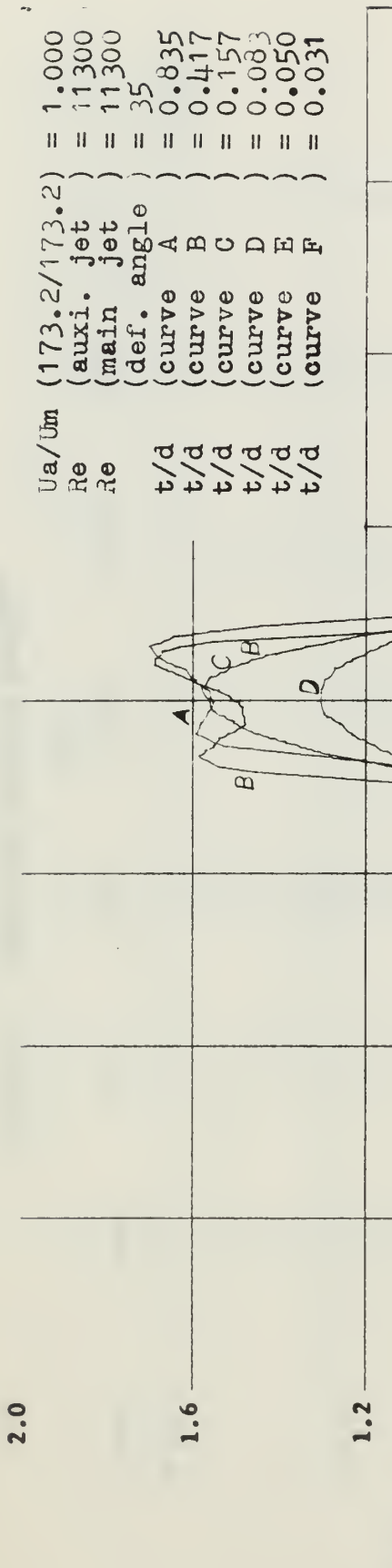


FIGURE 30 LOCALIZED VELOCITY PROFILES

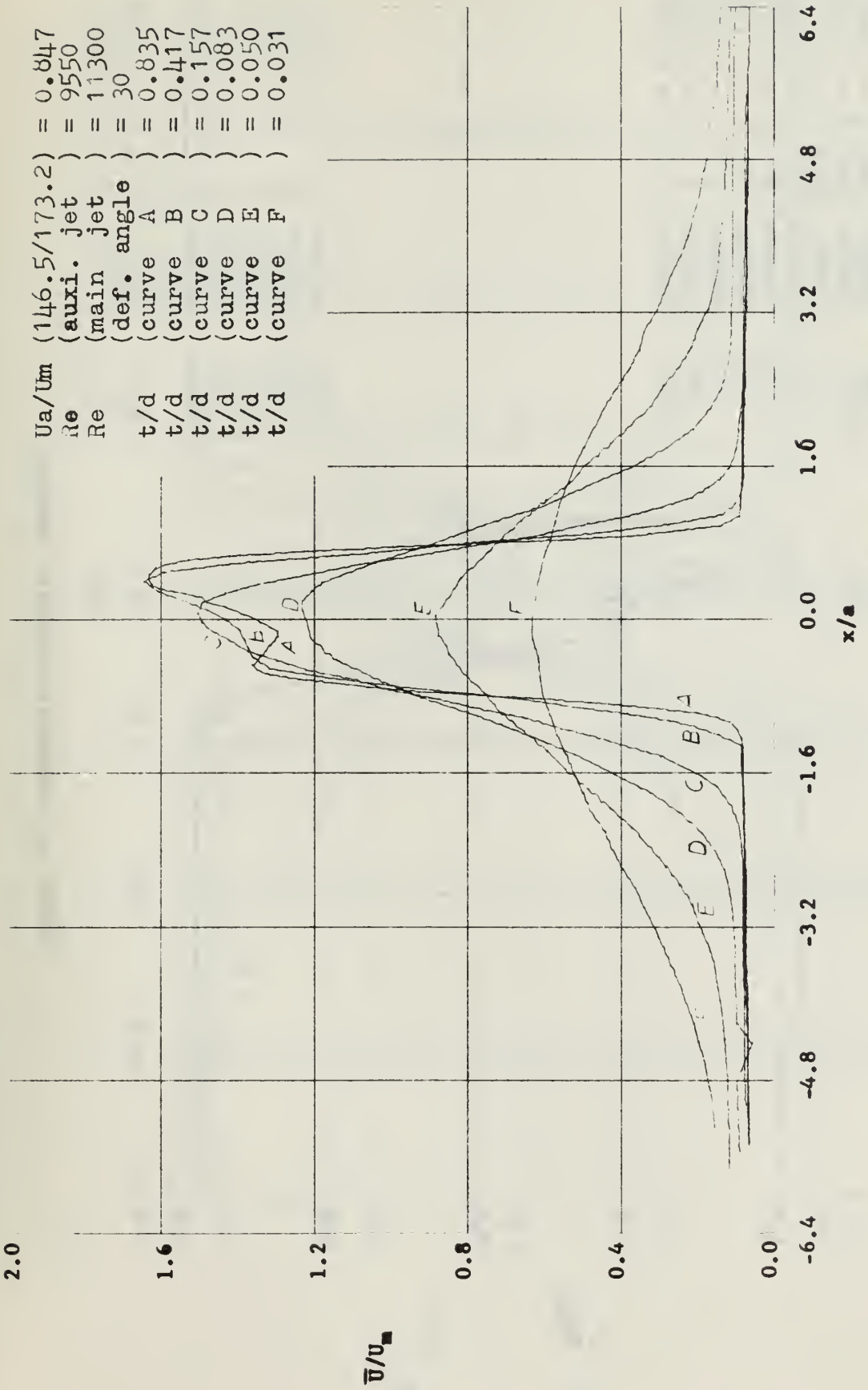


FIGURE 31 NORMALIZED VELOCITY PROFILES

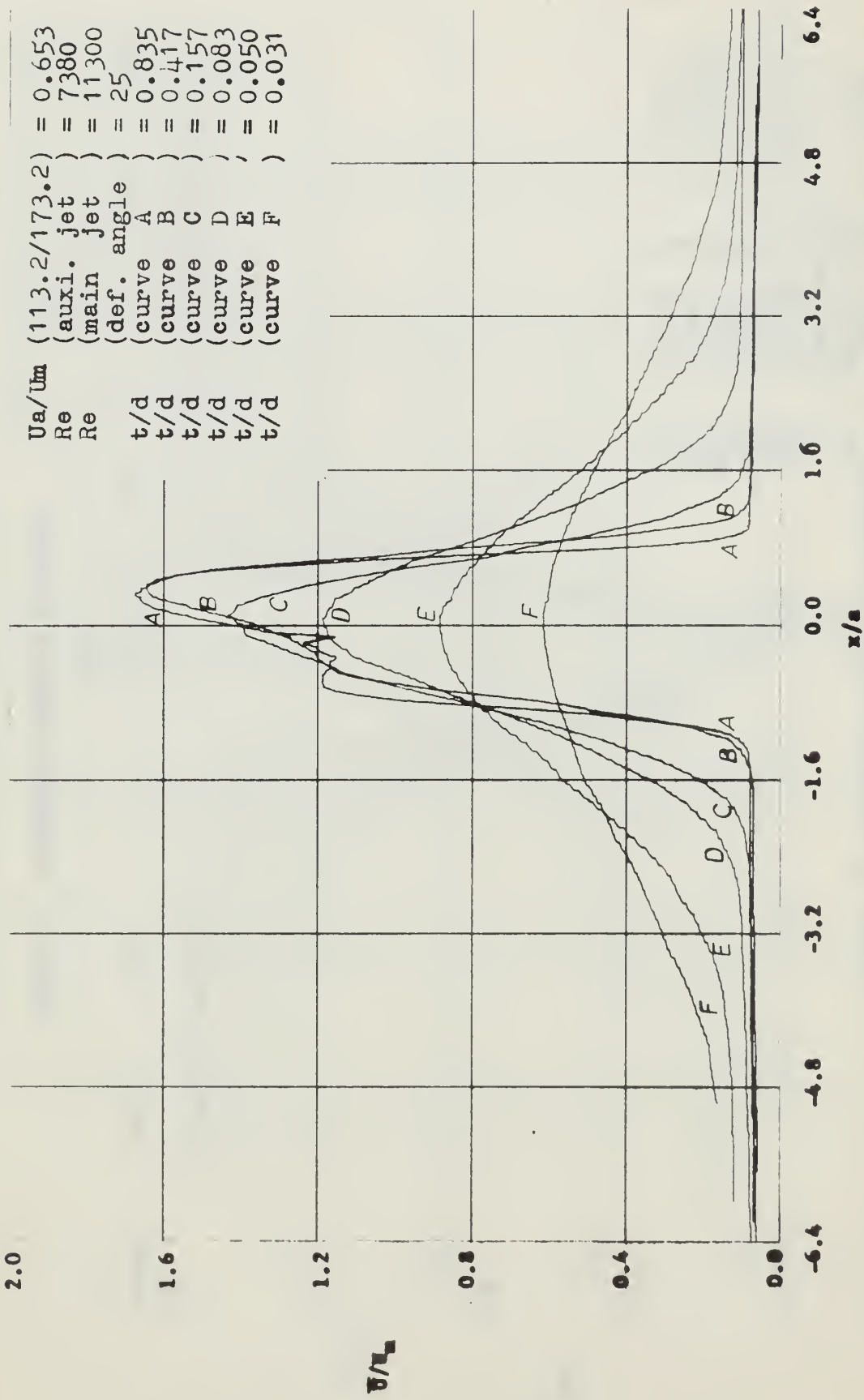


FIGURE 32 NORMALIZED VELOCITY PROFILES

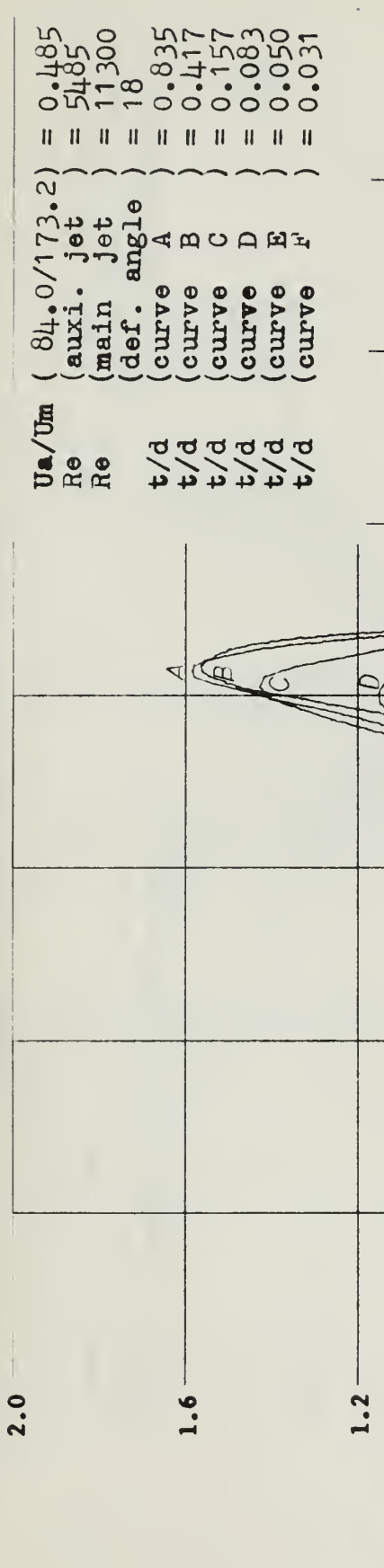


FIGURE 33 NORMALIZED VELOCITY PROFILES

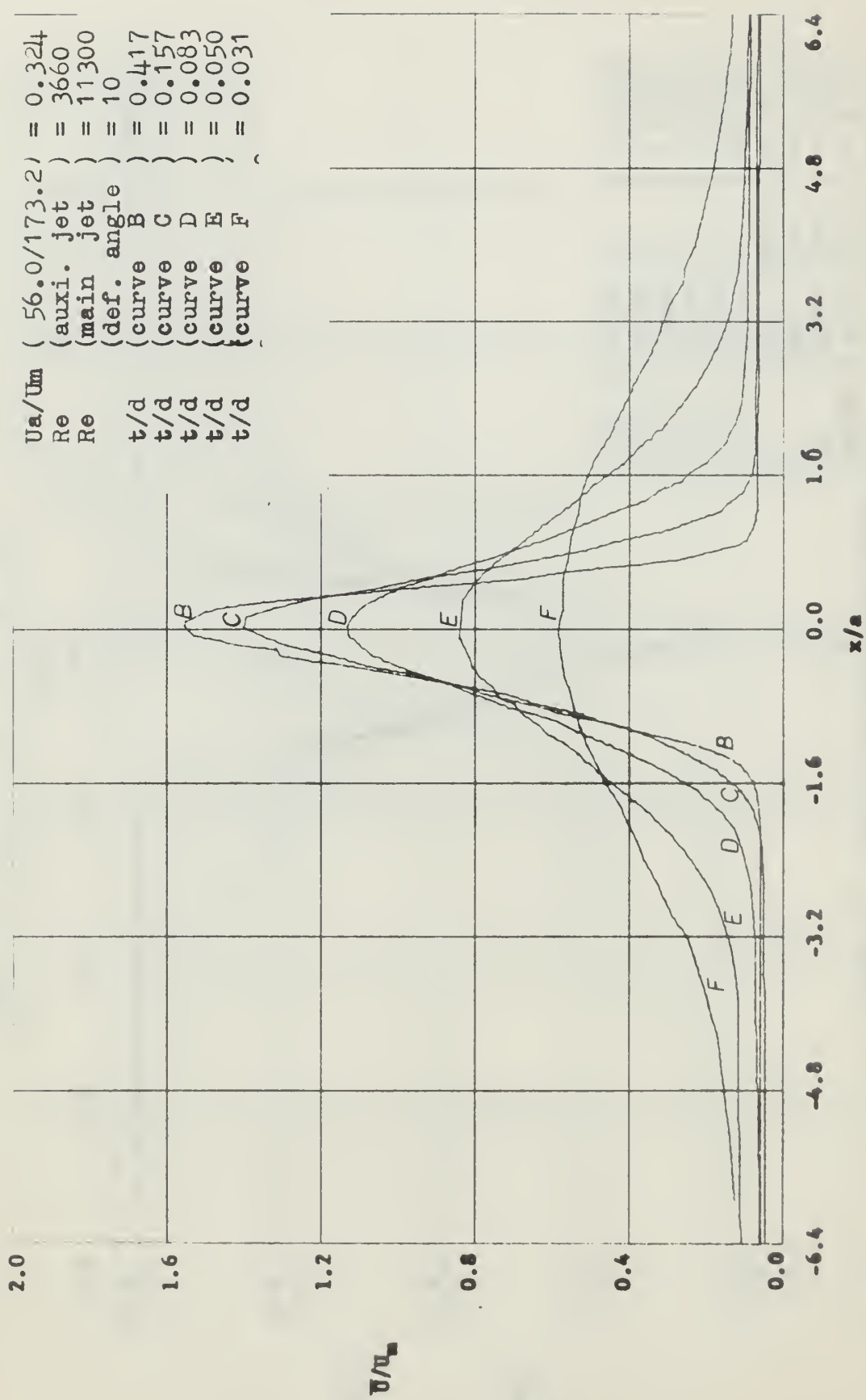


FIGURE 34 NORMALIZED VELOCITY PROFILES

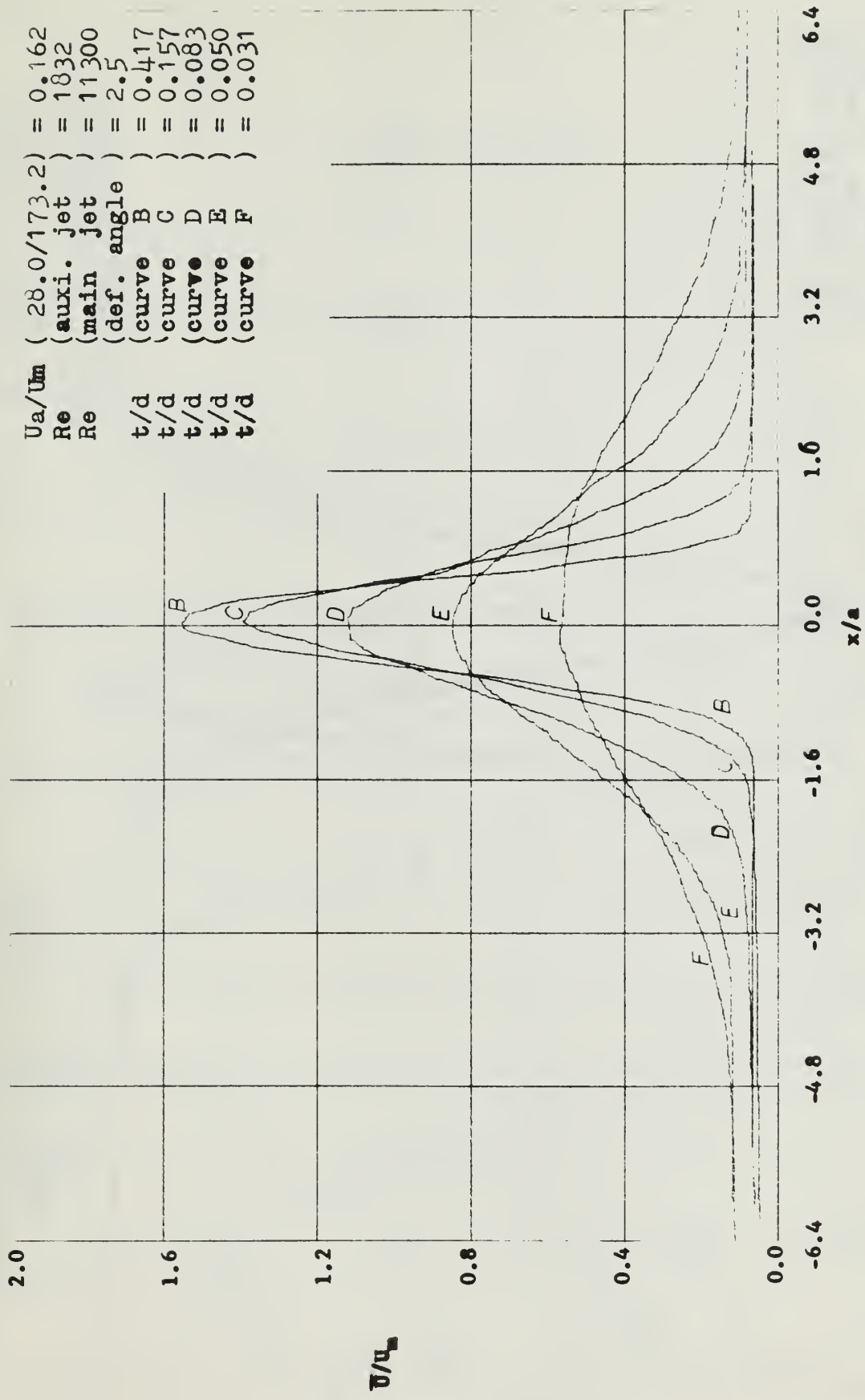


FIGURE 35 NORMALIZED VELOCITY PROFILES

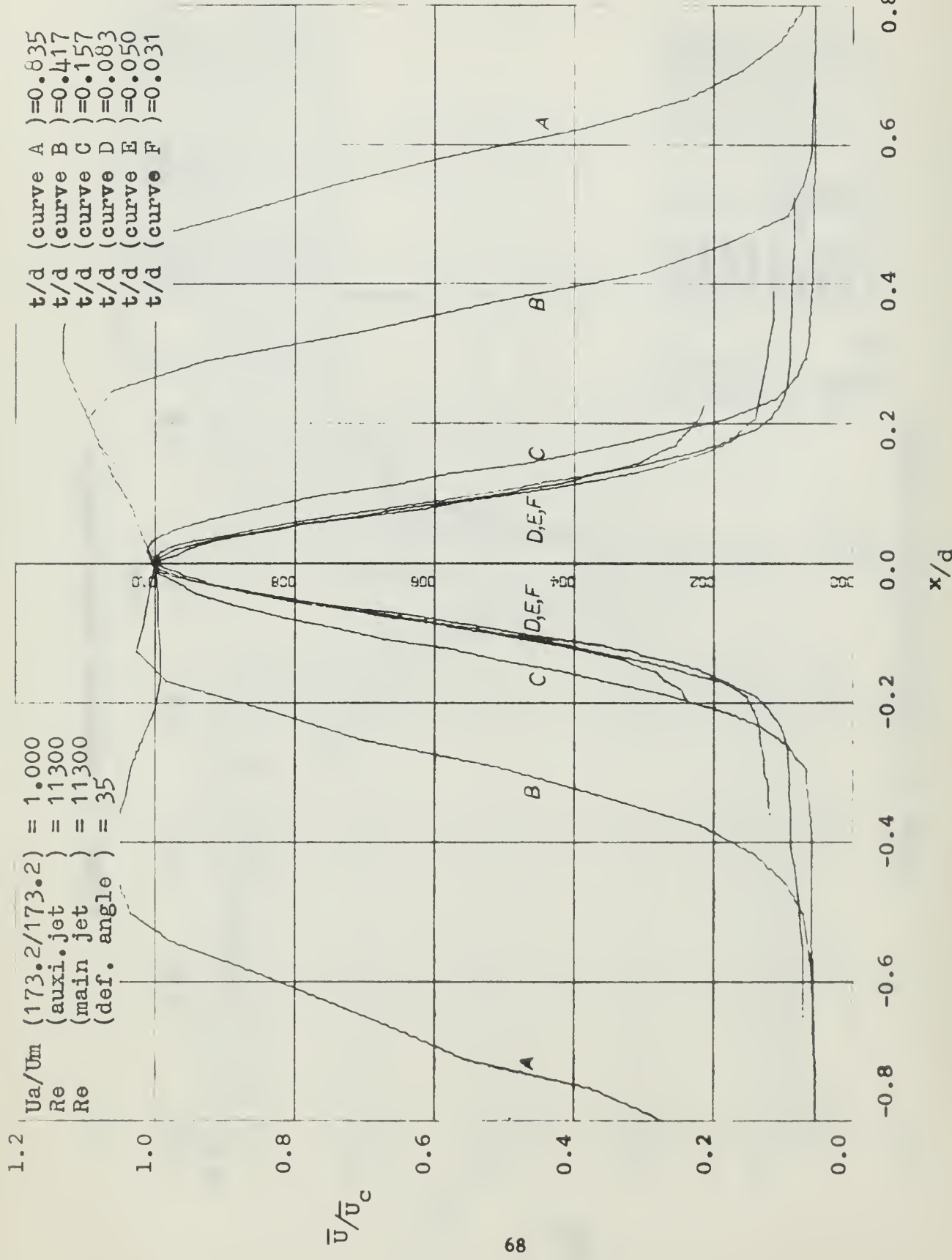


FIGURE 36 NORMALIZED VELOCITY PROFILES

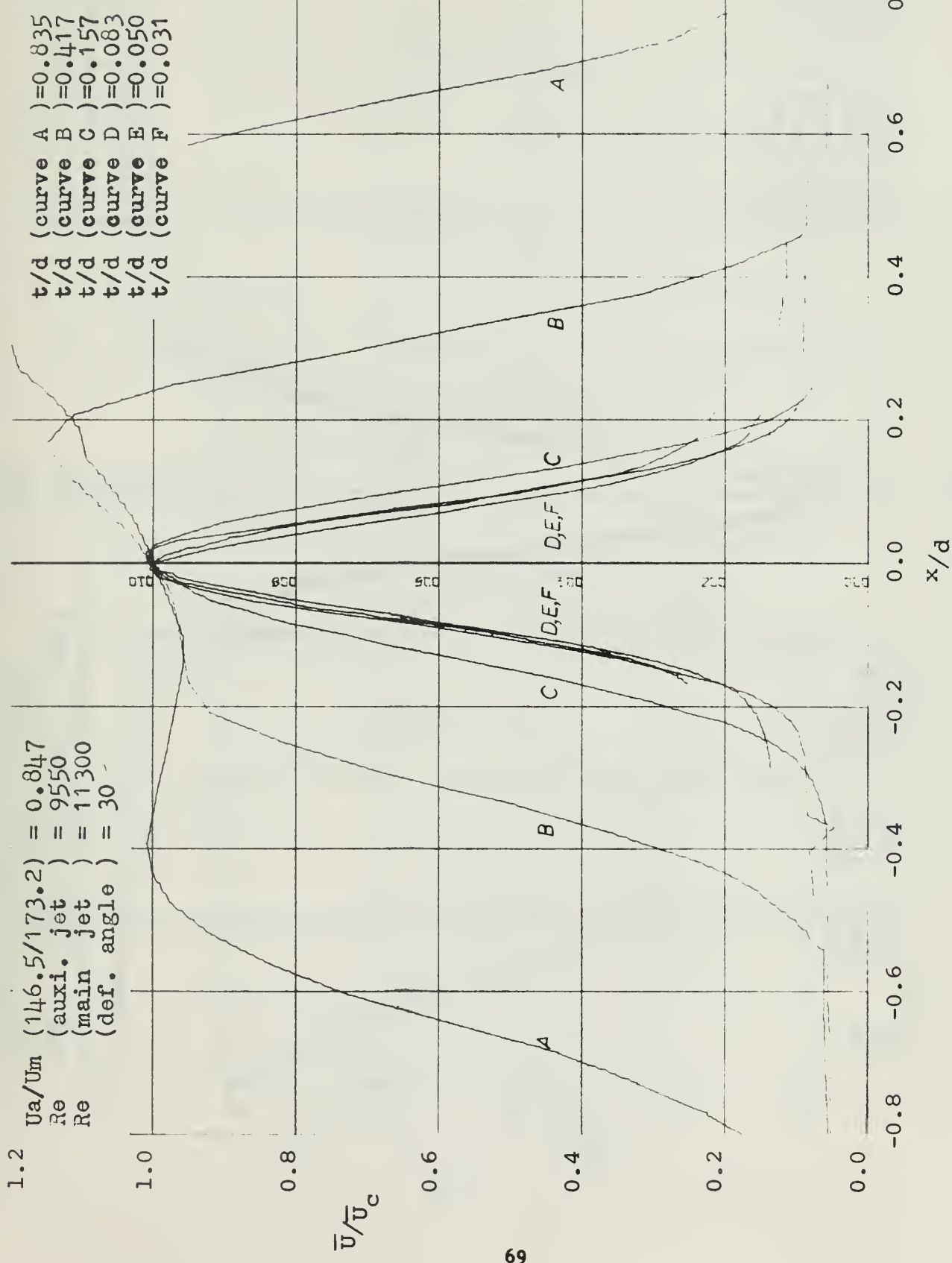


FIGURE 37 NORMALIZED VELOCITY PROFILES

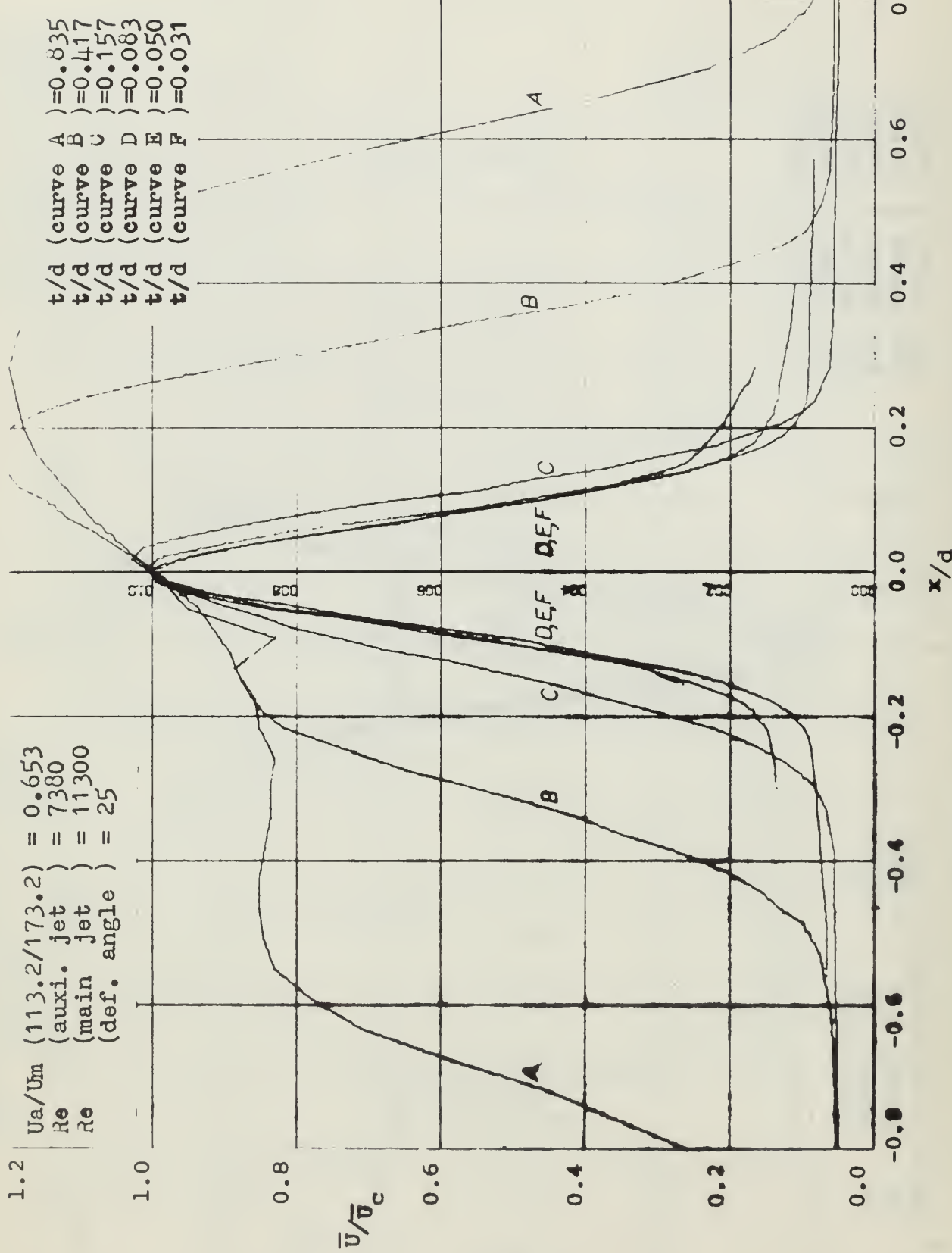


FIGURE 36 NORMALIZED VELOCITY PROFILES

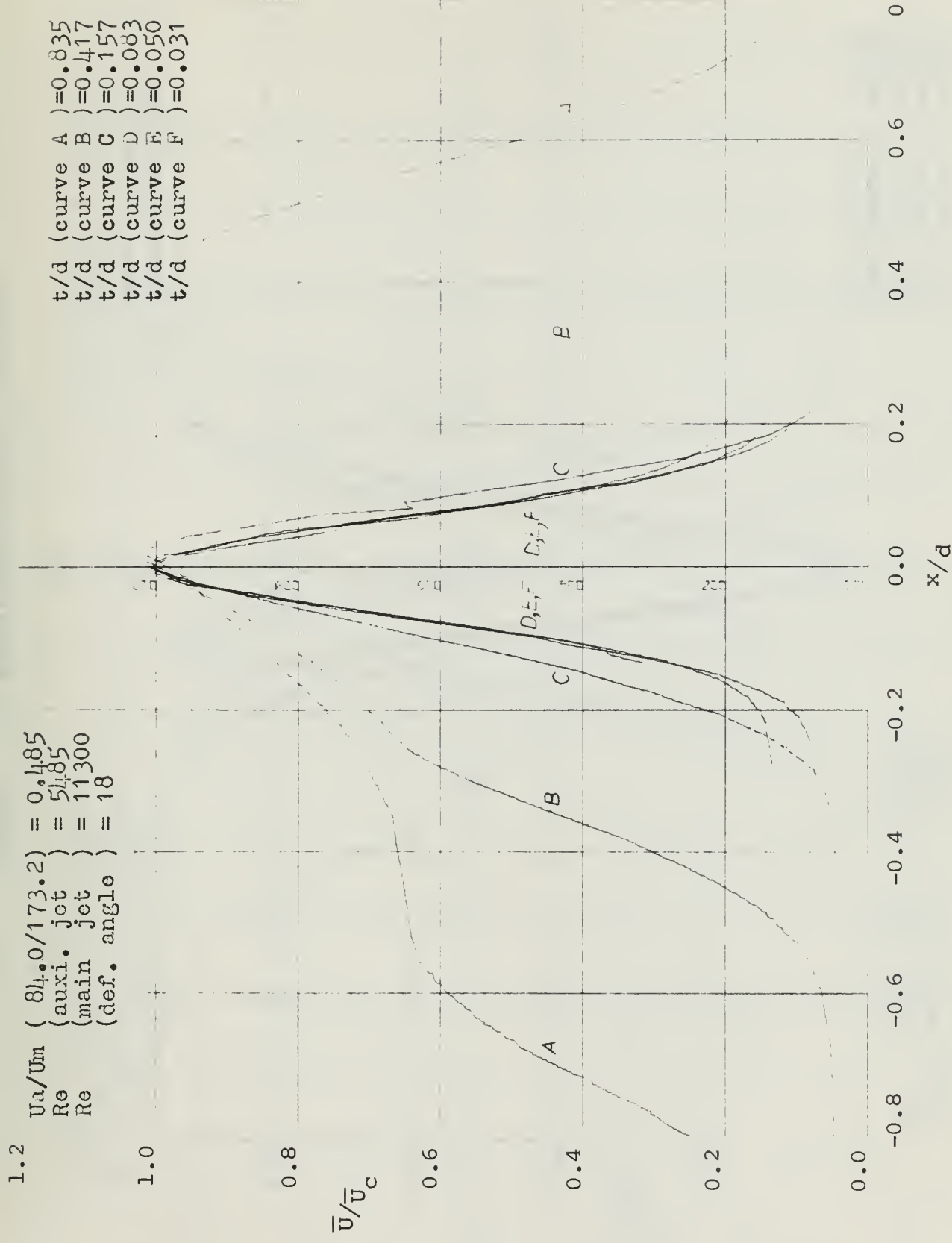


FIGURE 39 NORMALIZED VELOCITY PROFILES

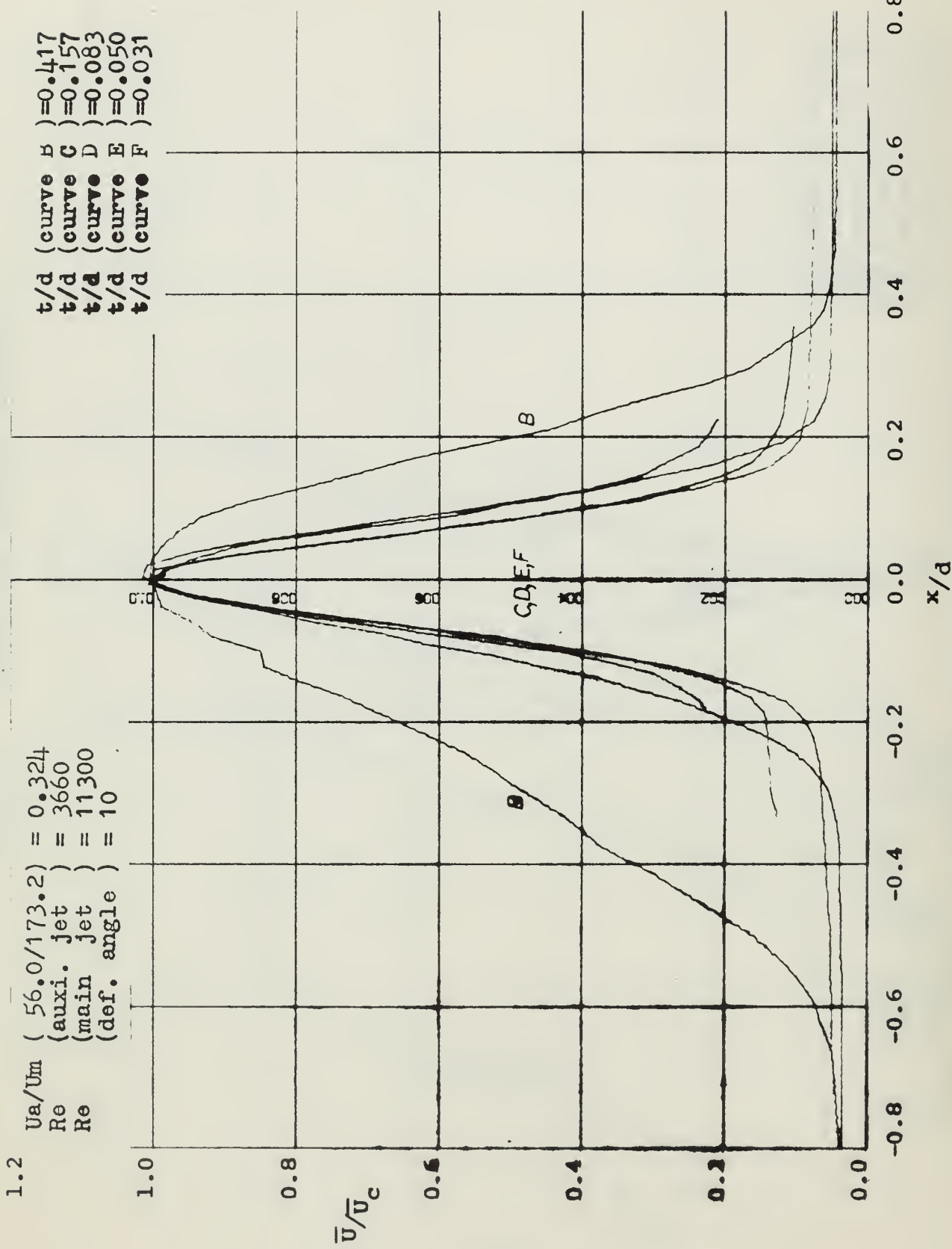


FIGURE 40 NORMALIZED VELOCITY PROFILES

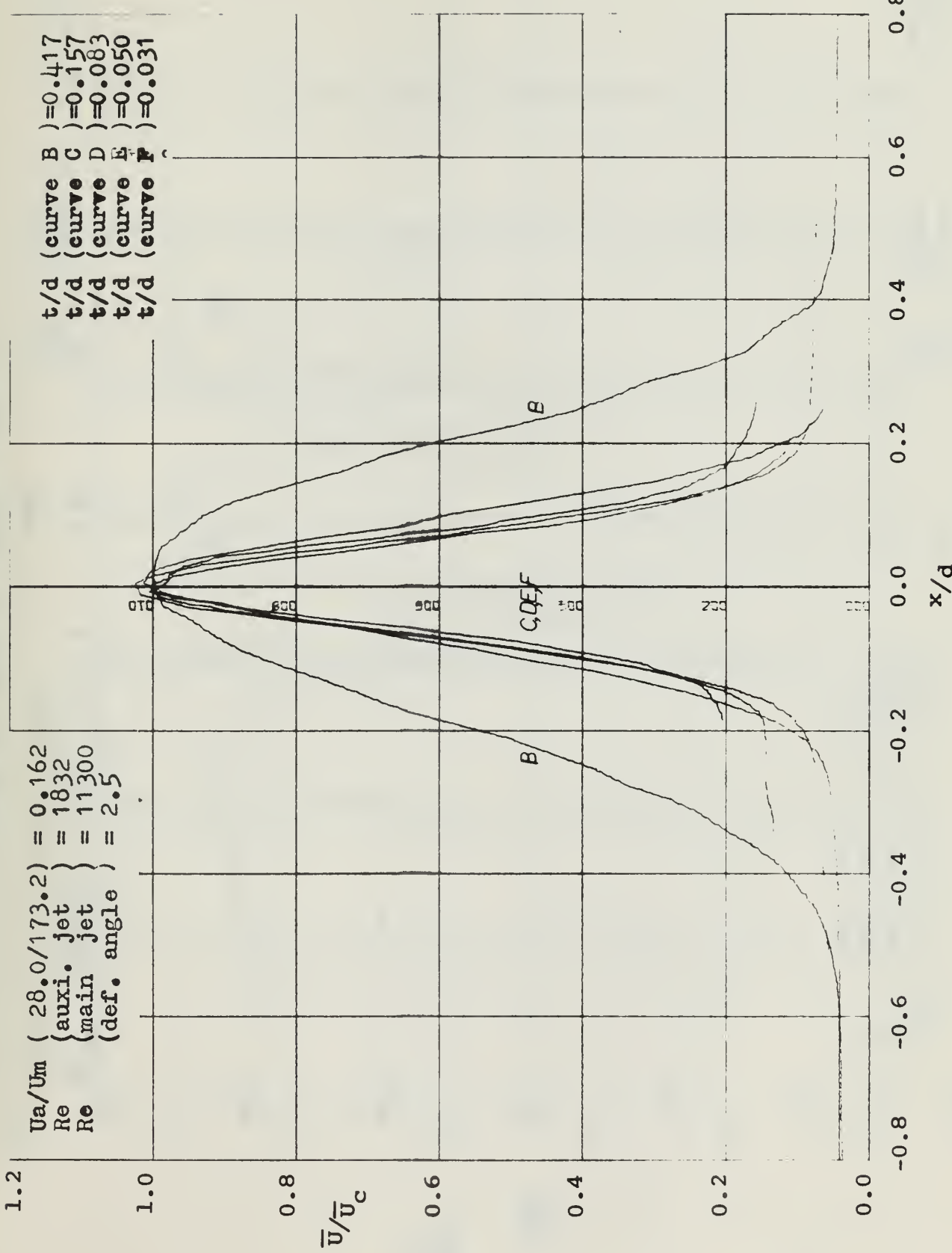


FIGURE 41 NORMALIZED VELOCITY PROFILES

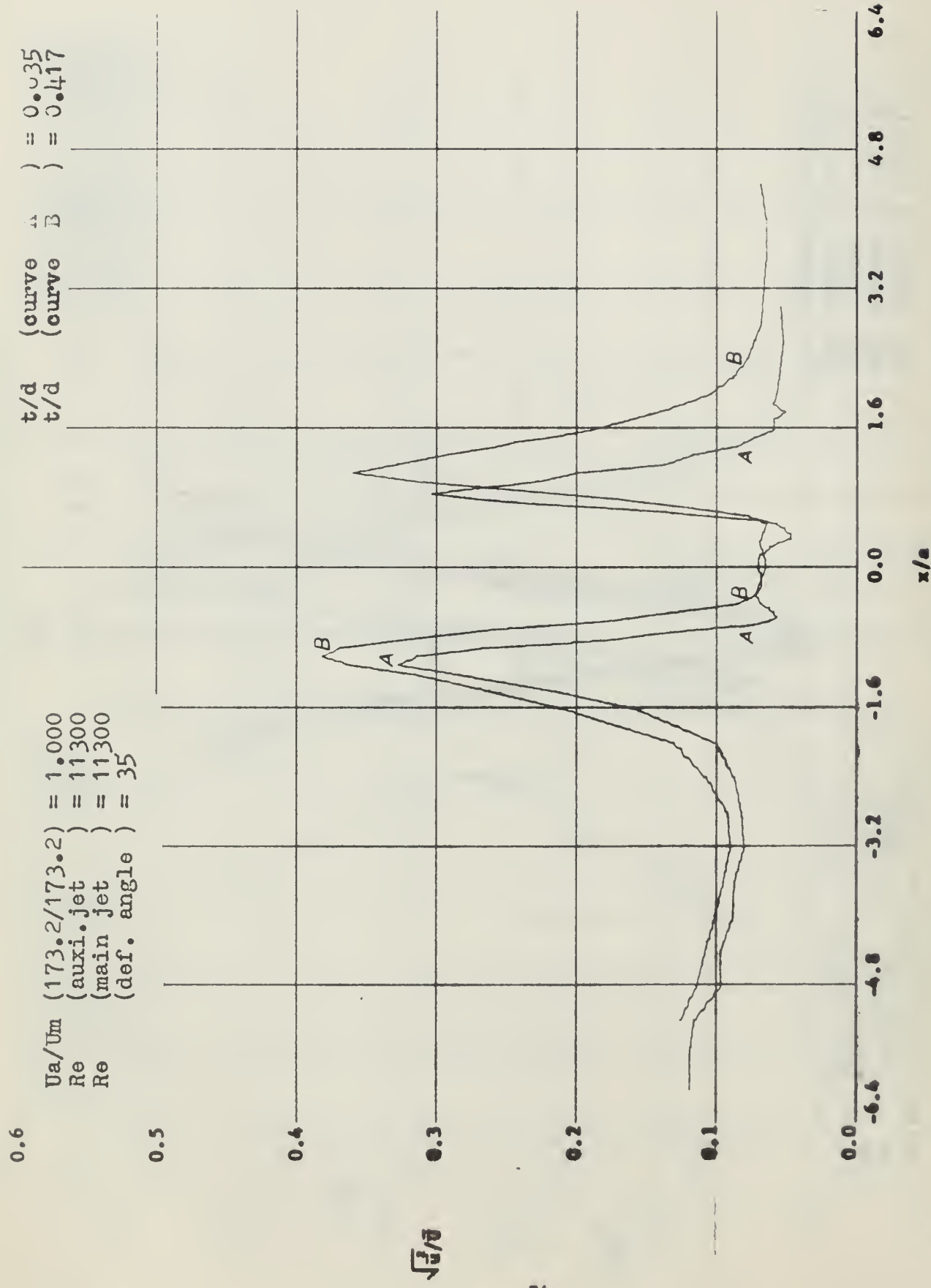
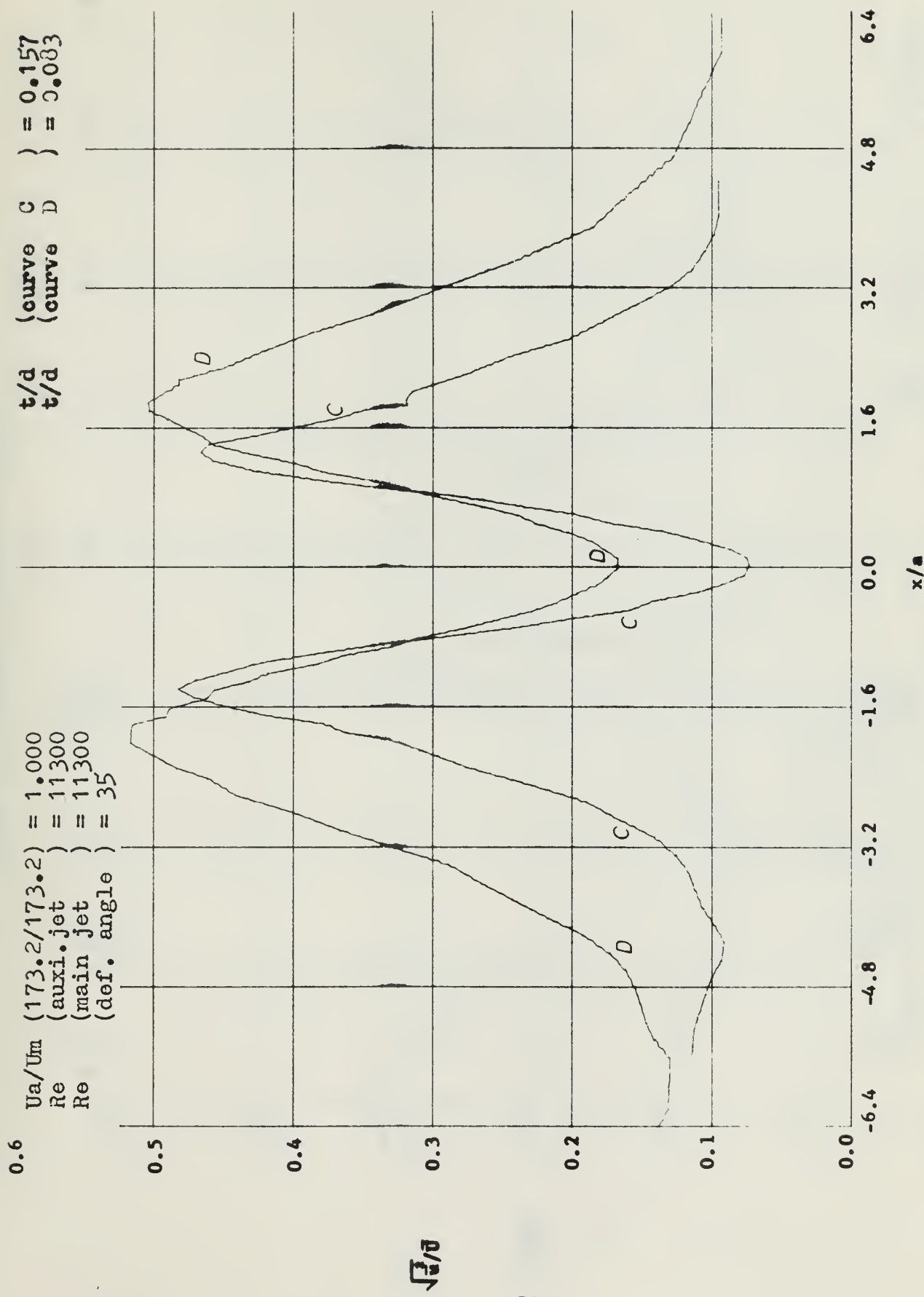


FIGURE 4.2 TURBULENCE INTENSITY PROFILES

FIGURE 43 TURBULENCE INTENSITY PROFILES



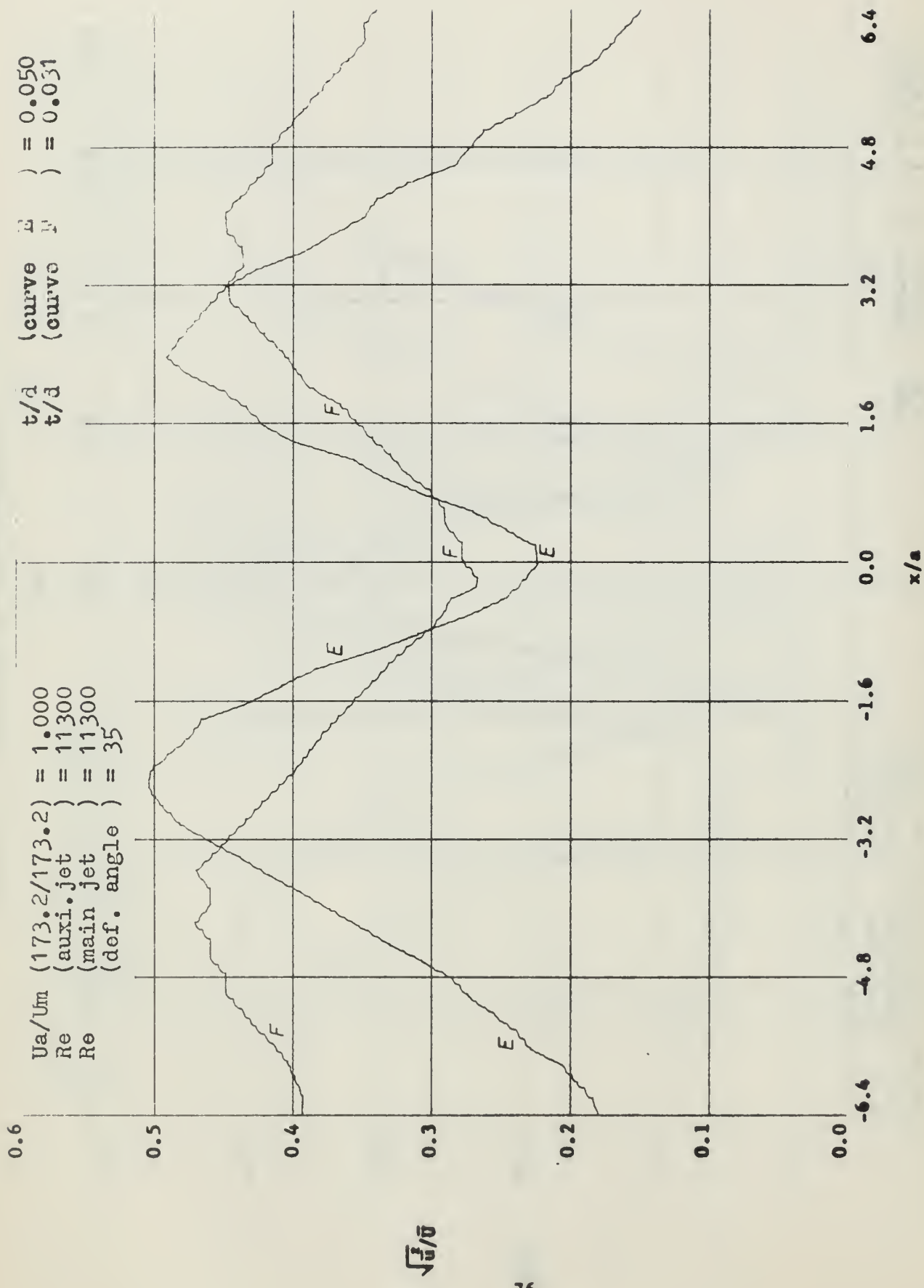


FIGURE 44 TURBULENCE INTENSITY PROFILES

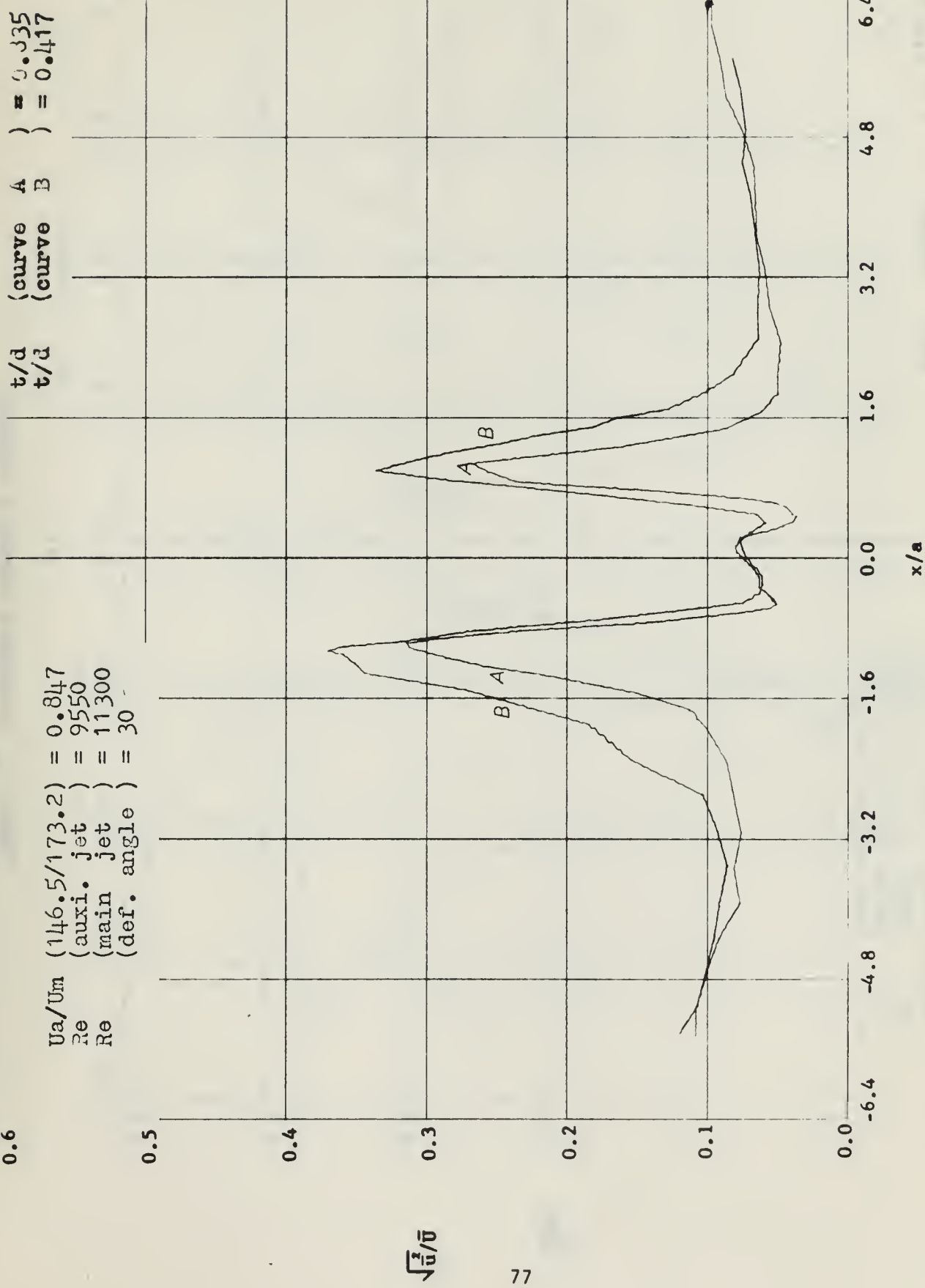


FIGURE 45 TURBULENCE INTENSITY PROFILES

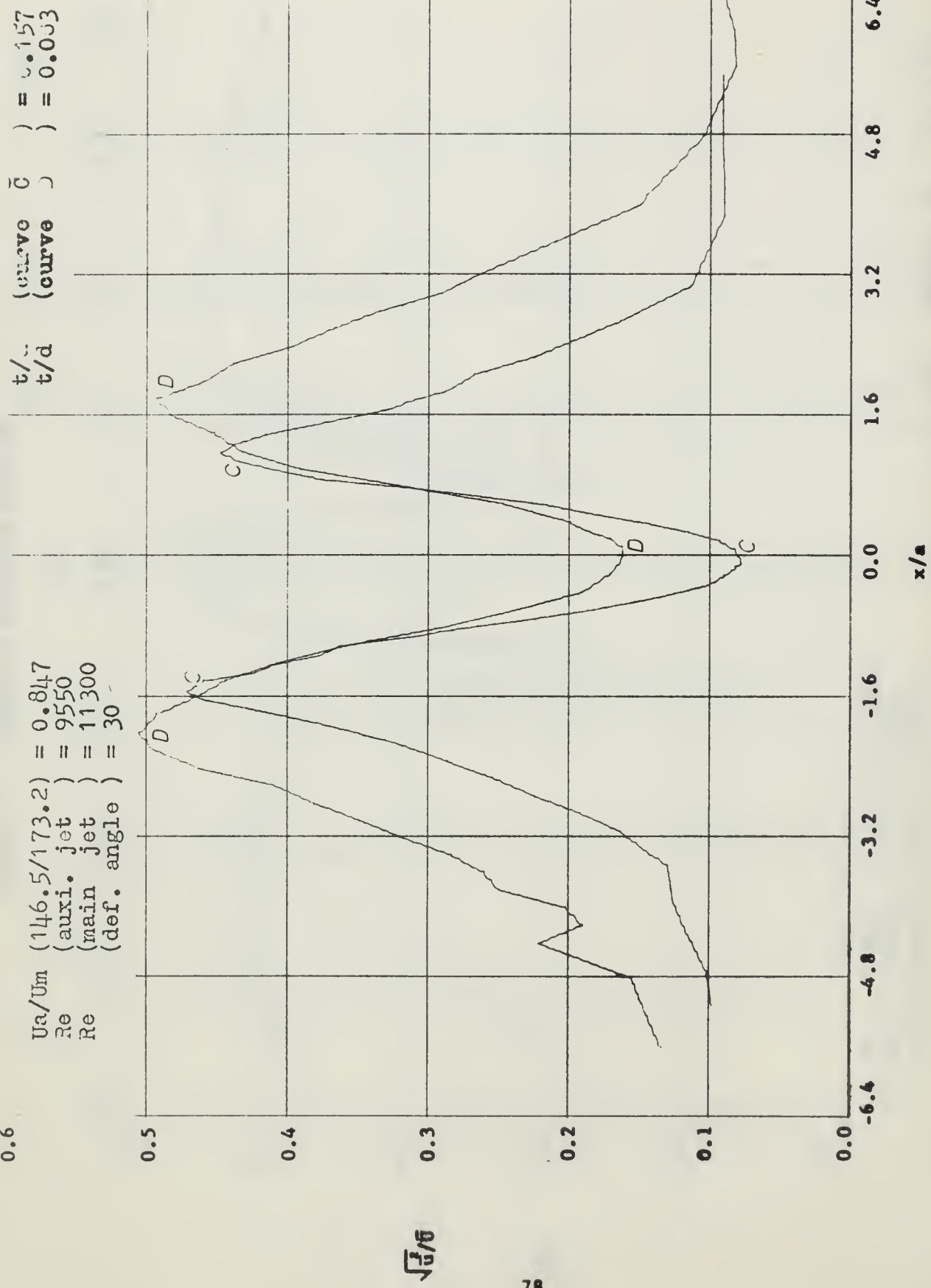


FIGURE 46 TURBULENCE INTENSITY PROFILES

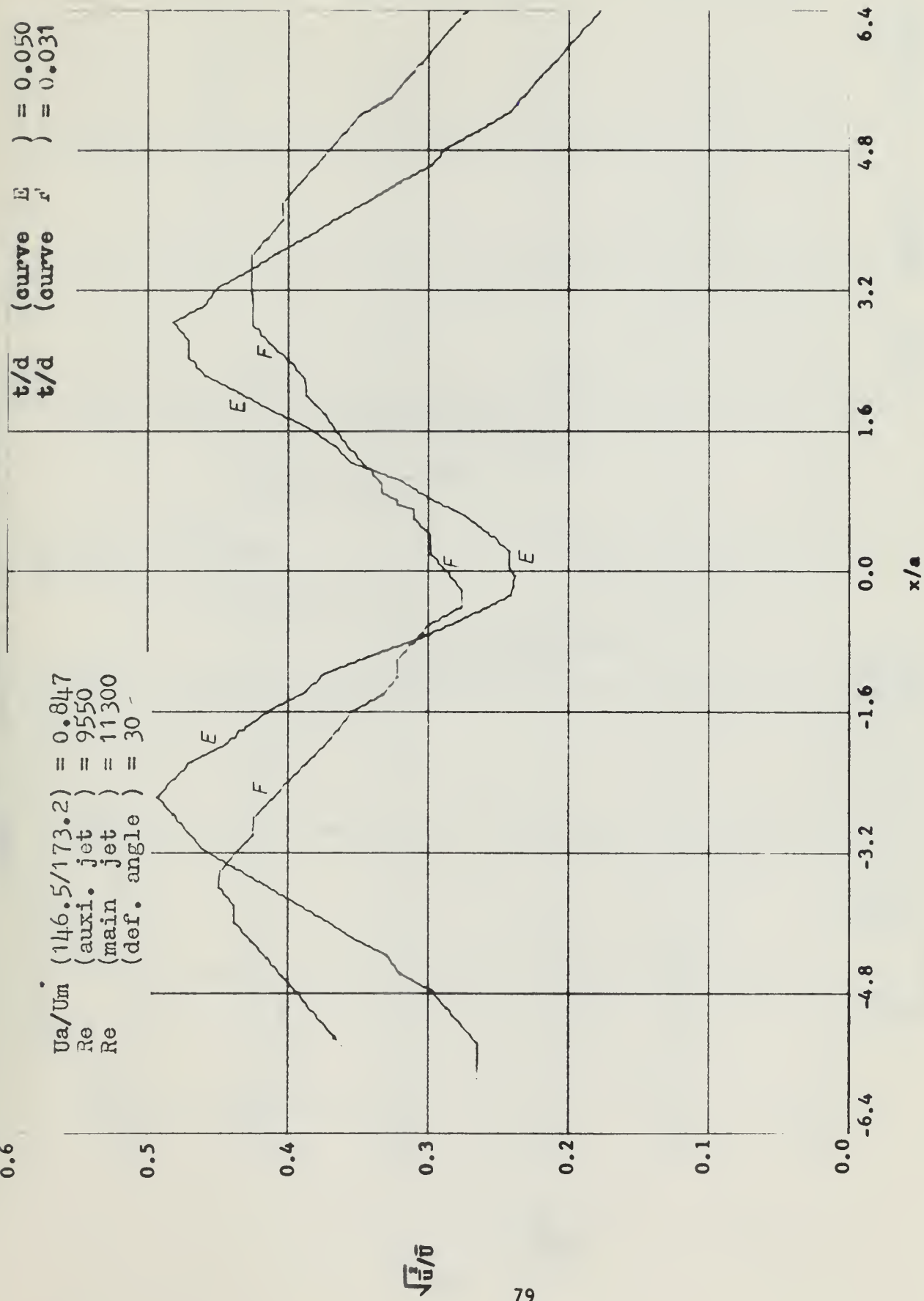
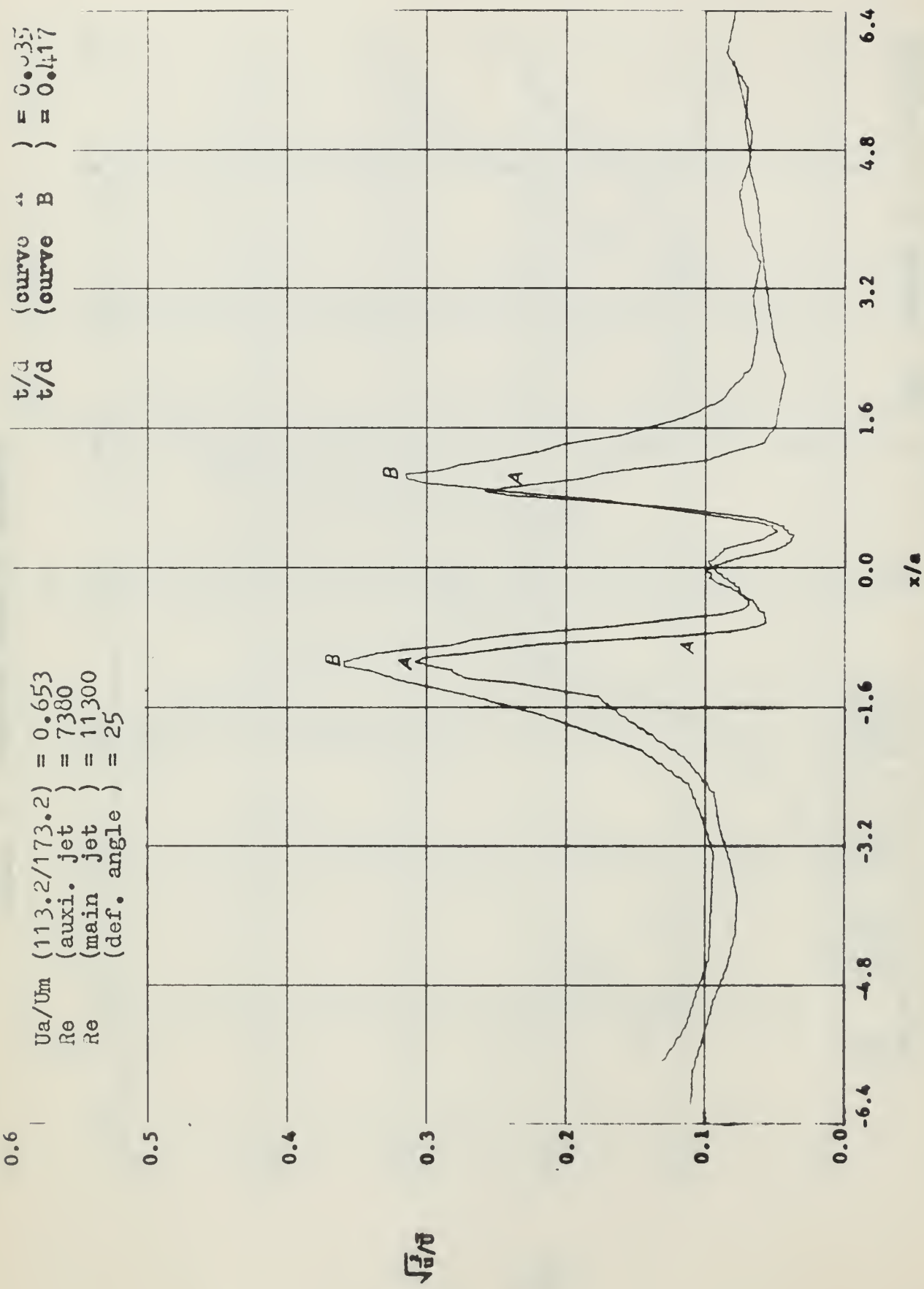


FIGURE 47 TURBULENCE INTENSITY PROFILES

FIGURE 48 TURBULENCE INTENSITY PROFILES



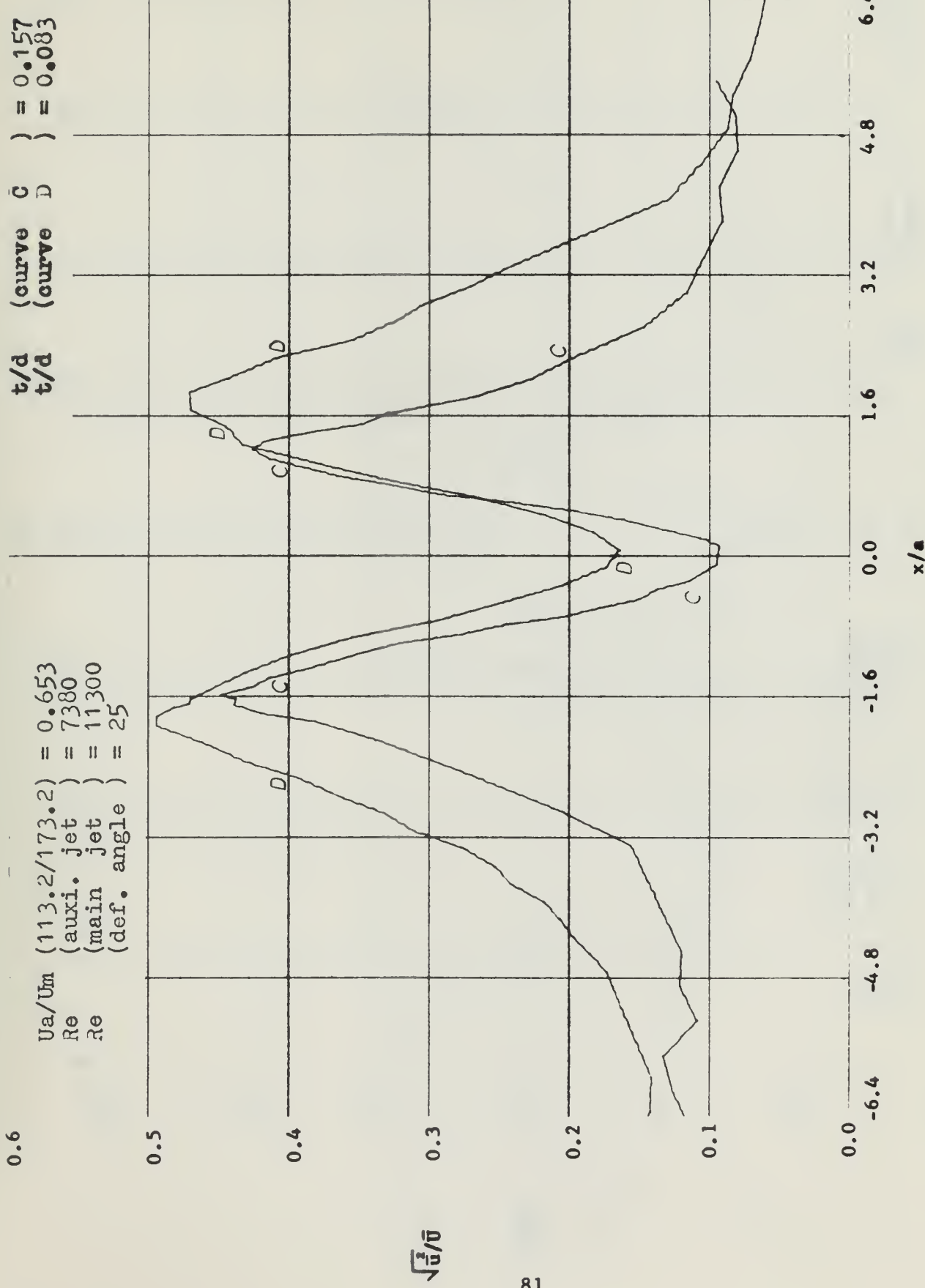


FIGURE 49 TURBULENCE INTENSITY PROFILES

$U_a/U_m = (113.2/173.2) = 0.653$
 $\text{Re}_{\text{auxi. jet}} = 7380$
 $\text{Re}_{\text{main jet}} = 11300$
 $\text{Re}_{\text{def. angle}} = 25$

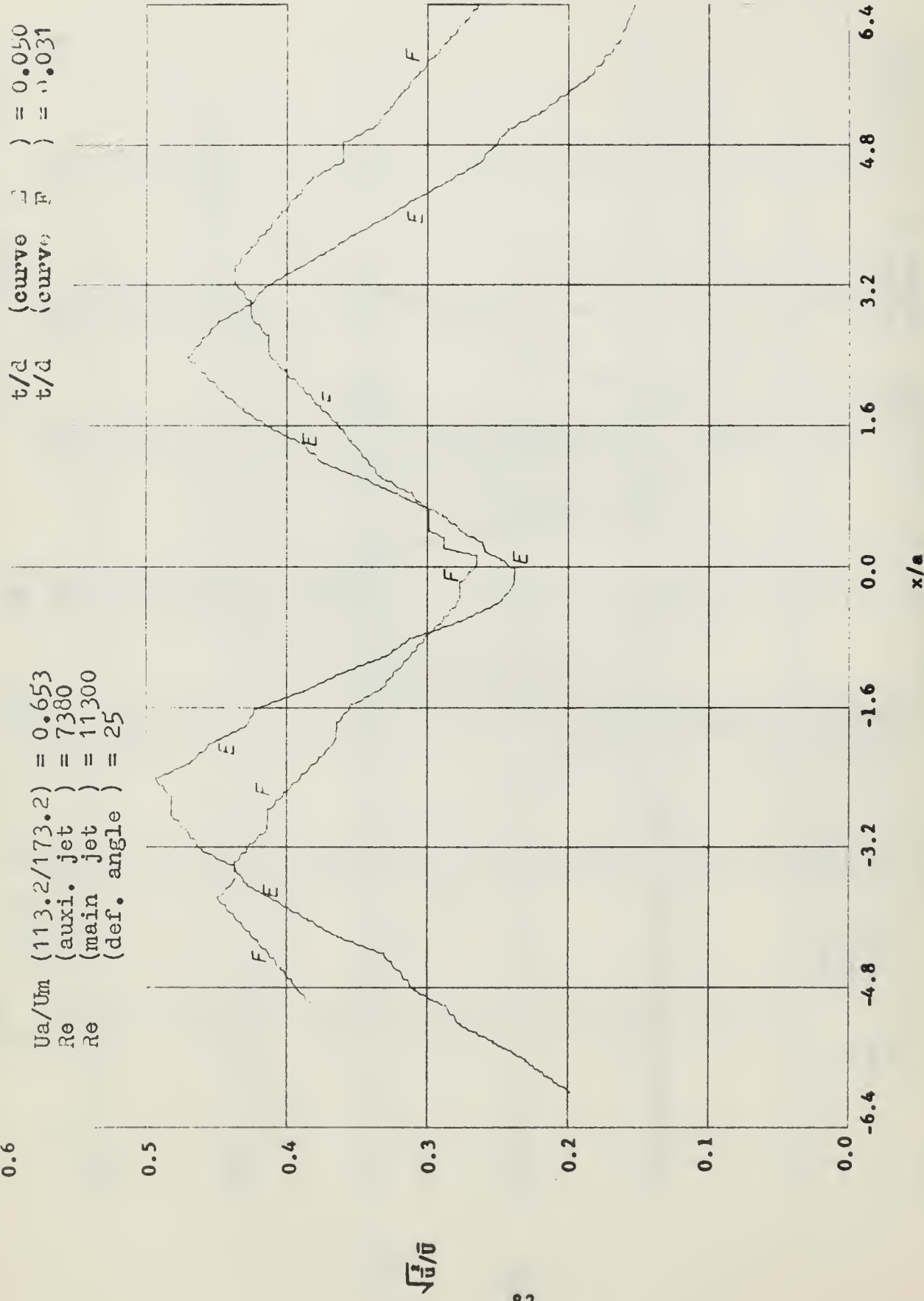


FIGURE 50 TURBULENCE INTENSITY PROFILES

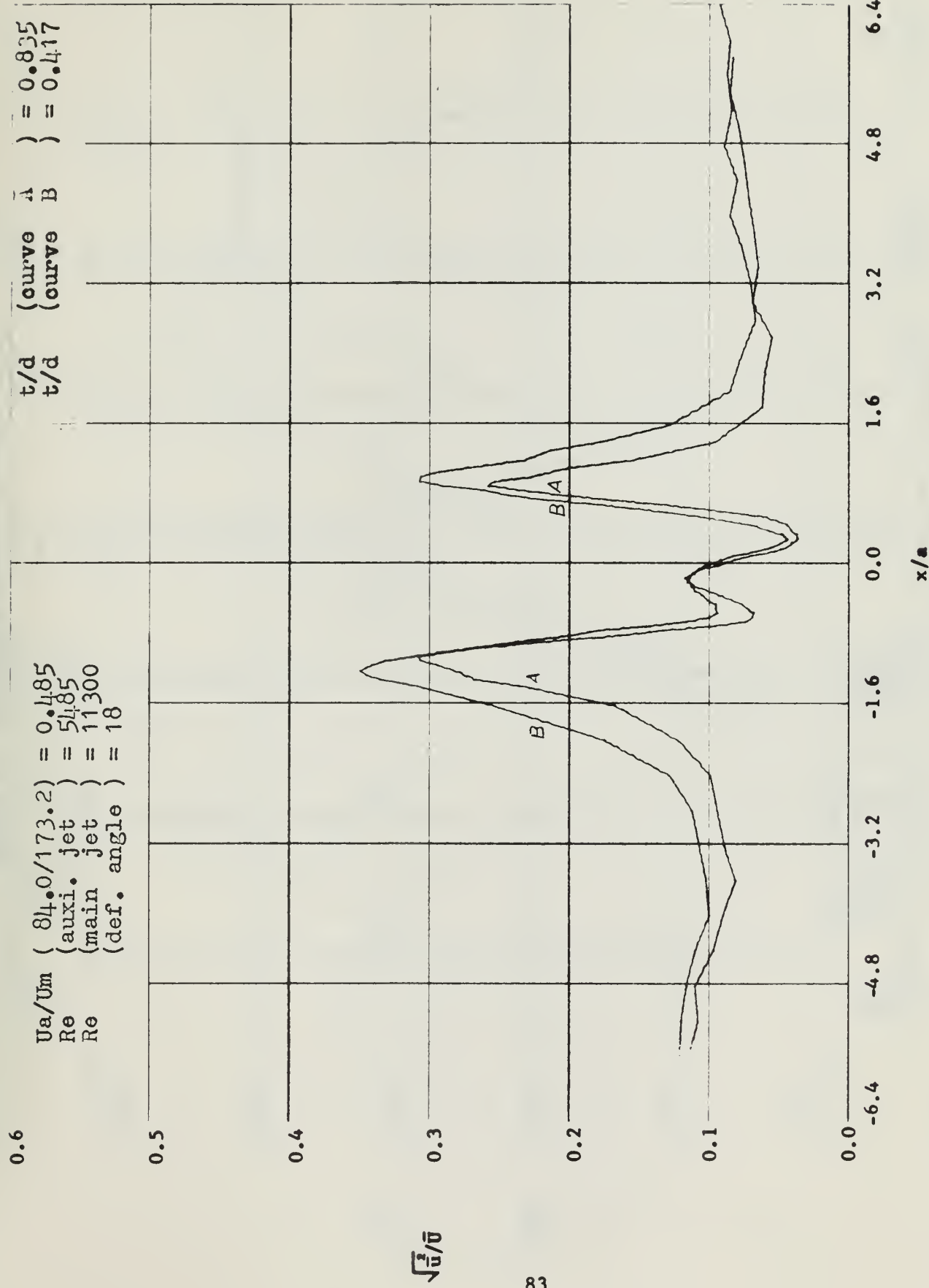


FIGURE 5'1 TURBULENCE INTENSITY PROFILES

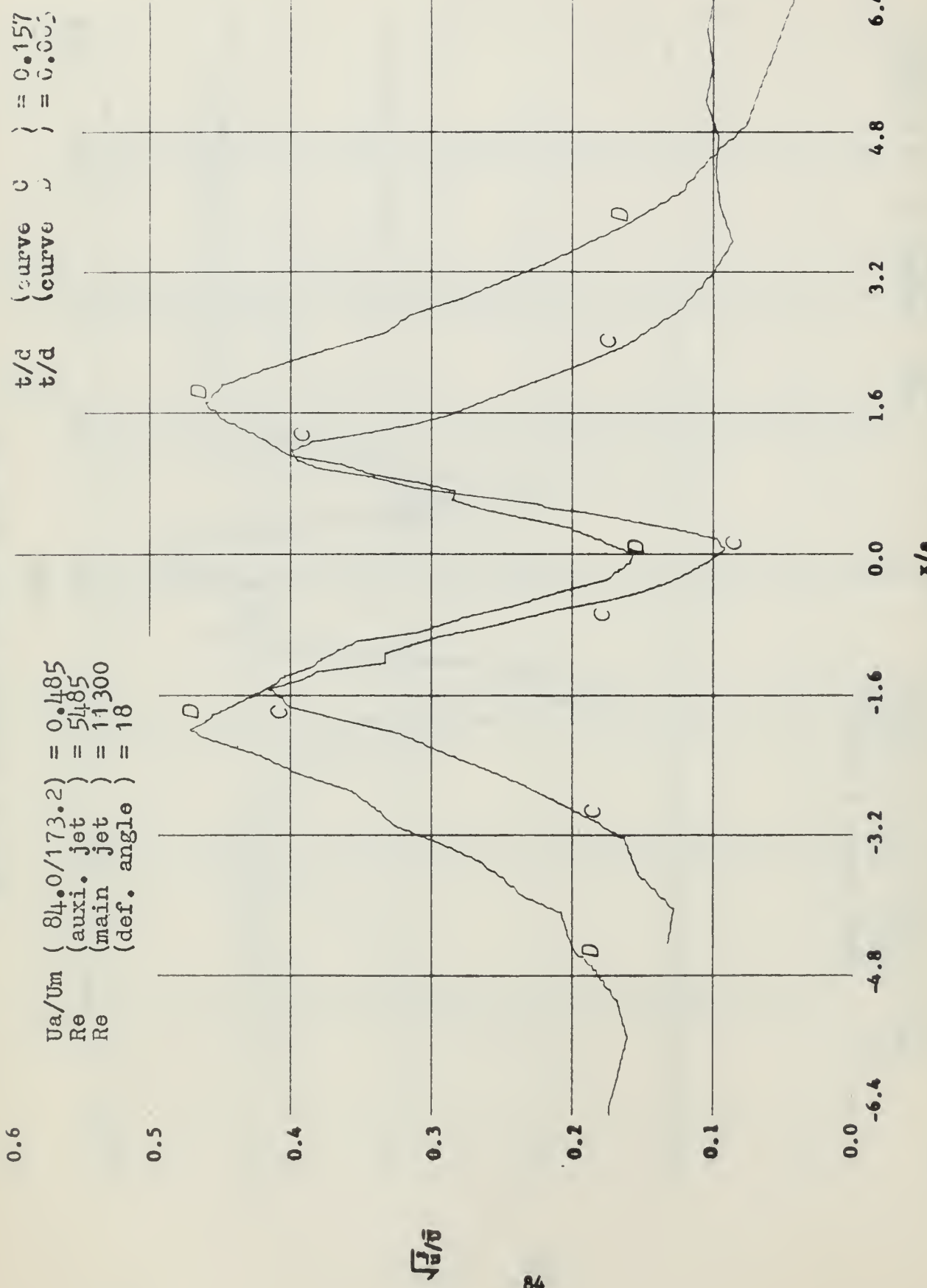


FIGURE 52 TURBULENCE INTENSITY PROFILES

$U_a/U_m = 84.0/173.2 \equiv 0.485$
 $R_e \quad \text{auxi. jet} \quad \equiv 54.85$
 $R_e \quad \text{main jet} \quad \equiv 11300$
 $(\text{def. angle}) \theta \quad \equiv 18^\circ$

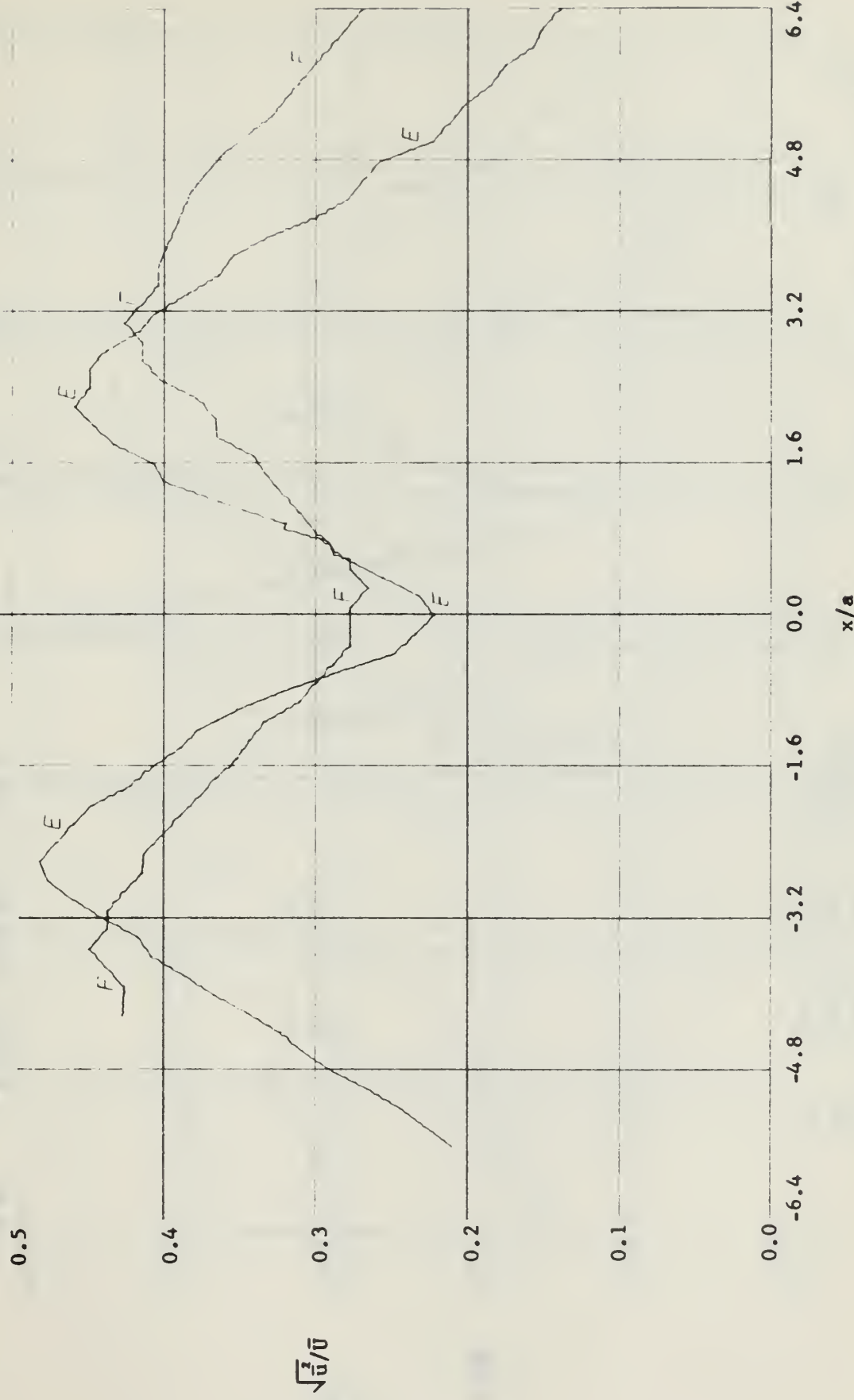


FIGURE 53 TURBULANCE INTENSITY PROFILES

$$\begin{aligned} U_a/U_m & \left(56.0/173.2 \right) = 0.324 \\ Re & \left(\text{auxili. jet} \right) = 3660 \\ Re & \left(\text{main jet} \right) = 11300 \\ (\text{def. angle}) & = 10^\circ \end{aligned}$$

$$\begin{aligned} t/d & \quad \{ \text{curve B} \quad \} = 0.417 \\ t/d & \quad \{ \text{curve C} \quad \} = 0.157 \end{aligned}$$

0.6

0.5

0.4

0.3

0.2

0.1

0.0

-0.1

-0.2

-0.3

-0.4

-0.5

-0.6

$\sqrt{f_u}$

86

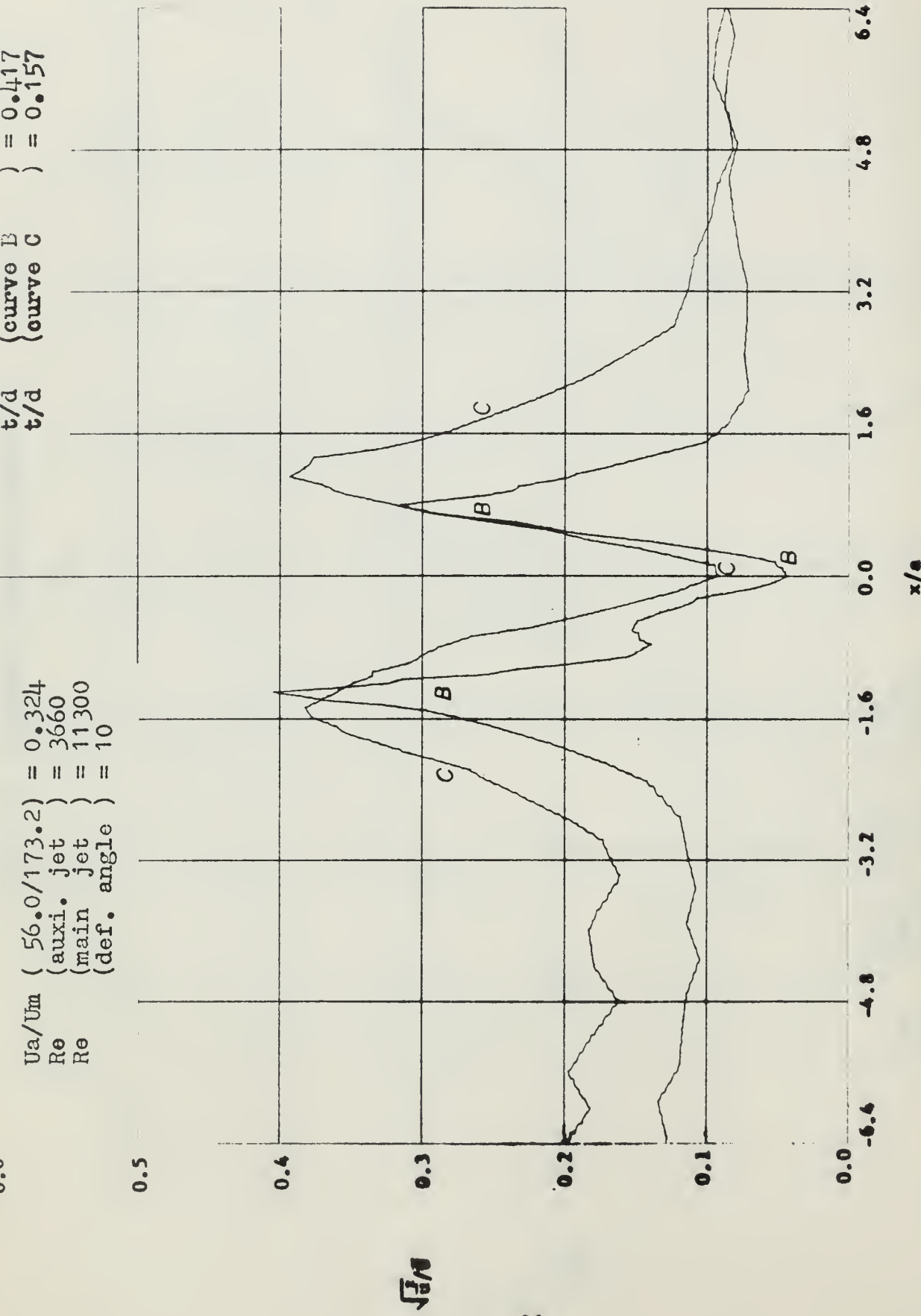


FIGURE 54 TURBULENCE INTENSITY PROFILES

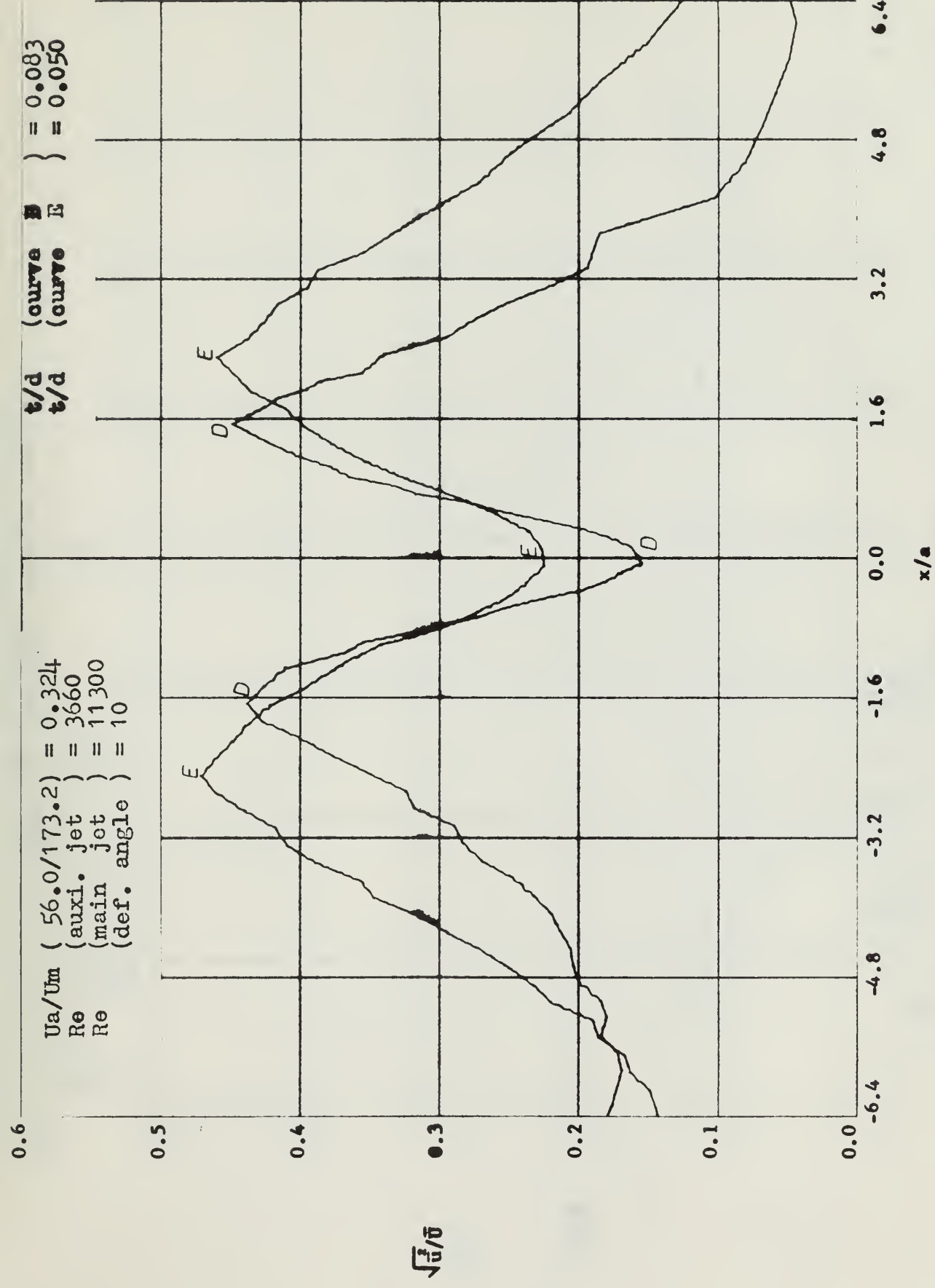


FIGURE 55 TURBULENCE INTENSITY PROFILES

FIGURE 56 TURBULENCE INTENSITY PROFILES

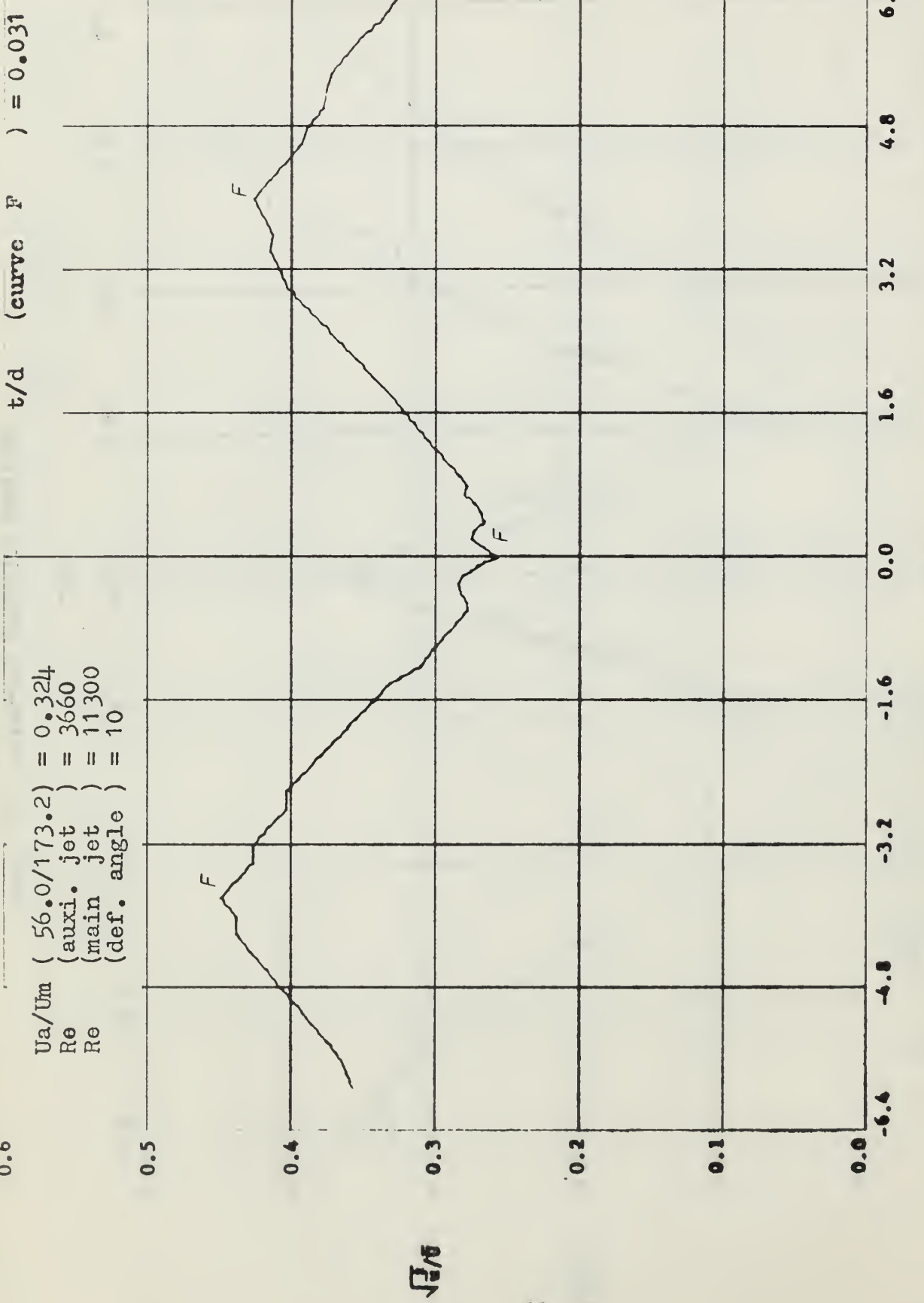


FIGURE 57 TURBULENCE INTENSITY PROFILES

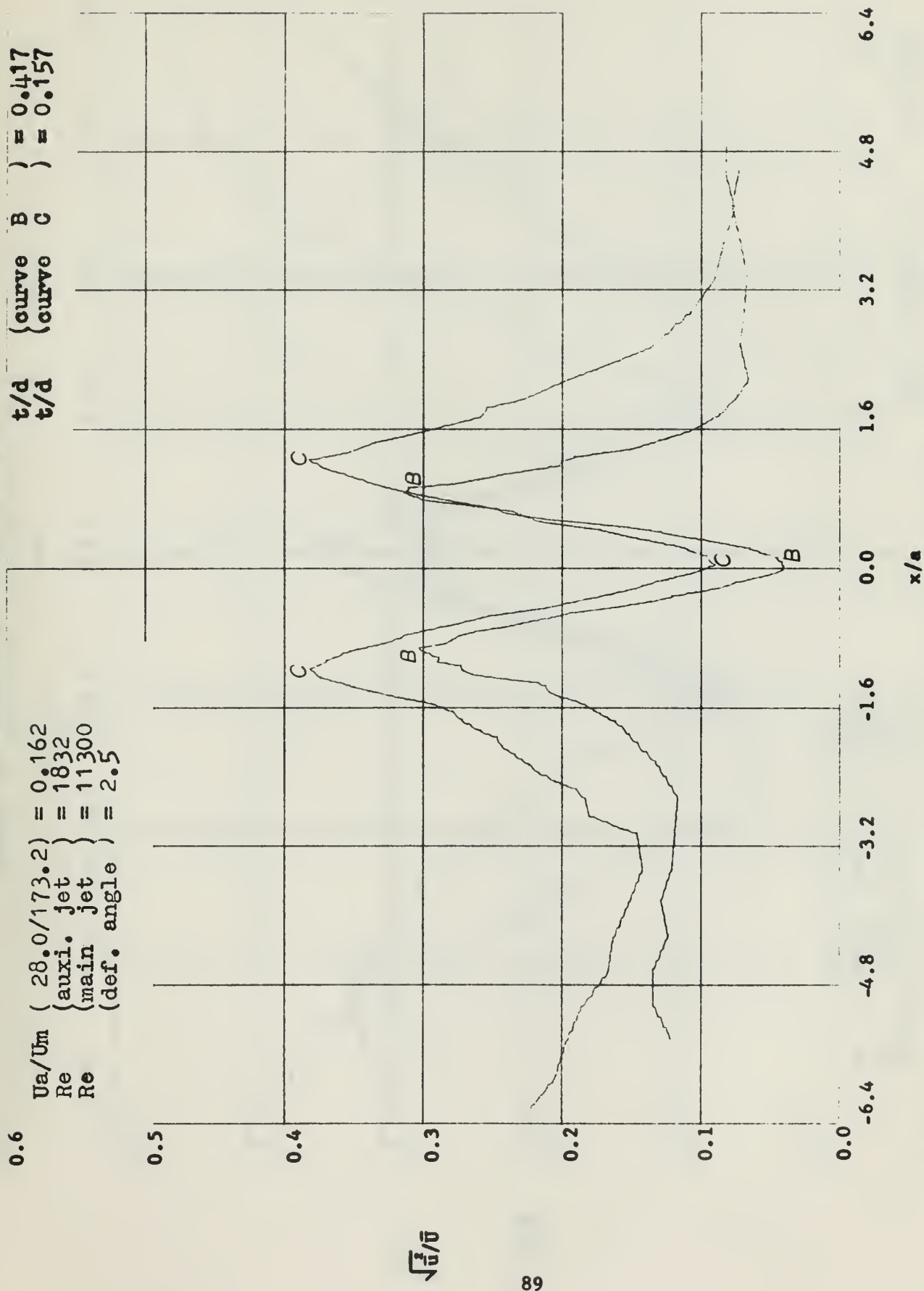
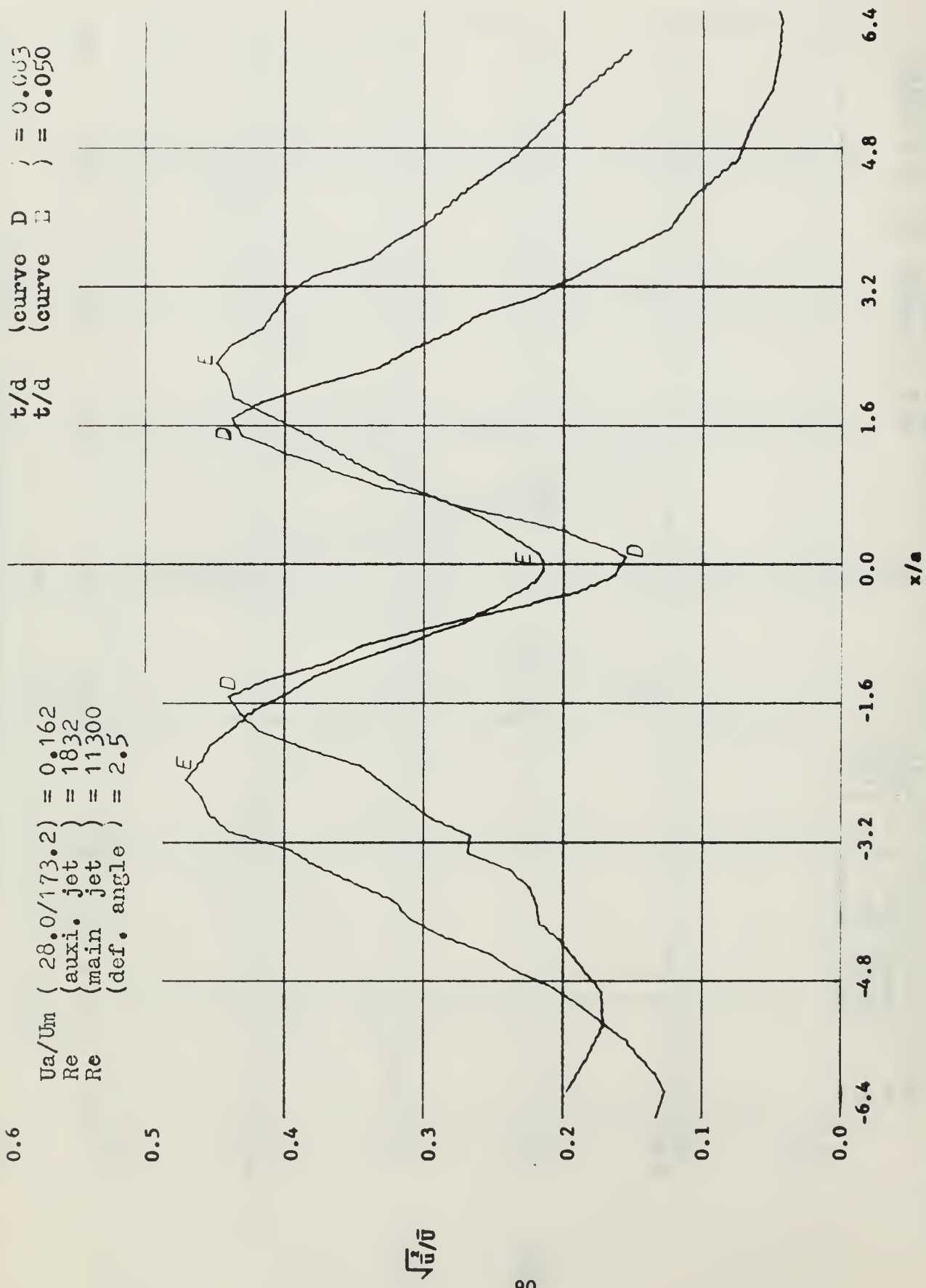


FIGURE 56 TURBULENCE INTENSITY PROFILES



t/d (curve 2) = 0.031

$$\begin{aligned} \frac{U_a}{U_m} &= 28.0 / 173.2 = 0.162 \\ \text{Re}_\text{auxi. jet} &= 1832 \\ \text{Re}_\text{main jet} &= 11300 \\ (\text{def. angle}) &= 2.5 \end{aligned}$$

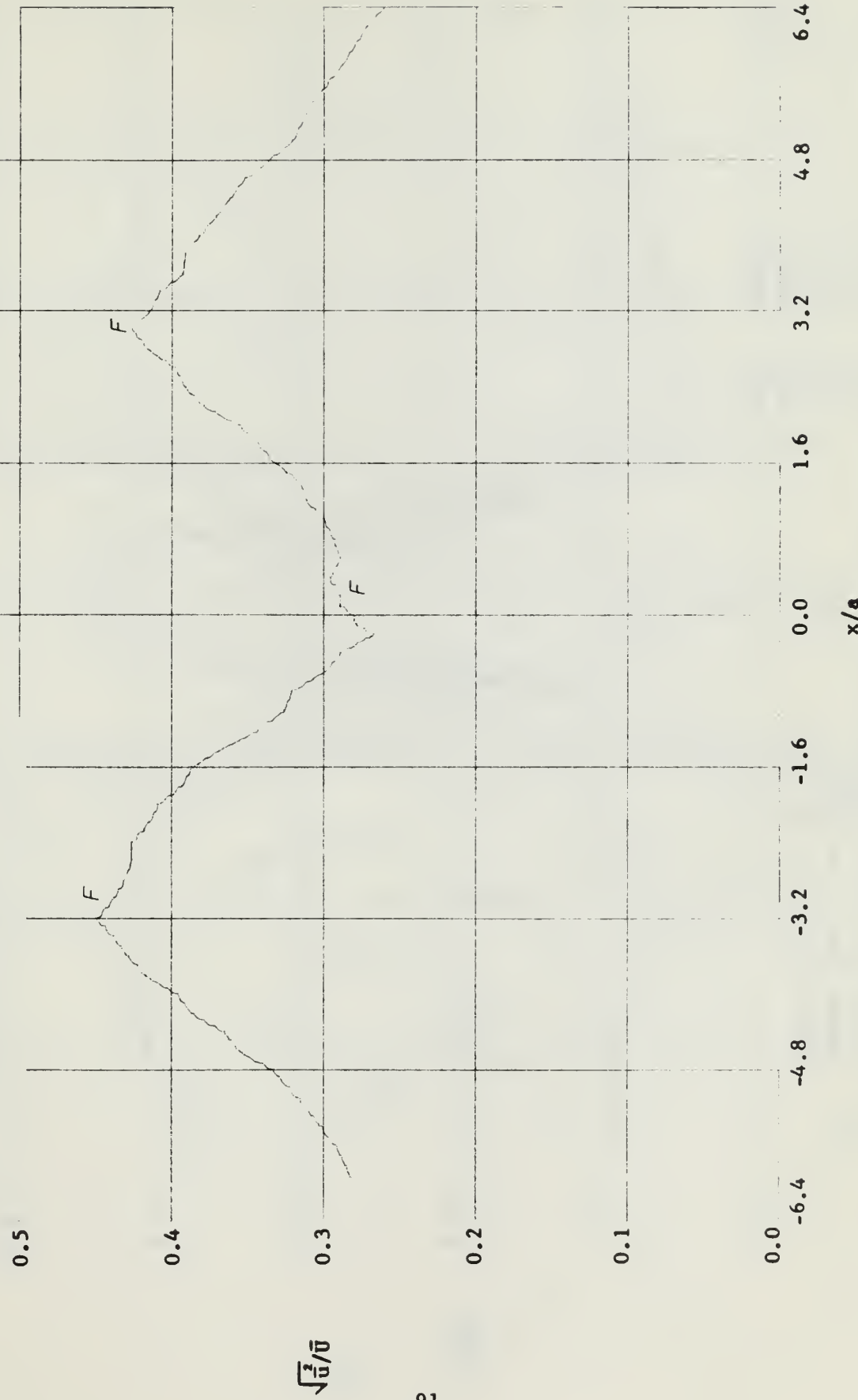


FIGURE 59 TURBULANCE INTENSITY PROFILES

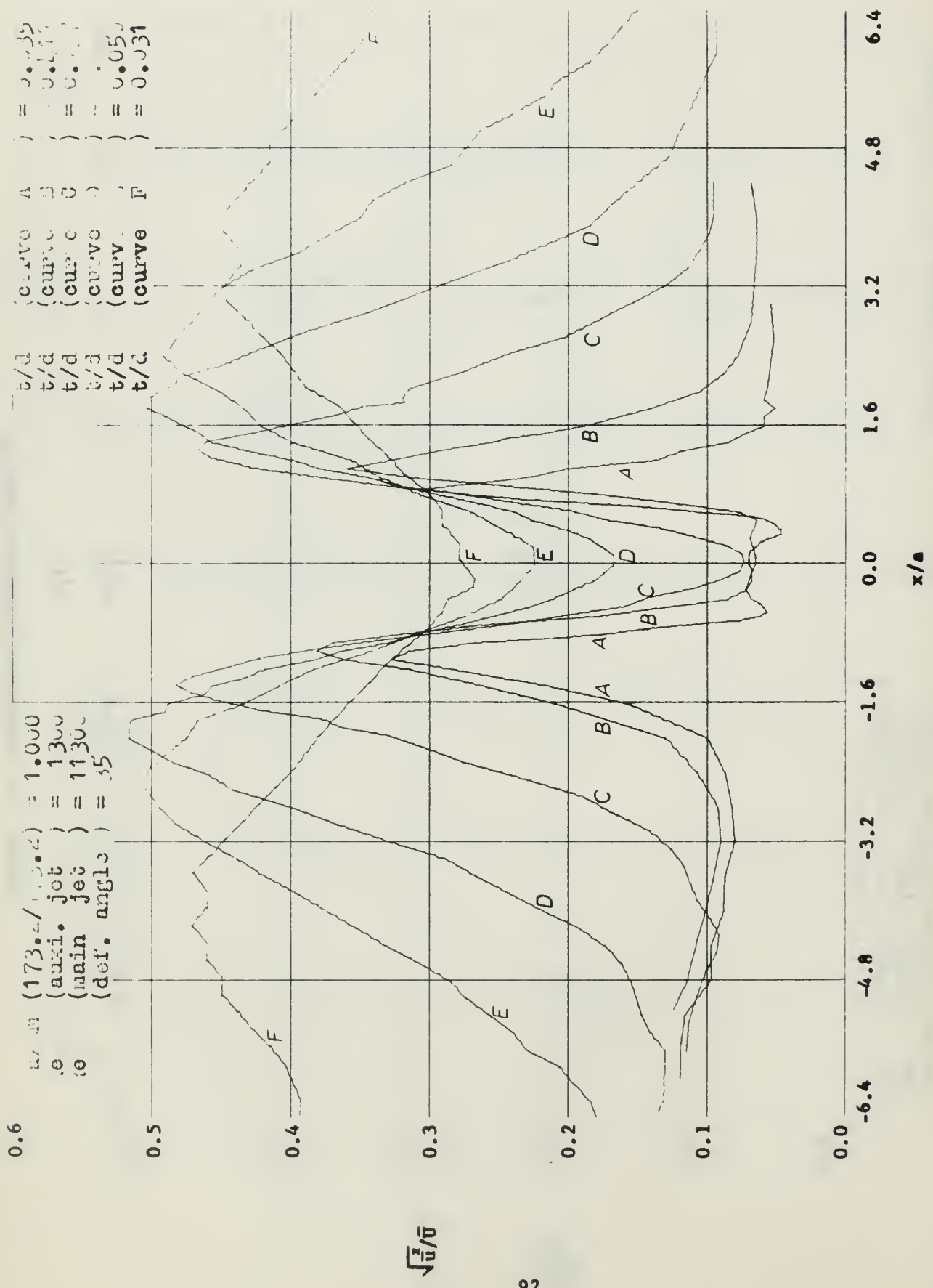


FIGURE 60 TURBULENCE INTENSITY PROFILES

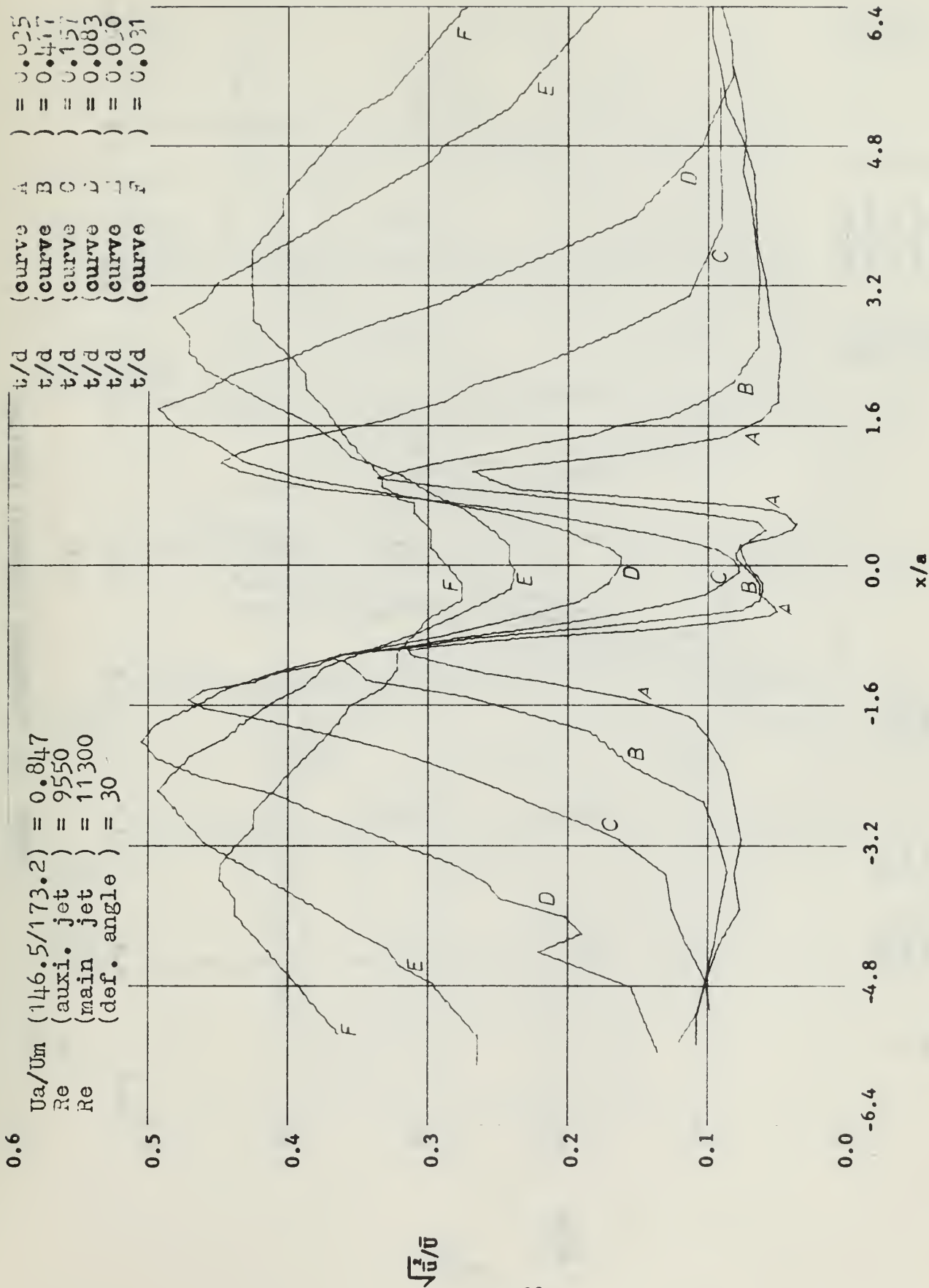
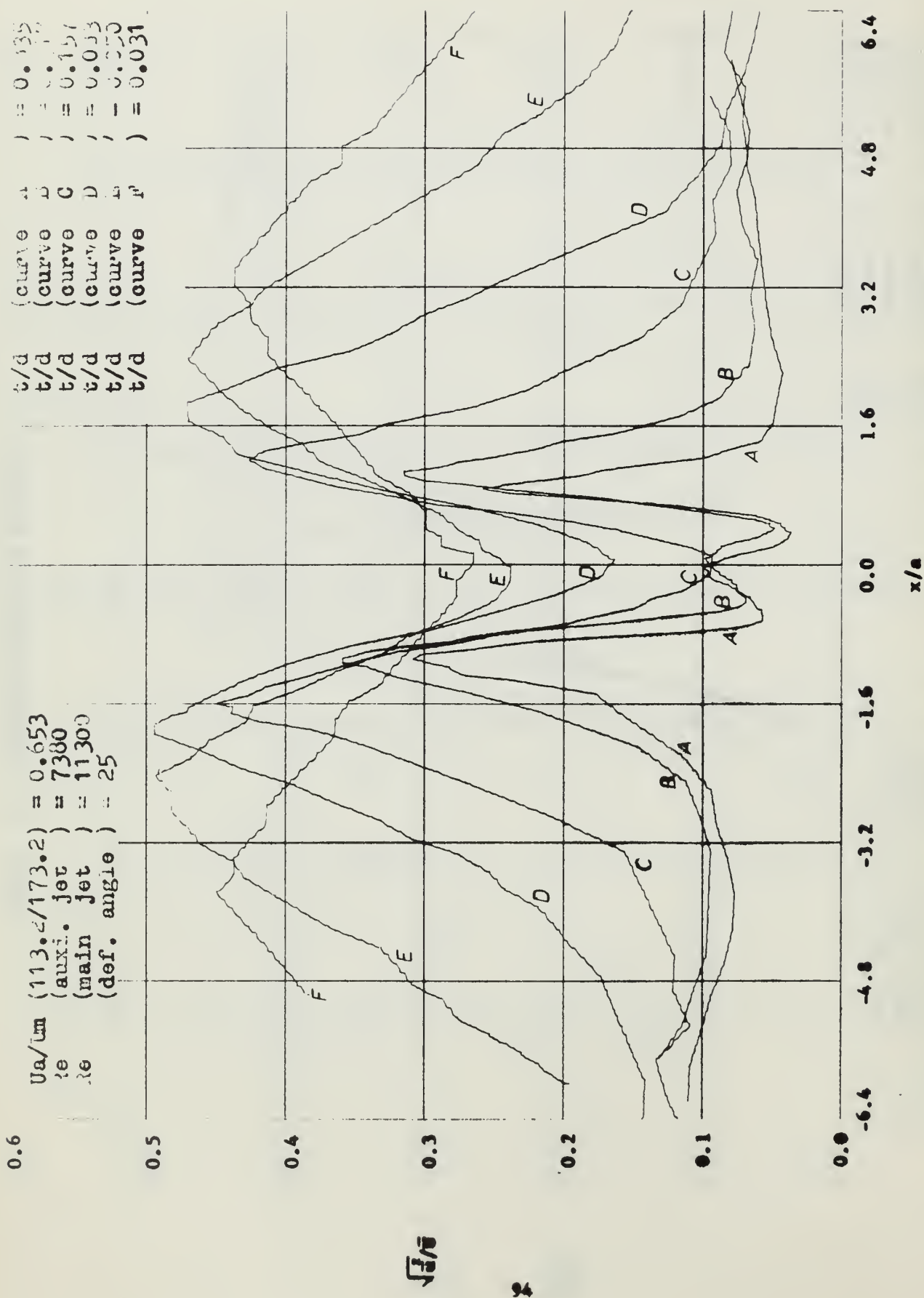


FIGURE 61 TURBULANCE INTENSITY PROFILES

FIGURE 62 TURBULENCE INTENSITY PROFILES



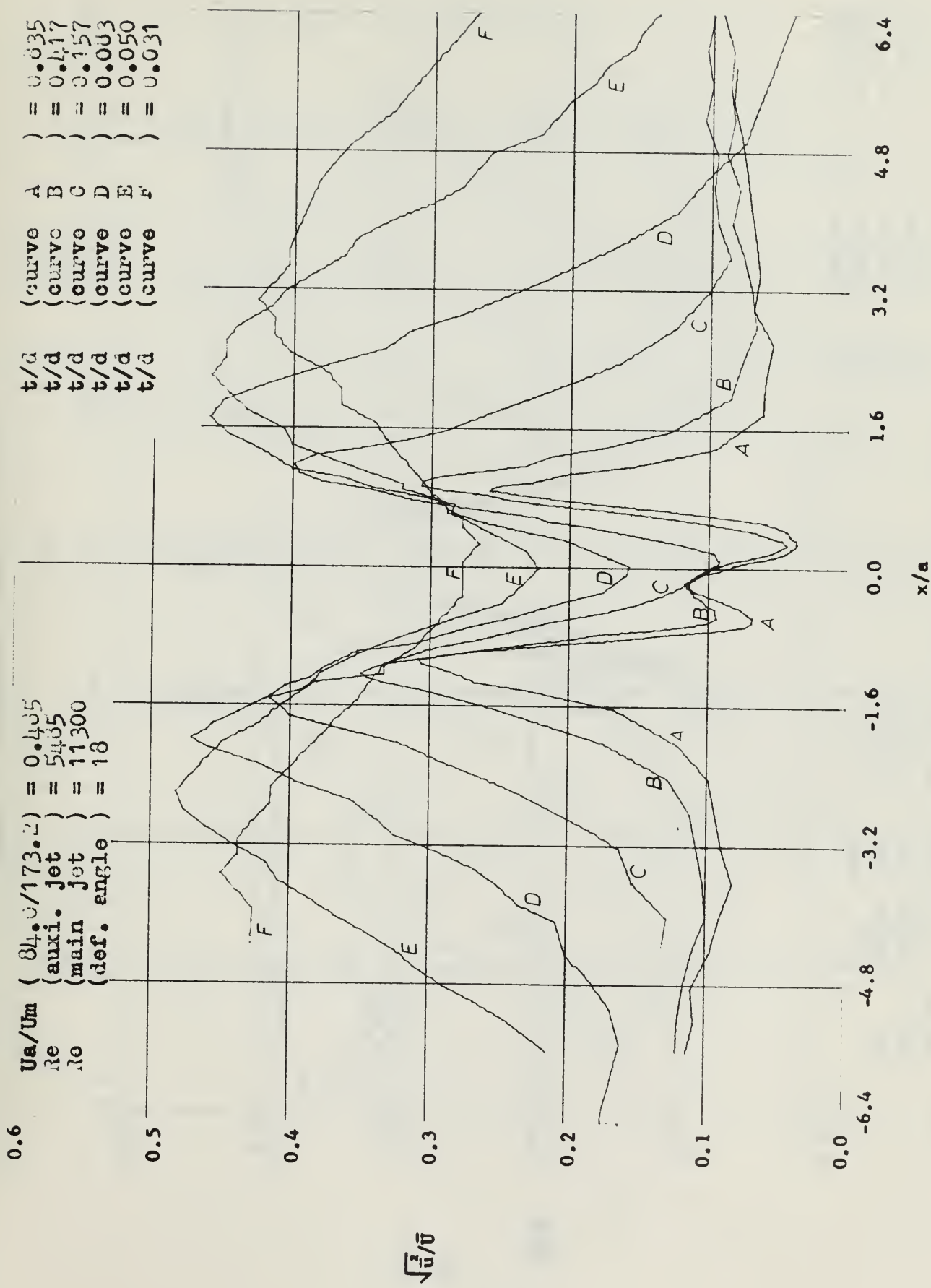


FIGURE 63 TURBULENCE INTENSITY PROFILES

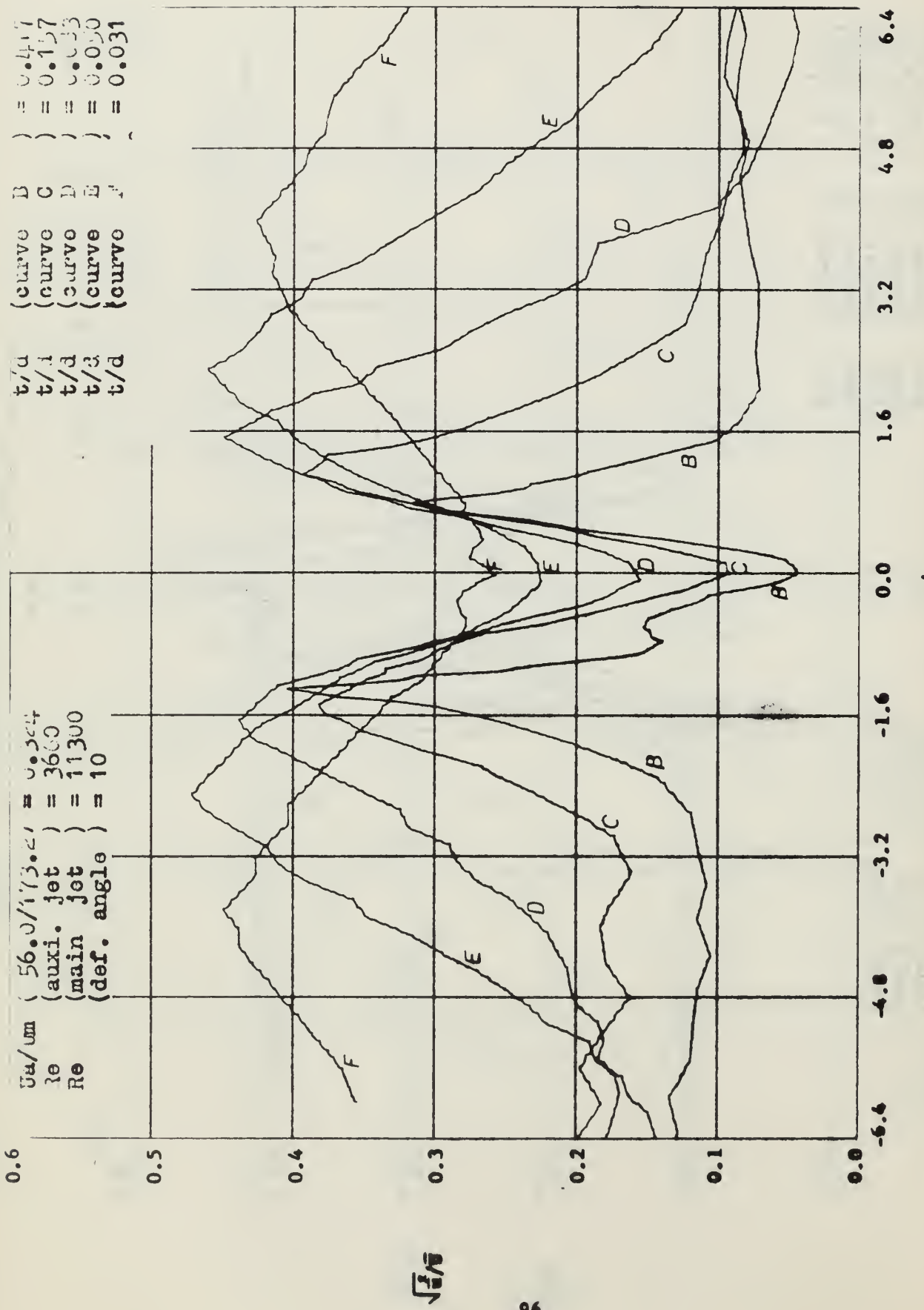


FIGURE 64 TURBULENCE INTENSITY PROFILES

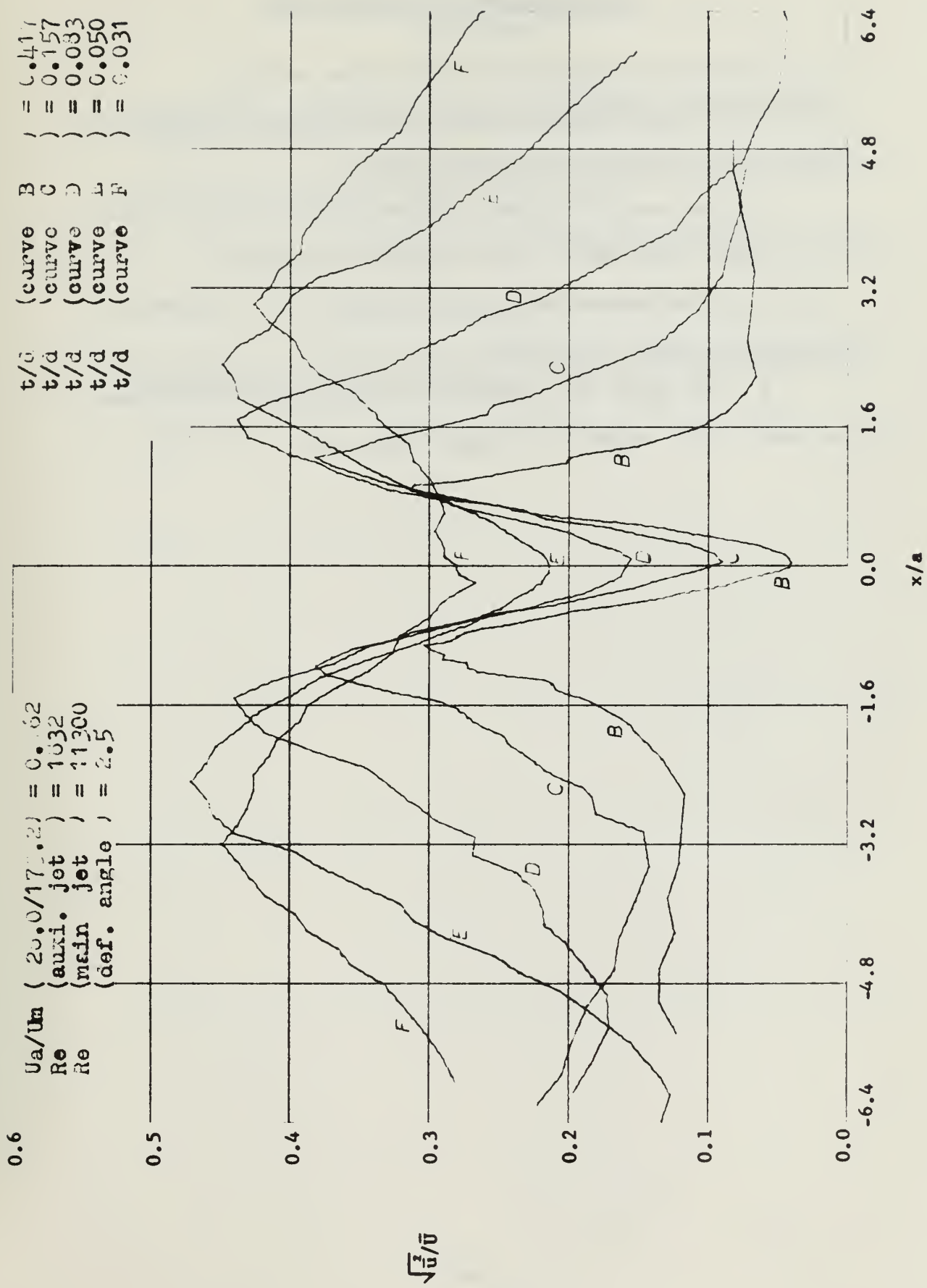


FIGURE 65 TURBULENCE INTENSITY PROFILES

VI. RECOMMENDATIONS FOR FURTHER WORK

The following are recommendations for further studies:

- a. Jet deflection, velocity and turbulence distributions be studied for other set-back and channel widths.
- b. The study of the above parameters be extended to lower Reynolds numbers where one or both of the jets are laminar.
- c. A theoretical analysis be carried out for unidentical free-stream velocities, and finally,
- d. The aspect ratio (the ratio of the width of the channel to the depth of the channel) be changed from 2 to 8.

BIBLIOGRAPHY

1. Mangion, C., and Weathers, T. M., Aerospace Fluid Component Designer's Handbook, TRW Systems, Redonda Beach, Calif., 1969.
2. Helmholtz, H., Über Discontinuirliche Flussigkeitsbewegungen, Monatsberichte Akad d. Wiss., Berlin, 1868.
3. Kirchhoff, G., Zur Theorie Freier Flussigkeitsstrahlen, Crelle, Vol. 70, 1869., pp. 289-298.
4. Streeter, V. L., Fluid Dynamics, McGraw-Hill Book Co., 1948.
5. Operating and Service Manual 1050 Series, Constant Temperature Anemometers and Related Accessories, Thermo-System, Inc.,
6. Abromovich, G. N., Theory of Turbulent Jet, M.I.T. Press, 1963.

APPENDIX A

Evaluation of the Integrals

The integrals indicated by Eq. 11 may be evaluated as follows:

$$I_1 = \int \frac{c\sqrt{t+1}}{t} dt = c \left\{ 2\sqrt{t+1} - \ln \frac{\sqrt{t+1} + \sqrt{1}}{\sqrt{t+1} - \sqrt{1}} \right\}$$

$$I_2 = -a\delta \int \frac{\sqrt{t+1}}{t-k} dt = -a\delta \left\{ 2\sqrt{t+1} - \sqrt{k+1} \ln \frac{\sqrt{t+1} + \sqrt{k+1}}{\sqrt{t+1} - \sqrt{k+1}} \right\}$$

$$I_3 = -e\eta \int \frac{\sqrt{t+1}}{t+f} dt = -e\eta \left\{ 2\sqrt{t+1} + 2\sqrt{f-1} \tan^{-1} \sqrt{\frac{f-1}{t+1}} \right\}$$

$$I_4 = c \int \frac{\sqrt{t-h}}{t} dt = c \left\{ 2\sqrt{t-h} + 2\sqrt{h} \tan^{-1} \sqrt{\frac{h}{t-h}} \right\}$$

$$I_5 = -a\delta \int \frac{\sqrt{t-h}}{t-k} dt = -a\delta \left\{ 2\sqrt{t-h} - \sqrt{k-h} \ln \frac{\sqrt{t-h} + \sqrt{k-h}}{\sqrt{t-h} - \sqrt{k-h}} \right\}$$

$$I_6 = -e\eta \int \frac{\sqrt{t-h}}{t+f} dt = -e\eta \left\{ 2\sqrt{t-h} + 2\sqrt{f+h} \tan^{-1} \sqrt{\frac{f+h}{t-h}} \right\}$$

The above results are evaluated between proper limits to yield the normalized distances s/a and t/a given by Eqs. (12) and (14). Note that regardless of the integration limits the sum of the first terms in the integrated expressions is zero because of continuity (see Eq. (13)).

APPENDIX B

Determination of the Coefficients of the Polynomial

One of the computer programs for the determination of the coefficients of the polynomials describing the two parts of the calibration curve is shown on page

The polynomials for either part of the calibration curve were assumed to be of the following type.

$$\bar{U}(\bar{E}) = a_1 + a_2 \Delta \bar{E} + a_3 (\Delta \bar{E})^2 + a_4 (\Delta \bar{E})^3 + a_5 (\Delta \bar{E})^4$$

The coefficients a_n and b_n for the two polynomials are tabulated below:

<u>a_n</u>	<u>b_n</u>
$a_1 = 0.764$	$b_1 = 3728.036$
$a_2 = 17.491$	$b_2 = -9160.219$
$a_3 = 20.558$	$b_3 = 8384.484$
$a_4 = -20.184$	$b_4 = -3353.178$
$a_5 = 24.969$	$b_5 = 512.192$

The second program used in the determination of the coefficients is not presented herein for it was identical in every aspect with the program used for the first part of the calibration curve with the exception of course, of the test data and the range of iteration. The resulting calibration curve and the test data are shown in Fig. 7.

APPENDIX C

Analysis of the Turbulence Measurement

Evaluation of the intensity of the turbulence is based on the well-known King's Law given as $E^2 - E_0^2 = BU^{1/n}$ where

E_0 is the anemometer output at zero velocity, E is the output for the velocity U , and B is a constant. The exponent n is ordinarily assumed to be 2. In most of the hot-wire work covering a large range of velocity, the exponent may deviate considerably from 2 and it is for this reason that in precision work one must use a calibration curve. The evaluation of such a calibration curve was described in the previous appendix. In the following the evaluation of the corresponding turbulence intensities will be described.

For a turbulent flow the instantaneous value of the anemometer output is given by $E = \bar{E} + \sqrt{\bar{e}^2}$

Where \bar{E} is the voltage output corresponding to the mean velocity at a given point and $\sqrt{\bar{e}^2}$ is the Root Mean Square value of the voltage output corresponding to $\sqrt{\bar{u}^2}$ (RMS value of the fluctuating component of velocity).

Writing

$$\bar{E} = f(\bar{U}), \quad d\bar{E} = f'(\bar{U}) d\bar{U}$$

and

$$U = \bar{U} + \sqrt{\bar{u}^2}$$

or

$$f(U) = f(\bar{U} + \sqrt{\bar{u}^2}) \cong f(\bar{U}) + \sqrt{\bar{u}^2} f'(\bar{U})$$

and noting that

$$\sqrt{\bar{u}^2} = \frac{\sqrt{\bar{e}^2}}{f'(\bar{U})}$$

Thus the intensity of turbulence reduces to

$$\frac{\sqrt{\bar{u}^2}}{\bar{U}} = \frac{\sqrt{\bar{e}^2}}{\bar{U} f'(\bar{U})} = \frac{\sqrt{\bar{e}^2}}{\bar{U}} \frac{d\bar{U}}{d\bar{E}}$$

where

$$f'(\bar{U}) = \frac{d\bar{E}}{d\bar{U}}$$

The turbulence intensity $\sqrt{\bar{u}^2}/\bar{U}$ was evaluated once again through the use of computer by feeding in the measured values of $\sqrt{\bar{e}^2}$, \bar{U} , and the values of $d\bar{U}/d\bar{E}$ as obtained from the two polynomials for respective parts of the calibration curve.

```

C 1 A' CALCULATION OF T/A, S/A, ANGLE BETA.
C TO FIND S/A T/A AND ANGLE BETA THE FOLLOWING PROGRAM WAS
C INTRODUCED AS THE EQUATIONS ARE NONINTEGRAL MAKES IT MANDATORY
C THAT ONE ASSUMPTION IS MADE. THE PARAMETERS F, H, K, AND G (=1)
C SYSTEMATICALLY OBTAIN CORRESPONDING VALUES OF T/A, S/A AND
C ANGLE BETA. FOR THE EQUATION SEE RELATED SECTION. THIS PROGRAM
C CONTAINS MORE INFORMATION FOR FURTHER CALCULATIONS. BESIDES
C S/A T/A ANGLE BETA.

C IMPLICIT INTEGER(I,J,L), REAL(A-H,K,M-Z)
C PI =3.1415926
C TO GENERALIZE THE PROGRAM , PARAMETER G IS USED IN EQUS. BELOW.
C IN THIS PROBLEM G=1.

C TO ALLOW THE ANGLE BETA UP TO 90 DEGREES, 10 DEGRES STEPS WERE USED
C G=1.0
P=SORT(G)

C TO ALLOW THE ANGLE BETA UP TO 90 DEGREES, 10 DEGRES STEPS WERE USED
L=9
DO 102 I=3,L
  BETA=(2.0*I-1.0)*PI/36.0
  C FROM THE EQUATION DERIVED FOR PARAMETER H.
  H=(TAN(BETA))**2
  Q=SORT(H)
  WRITE(6,103) BETA,H
101 J=1,70
  AS F-1 APPEARS UNDER SQUARE ROOT THE PARAMETER F MUST BE GREATER
  THAN F=1. THE INCREMENT CAN BE CHANGED FOR INTERESTING REGION OFF F.
  F=1.02*(0.02*j)
  DEL=0.01
  DO 100 K=1,50
    C FOR SAME REASON, THE PARAMETER K IS GREATER THAN 1
    C K INCREASES SYSTEMATICALLY TO COVER THE INTERESTING RANGE.
    C K=(1+EPS)*H+DEL*1/K
    C DEFINE ALL TERMS UNDER SQUARE ROOT.
    C SORT(H+G)
    R=SORT(K+G)
    C SORT(K-H)
    D=SORT(F-G)
    E=SORT(F+H)
    ALFA=A/(B+C)
    ETAE=A/(D+E)
    COA=ALFA+ETAE
    SEE THE EQUATIONS UNDER THE OPTICAL ANALYSIS SECTION.
    C ALFA IS APPEAR IN THIS SECTION AS DELTA.
    C SEE EQU.
    12
    SDA=-(CCAA*PI*D - PI*ALFA*B + ETAE*ALOG((F+A)/(F-A)))
    C C - CNA*Q*ALOG((A+Q)/(A-Q)) - 2.0*ALFA*C*ATAN(C/A)/(D*I*A)
    C SEE EQU. 14

```

```

TOA=-(C*DA*D*ALOG((A+P)/(A-P)) + ALFA*B*ALOG((B+A)/(B-A)))
C + CDA*PI*Q - 2.0*ETA*D*ATAN(D/A) - PI*ETA*E)/(DI*DA)
C*WDA=-(COA*P*Q*ALOG((G/H)*(A+Q)/(A-Q)))
C + 2.0*C*ALFA*P*C*(ATAN(C/A)-ATAN(C/Q))
C + ETA*P*E*ALOG(((F+Q)*(F-A))/(E-Q)*(A+E)))
C - ALFA*Q*R*ALOG((B+P)/(R-P)) + 2.0*ETA*Q*D*ATAN(D/P)
C - ETA*Q*D*PI)/(PI*(G+H))
C*NOA=(COA*P*Q*ALOG((G/H)*((A-P)/(A+P))/-2.0*ALFA*P*C*ATAN(C/Q))
C + ALFA*D*C*PI + ETA*P*E*ALOG((E+Q)/(E-Q)/(E-Q))
C + 2.0*ETA*Q*ALOG((B+P)/(B-P)) + ALFA*Q*B*ALOG((R+A)/(R-A)))
C + 2.0*ETA*Q*D*(ATAN(D/P)-ATAN(D/A))/(PI*(G+H))
WRITE(6,104) F,K,ALFA,ETA,COA,SDA,MOA,NOA
100 CONTINUE
101 CONTINUE
102 FORMAT(1H1,'5X','BETA = ','F11.4',10X,'H = ','F11.4','/','T12.2','F','/','T25.1,
C 'K',T35,'ALFA',T49,'ETA',T62,'C/A',T75,'S/A',T88,'T/A',T101,'M/A',,
CT14,'N/A',/)
104 FORMAT(4X,9(F11.4,2X))
105 RETURN
END

```

```

PROGRAM 'R' APPROXIMATION OF CALIBRATION CURVE
C TO APPROXIMATE THE CALIBRATION CURVE IN TWO 4TH DEGREE OF
C POLYNOMIAL THE PROGRAM BELOW WAS INTRODUCED.
C DIMENSION X(100),Y(100),A(20),RX(20),RH(20)
C INTEGER R(20)
C P(PRESSURE IN INCHES OF WATER)=1/12*1/33.9*14.7*144=5.2 LB/F/FT**2
C L INCHES OF WATER(PRESSURE)=5.2 LB/F/FT**2
C V(VELLCITY)=SQRT(2*p/air density)
C AIR DENSITY WAS TAKEN 0.0744 LB/M/FT**3
C E=2.0*0.0744*32.2=868
C V=SQR(TIP*E).
C P(Z)=Z*5.2
C V(Z)=SQRT(Z*E)
C READ(5,1) NM,E
C 1 FORMAT(5I1) NM,E
C 2 FORMAT(5I2) Y(I),I=1,N
C C PRESSURE INCHES OF WATER
C C READ(5,2) Y(I),I=1,N
C 2 FORMAT(7F10.5)
C M1=M+1
C B=0.01
C X(1)=0.0
DO 100 I=1,10
X(I+1)=X(I)+B
CONTINUE
C=0.1
DO 200 I=11,14

```

```

2CC CONTINUE
  C = C
  DO 1 I=15,20
    X(I+1)=X(I)+C
 1 CONTINUE
 10 WRITE(6,3)
 3 FORMAT(10X,'DIN.WATER'),T25,'R(VOLT)',T45,'VELOCITY(FT/SEC)',//)
  DO 20 I=1,N
    C=X(I)
    CC=P(C)
    X(I)=V(CC)
    WRITE(6,4) C,Y(I),X(I)
    4 FORMAT(3F10.5)
    C WITH CALCULATED VELOCITIES AND ANEMOMETER READING DATA AND
    LISTING SUBROUTINE POLYNOMIAL COEFFICIENTS WEPE FOUND.
    CALL CHBFT(Y,X,N,A,M,RX,RH,R)
    WRITE(6,5)
    5 FORMAT(10X,'POLY.COFF.'//)
    WRITE(6,6) (A(I),I=1,M)
    6 FORMAT(5X,E14.7)
    REAL LABEL/1/
    REAL*8 TITLE(112) /' NIHAT GUNGOR RUNI
    * VFLCITY PROFILE
    CALL DRAW(21,X,Y,1,2,LABEL,ITITLE,40.,.4,0,0,0,0,9,6,1,L)
    Y=(Y(N)-Y(1))/3
    YZERO=Y(1)-DY
    DO 70 I=1,100
      Y(I)=YZERO+DY*I
    X(I)=A(M+1)
    DO 60 J=1,M
      JM=M1-J
      THE VELOCITIES WERE CALCULATED BY USING POLYNOMIALS AND
      ANEMOMETER READING (E-E(ZERO)) BY NESTING METHOD TO CHECK
      HOW THEY FIT EXPERIMENTAL VALUES.
      XC=X(I)*X(I)+A(JM)
      CONTINUE
      CALL DRAW(100,X,Y,3,0,LABEL,ITITLE,40.,.4,0,0,0,0,9,5,1,L)
      RETURN
    END
    SUBROUTINE CHBFT
    C
    C PURPOSE:
    C SUBROUTINE CHBFT EVALUATES THE COEFFICIENTS OF AN MTH ORDER
    C POLYNOMIAL P(X)=A(1)+A(2)*X+A(3)*X**2+...+A(M+1)*X**M SUCH
    C THAT THE MAXIMUM ERROR ABS(P(X(I))-Y(I)) IS A MINIMUM OVER
    C THE N (N GT M+1) SAMPLE POINTS X(I), Y(I) I=1,2,...,N.
    C X(I) MUST FORM A STRICTLY MONOTONIC SEQUENCE: I.E.,

```

X(1).LT.X(2).LT.X(3).LT...X(N). THIS SURCCUTINE IS A CONVERSIN FROM ALGOL TO FORTRAN OF ALGORITHM 318, CHERYSCHEF CURVE-FIT FROM "COMMUNICATIONS OF THE ACM" VOL 10, NUMBER 12, DECEMBER 1967. THE AUTHOR OF THE ALGOL VERSION WAS J. BOOTHROYD FROM THE UNIVERSITY OF TASMANIA.

USAGE: CALL CHBFT (X,Y,N,A,M,PX,RH,R)

DESCRIPTION OF PARAMETERS:
 X - ARRAY OF ABSISSAE DIMENSIONED REAL*4 X(N)
 Y - ARRAY OF ORDINATES DIMENSIONED RFAL*4 Y(N)
 N - NUMBER OF SAMPLE POINTS (INTEGER)
 A - ARRAY OF THE OUTPUTTED POLYNOMIAL COEFFICIENTS
 M - DIMENSIONED AT LEAST A(M+2) (REAL*4)
 R - ORDER OF DESIRED APPROXIMATING POLYNOMIAL
 RX - WORK ARRAY DIMENSIONED AT LEAST REAL*4 RX(M+2)
 RH - WORK ARRAY DIMENSIONED AT LEAST REAL*4 RH(M+2)
 R - INTEGER WORK ARRAY DIMENSIONED AT LEAST R(M+2)

REMARKS: THE POLYNOMIAL $P(x)$ IS A BEST-FIT POLYNOMIAL IN THE CHERYSCHFV SENSE AS DESCRIBED BY STIEFEL (NUMERICAL METHODS OF APPROXIMATION IN LANGER (ED.), "NON NUMERICAL CHEBYCHEFF APPROXIMATION" IN PRESS). THE PROCEDURE MUST TERMINATE AFTER A FINITE NUMBER OF STEPS. AT EXIT THE ABSOLUTE VALUE OF $A(M+1)$ YIELDS THE FINAL REFERENCE DEVIATION. NEGATIVE $A(M+1)$ INDICATES THAT THE PROCEDURE HAS BEEN TERMINATED FOLLOWING THE DETECTION OF CYCLING.

NOTE : DIVIDED DIFFERENCES AND NEWTON'S INTERPOLATING FORMULA IS USED FOR COMPUTING THE POLYNOMIAL COEFFICIENTS.

```

SUBROUTINE CHBRET(X,Y,A,M,RX,PH,P)
REAL*4 NEXTH
INTEGER RI,RJ,R(1)
DIMENSION X(1),Y(1),A(1),RX(1),RH(1)
MPLUS2=M+1
NPLUS2=M+2
PREVH=0.0
C DETERMINE INDEX VECTOR FOR INITIAL REFERENCE SET .
C R(NPLUS2)=1
R(NPLUS2)=N
D=(N-1)/MPLUS1
H=D
DO 1 I=2,MPLUS1
R(I)=H+1.0
1 H=H+D
H=-1.0
C SELECT M+2 REFERENCE PAIRS AND SET ALTERNATIVE DEVIATION VECTOR
DO 2 I=1,MPLUS2
RI=R(I)
RX(I)=X(RI)
A(I)=Y(RI)
H=-H
C COMPUTE M+1 LEADING DIVIDED DIFFERENCES
DO 3 J=1,MPLUS1
I1=MPLUS2
A1=A(I1)
RH1=RH(I1)
I=MPLUS1
DENOM=RX(I1)-RX(I-J+1)
C A1=A(I)
RH=RH(I)
A(I1)=(A(I1)-A1)/DENOM
RH(I1)=(RH1-RH)/DENOM
I1=I
A1=A(I)
RH1=RH(I)
IF(I-J) 4,5,5
C CONTINUE
C EQUATE (M+1) THE DIFFERENCE TO ZERO TO DETERMINE H
C H=-A(MPLUS2)/RH(MPLUS2)
C WITH H KNOWN, COMBINE THE FUNCTION AND DEVIATION DIFFERENCES
DO 6 I=1,MPLUS2
A(I)=A(I)+RH(I)*H
C COMPUTE POLYNOMIAL COEFFICIENTS
J=M
7 XJ=RX(J)

```

```

I=J
AI=A(I)
JPLUS1=J+1
DO 8 I=JPLUS1,MPLUS1
AI=A(I)
AI=AI-XJ*AI
AI=AI
I=I
9 J=J-1
IF(J-1) 9,7,7
C CONTINUE IF THE REFERENCE DEVIATION IS NOT INCREASING MONOTONICALLY
C THEN EXIT
HMAX=ABS(H)
IF(HMAX.GT.PREVH) GO TO 29
A(MPLUS2)=HMAX
RETURN
C FIND THE INDEX,IMAX, AND VALUE,HIMAX, OF THE LARGEST ABSOLUTE
C ERROR FOR ALL SAMPLE POINTS
29 PREVH=HMAX
IMAX=R(1)
HIMAX=H
J=1
RJ=R(J)
DO 110 I=1,N
IF(I.EQ.RJ) GO TO 11
XI=X(I)
HI=A(MPLUS1)
K=M
12 HI=HI*XI+A(K)
K=K-1
IF(K-1) 112,12,12
HI=Y(I)
ABSHI=ABS(HI)
IF(LARSHI.LE.HMAX) GO TO 11
HMAX=ABSHI
HIMAX=HI
IMAX=I
GO TO 110
11 IF(J.GE.MPLUS2) GO TO 110
J=J+1
RJ=R(J)
110 CONTINUE
C IF THE MAXIMUM ERROR OCCURS AT A NONREFERENCE POINT, EXCHANGE THIS
C POINT WITH THE NEAREST REFERENCE POINT HAVING THE
C SAME SIGN AND REPEAT
C IF(IMAX.EQ.R(1)) RETURN

```

```

DO 14 I=2,MPLUS2      GO TO 15
14 CONTINUE
15 IF(IMAX.LT.R(I)) NEWTI=-H
    IF((I-1)*2*2).GT.NEXTI) NEXTI=0
    IF(HIMAX*NEXTI.GE.0) GO TO 115
    IF((IMAX.GF.R(I))) GO TO 116
    J1=MPLUS2
    J=N
    R(J1)=R(J)
    J1=J
    J=J-1
    IF((J-1).LT.118,117,117
    R(1)=IMAX
    GO TO 2
116 IF((IMAX.LF.R(MPLUS2))) GO TO 120
    J=1
    DO 121 J1=1,MPLUS2
    R(J)=R(J1)
    J=J1
    R(MPLUS2)=IMAX
    GO TO 2
115 R(1)=IMAX
    GO TO 2
120 R(I-1)=IMAX
    GO TO 2
END

C PROGRAM 'C' CALCULATION OF VELOCITIES AND TURBULANCE
C TO CALCULATE AND DRAW THE TURBULENCE INTENSITY PROFILES BY
C EVALUATING THE TWO POLYNOMIALS (SEE APPENDIX B)
C THE PROGRAM BELOW WAS INTRODUCED
C THIS PROGRAM AS VELOCITIES IT CAN BE USED TO DRAW THE VELOCITY PROFILES.
C WITH MINOR CHANGES IT CAN BE USED TO DRAW THE VELOCITY PROFILES.
C DIMENSION A1(10),A2(10),A3(10),A4(10),R(100),R1(100),R2(100),
C *Y(100),W(100),TURIN(100),X(100)
C REAL LABLE/
C REAL*TITLF(12)
C A1(I) AND A2(I) ARE THE COEFFICIENTS OF POLYNOMIALS AND
C A3(I) A4(I) ARE THE COEFFICIENTS OF DERIVATIVES OF THIS
C POLYNOMIALS
C READ(5,10) (A1(I),I=1,5)
C READ(5,10) (A2(I),I=1,5)
1C FORMAT(5F14.7)
C READ(5,11) (A3(I),I=1,4)
C READ(5,11) (A4(I),I=1,4)
11 FORMAT(4F14.7)

```

21
DO 900 IAB=1,4
READ(5,21)(TITLE(IKA),IKA=1,12)
FORMAT(6,8)
NC 800 IAB=1,5

K=2
IF(IAB.EQ.1) K=1
IF(IAB.EQ.6) K=3
READ(5,30) K1,L,M,NK,J,IK,S,RZERO,IH
30 FORMAT(7I5,2F10.5,I5)
C ANEMOmeter READINGS WERE INTRODUCED.
READ(5,20)(R(I),I=1,IH)
READ(5,20)(R2(I),I=1,IH)
20 FORMAT(7F10.5)
C THE INCREMENTS ON THE TRAVERSING LINE WAS CALCULATED.
X(1)=S
DO 40 I=1,K1
X(I+1)=X(I)+0.050
40 CONTINUE
IA=KI+1
DO 50 I=IA,L
X(I+1)=X(I)+0.0250
50 CONTINUE
IB=L+1
DO 60 I=IB,M
X(I+1)=X(I)+0.0125
60 CONTINUE
IC=M+1
DO 80 I=IC,NK
X(I+1)=X(I)+0.00625
80 CONTINUE
ID=NK+1
DO 90 I=ID,J
X(I+1)=X(I)+0.0125
90 CONTINUE
IE=J+1
DO 100 I=100 IE,IK
X(I+1)=X(I)+0.0250
100 CONTINUE
IG=IK+1
DO 110 I=IG,IJ
X(I+1)=X(I)+0.050
110 CONTINUE
DO 120 I=120 I=IH
R1(I)=R(I)-RZERO
120 CONTINUE
DO 200 I=1,IH
IF(R1(I).GT.1.300) GO TO 300
Y(I)=A1(5)

```

DN 201 JA=1 ,4
C VELocities WAS EVALUATED BY NESTING METHOD.
201 CONTINUE
202 DO 500 I=1,200
300 Y(I)=A2(5)
DO 202 JA=1 ,4
JM=5-JA
Y(I)=Y(I)*P1(I)+A2(JM)
202 CONTINUE
DO 500 I=1,IH
IF(R1(I).GT.1.460) GO TO 600
W(I)=A3(4)
DO 501 JB=1 ,3
JN=4-JB
W(I)=W(I)*R1(I)+A3(JN)
C DERIVATIVES OF THE POLYNOMIALS WERE CALCULATED.
501 CONTINUE
GO TO 500
W(I)=A4(4)
DO 502 JB=1 ,3
JN=4-JB
W(I)=W(I)*R1(I)+A4(JN)
502 CONTINUE
DO 700 I=1,IH
TURIN(I)=(R2(I)/Y(I))*W(I)
700 CONTINUE
CALL DRAW(IH,X,TURIN,K,O,LABLE,ITITLE,.2,.1,0,0,0,9,6,1,L)
WRITE(6,1)
1 FORMAT(10X,'X''T25','R1','T35','R2','T45','Y''T55','TURIN!',//)
2 WRITE(6,2)
2 FORMAT(15F12.5)
800 CONTINUE
900 RETURN
END

```

INITIAL DISTRIBUTION LIST

	No. Copies
1. Defense Documentation Center Cameron Station Alexandria, Virginia 22314	20
2. Library Naval Postgraduate School Monterey, California 93940	2
3. Naval Ship Systems Command (Code 2052) Department of the Navy Washington, D. C. 20360	1
4. Professor T. Sarpkaya Chairman, Department of Mechanical Engineering Naval Postgraduate School Monterey, California 93940	5
5. Department of Mechanical Engineering Naval Postgraduate School Monterey, California 93940	2
6. LT Nihat Gungor Huseyin Rahmi Bey Sokak. No. 6/1, Heybeliada, Istanbul, Turkey	4
7. Dz. kv. Komutanligi Ankara, Turkey	1
8. Deniz Harp okulu Komutanligi Heybeliada, Istanbul, Turkey	1
9. Istanbul Teknik Universitesi Istanbul, Turkey	1
10. Trabzon Teknik Universitesi Trabzon, Turkey	1
11. Middle East Technical University Ankar, Turkey	1
12. Robert College Istanbul, Turkey	1
13. Professor N. P. Tyvand (59Tv) Mechanical Engineering Department Monterey, California 93940	1

- | | |
|--|---|
| 14. Professor R. H. Nunn (Code 59Nn)
Mechanical Engineering Department
Naval Postgraduate School
Monterey, California 93940 | 1 |
| 15. LT Gerardo L. Hiriart
Naval Postgraduate School
SMC Box 1342
Monterey, California 93940 | 1 |

DOCUMENT CONTROL DATA - R & D

(Security classification of title, body of abstract and indexing annotation must be entered when the overall report is classified)

1. ORIGINATING ACTIVITY (Corporate author) Naval Postgraduate School Monterey, California 93940	2a. REPORT SECURITY CLASSIFICATION Unclassified
	2b. GROUP

3. REPORT TITLE

A Theoretical and Experimental Study of the Impingement of Two Subsonic Jets

4. DESCRIPTIVE NOTES (Type of report and, inclusive dates)

Master's Thesis; June 1969

5. AUTHOR(S) (First name, middle initial, last name)

Nihat Gungor, Turkish Navy

6. REPORT DATE June 1969	7a. TOTAL NO. OF PAGES 114	7b. NO. OF REFS 6
8a. CONTRACT OR GRANT NO.	9a. ORIGINATOR'S REPORT NUMBER(S)	
b. PROJECT NO. MIPR. No: R-68-9 (T. Sarpkaya)	9b. OTHER REPORT NO(S) (Any other numbers that may be assigned this report)	
c.		
d.		

10. DISTRIBUTION STATEMENT

Distribution of this document is unlimited.

11. SUPPLEMENTARY NOTES The research was funded by the U. S. Army Materiel Command, Harry Diamond Laboratories, Washington, D. C.	12. SPONSORING MILITARY ACTIVITY Naval Postgraduate School Monterey, California 93940
--	---

13. ABSTRACT

A theoretical and experimental investigation has been performed on the determination of the characteristics of two impinging plane turbulent jets for the purpose of understanding the performance of proportional fluid amplifiers and momentum-exchange devices. The jet deflection angle was determined through the application of the free-streamline theory for two normally impinging jets with arbitrary throat widths and wall set-backs. The deflection angle and the velocity and turbulence distributions across and at various distances along the jet were determined through the use of a hot-wire anemometer system. The results are presented in terms of normalized parameters suitable for comparison with the theoretical predictions. The deflection angles predicted theoretically were found to be in good agreement with those obtained experimentally.

Unclassified

- Security Classification

14	KEY WORDS	LINK A		LINK B		LINK C	
		ROLE	WT	ROLE	WT	ROLE	WT
	Mixing of Turbulent Jet						
	Momentum Exchange						
	Plane Turbulent Jet						
	Proportional Amplifiers						

